UNIVERSITÀ DI PARMA

UNIVERSITA' DEGLI STUDI DI PARMA

DOTTORATO DI RICERCA IN
INGEGNERIA INDUSTRIALE

CICLO XXXIV

ACTIVE NOISE CANCELLATION SYSTEM DEVELOPMENT FOR AGRICULTURAL TRACTOR CABS

Coordinatore:
Chiar.mo Prof. Gianni Royer Carfagni

Tutore:
Chiar.mo Prof. Luca Collini

Dottorando: Costante Belicchi

Anni Accademici 2018/2019 – 2020/2021

Abstract

This work describes the implementation process of an Active Noise Cancellation system for agricultural tractor cabs. The most interesting feature of this implementation is the use of general-purpose hardware, without the need of expensive and hard-to-program Digital Signal Processing (DSP) devices. In particular, the reference signals, provided by accelerometers properly placed on noise-generating parts, and the error feedback signals are collected by means of a USB interface. All signal processing, aimed at primary path estimation and anti-noise audio signal generation, is performed using Simulink running on a commercial mini PC. The Exponential Sine Sweep (ESS) method is adopted for the measurement of the secondary path from the cancellation loudspeakers to the error microphones. An adaptive Filtered-x Least Mean Square (FxLMS) algorithm determines the anti-noise audio signal to be emitted. The system has been installed and tested on a commercial agricultural tractor cabin mounted over electromagnetic shakers to emulate realistic operating conditions. Two error microphones are attached to the headrest, close to the driver's ears. The resulting ANC system relies on the use of very small buffers (for audio/accelerometric data), with a latency comparable to that of more complex and expensive specific DSP systems used in this kind of applications. In terms of acoustic performance, a significant reduction of annoying peaks in the 200-500 Hz range and a broadband noise reduction at lower frequencies are observed, thus improving the overall sound quality experience. In conclusion, the implementation of an effective ANC system, employing common audio devices and a relatively simple Simulink program, was obtained. This paves the way to straightforward experimentation (in Matlab/Simulink) of new ANC processing algorithms, allowing direct testing of simulation-based solutions, without the need of porting them to proprietary DSP-based platforms.

Contents

Acknowledgements

At the end of my PhD program, the time has finally come to thank all those who have played a fundamental role in this experience of cultural, professional and personal growth.

The first thanks go to Professors Luca Collini and Angelo Farina, of the University of Parma, for giving me the invaluable opportunity to undertake this path. In particular, it was an immense honour and a source of pride to be guided and supported in the research by a figure of such high cultural and personal depth as Professor Farina.

I thank all the team of people from the University of Parma who have made their support and experience available to me in this project. In particular I would like to mention Daniel Pinardi, Marco Binelli, Lorenzo Ebri, Andrea Toscani, Marco Martalò, Nicolò Strozzi and Prof. Gianluigi Ferrari.

Of course, I thank Argo Tractors S.P.A. for giving me the opportunity to work in the field of agricultural tractors, to which I have been linked since I was a child. I do not deny that it was a dream that came true. In particular I would like to thank Giovanni Esposito, Leonardo Pilò, Giordano Cordioli and Francesco Annunziata.

I reserve a special thanks to Alessandro Opinto, of the University of Parma. He shared with myself the most demanding part of the project, made up of successes but also of many difficulties. His skills and his work played a fundamental role in achieving the results.

Finally, I reserve my heartfelt thanks and I dedicate this work to all the important figures in my life: my parents, my friends, myself.

Costante

Chapter 1: Introduction

Acoustic comfort, in the use of a motorized vehicle of any type, has become a dominant factor both for the commercial success of the machine and in terms of safety for the health of the driver and passengers. In particular, in the context of work on agricultural and earth-moving machinery, the reduction of the driver's exposure to noise is important. Persistent high noise levels over time can cause on the worker occupational diseases as well as psychophysical problems such as fatigue and loss of attention in the medium-short term. In this regard, there are regulations that define the daily and weekly limit levels of worker exposure to noise. For example, in Italian legislation, these limit values are dictated in a specific section of Law 81/2008 [1]. This thesis work summarizes part of the activities carried out as part of a large project called *CleverCab*. The objective of the latter was to significantly improve the comfort and safety of those who work on board tractors, with particular attention to those with medium-large cabs, such as those produced by the company Argo Tractors S.P.A. [2] which has participated in the project. This objective was pursued through the redesign of the tractor cab itself. On the one hand, managed by the Polytechnic of Milan (Italy), a new system of active cab suspension was developed with the aim of obtaining a considerable attenuation of the vibrations that are transmitted to the driver's seat. On the other hand, managed by the University of Parma (Italy), an advanced *Active Noise Cancellation* (*ANC*) system has been implemented to act on the medium-low frequencies of the noise that reaches the cabin. This work will focus on the latter implementation process of the ANC system starting from the experimental characterization of the acoustic field present in the cabin of a real tractor, up to the installation and test of the prototype system on board a cabin deriving from a production vehicle. In particular, the model on which the research was carried out is the one called *McCormick X7.690* in production in year 2018.

1.1 Characteristics of Agriculture Interior Noise

In order to design a high-performance active noise cancellation system, it is primarily necessary to know the possible sources that determine the acoustic field inside the cabin. In fact, in general, ANC systems must be developed based on the noise sources whose effects it is intended to reduce. The acoustic field is composed of a mix of components due to various causes that must be

correctly identified. Studies on this subject are available in the literature, such as that of Abd-El-Tawwab et al [3], which show that within the cabs of agricultural machinery, the noise at the driver's ear is characterized, mostly, by low and medium frequency components deriving from sources such as the engine or road-tire interaction.

The components of noise inside a generic passenger compartment can be divided into two categories: *air-borne* noise and *structure-borne* noise. The air-borne noise is that component of the noise that is transmitted from the outside into the cabin through the boundary surface or through existing openings. Typical cases of air-borne noise are represented by the noise that crosses the glass surfaces of the cabin or that creeps through the inefficient seals of the doors. The structure-borne noise is represented by that component that arises as vibration, corresponding to the mechanical parts of the system, which is transmitted through the structures until it is radiated in an acoustic form from the interior surfaces of the passenger compartment.

The noise components in the cabin can also be catalogued based on the characteristics of their spectrum:

- Tonal noise, characterized by the concentration of sound energy at certain frequencies;
- Random or broadband noise, characterized by a homogeneous distribution of energy over a more or less extended frequency band.

Figure 1.1 shows, as an example, the spectrum of the signal acquired by a microphone placed at the ear of the driver of a tractor driving on an asphalt road at 40 km/h and 1700 rpm of the engine. The prevalence of energy at medium-low frequencies below 1000 Hz is evident. In addition, peaks due to tonal noise are visible. These components can affect the *sound quality* in the cabin because they can be perceived as psycho-acoustically annoying. In fact, as reported in texts, such as that of Fastl and Zwicker [4], a tone is annoying if it significantly prevails over the rest of the noise within the third octave of the spectrum to which it belongs. Furthermore, the presence of high frequency tonal noise raises the psycho-acoustic disturbance parameter called *sharpness* [5].

From the data available in the literature and from the measurements that will be described in Chapter 3, the main sources of noise identified on board the tractor are the following:

- *Engine*: low-frequency noise of the tonal type characterized by a fundamental frequency and by harmonics commonly defined as *orders* of the engine;
- *Distribution pump group*: medium frequency tonal noise characterized by a fundamental frequency usually between 300 and 600 Hz and by harmonic components;
- *Rear wheel transmission reducer*: also in this case it is a medium-low frequency tonal noise;
- *Tire-soil rolling interaction*: Low frequency random noise depending on the type of soil. It is predominant when the vehicle travels on an asphalted road at high speeds which for a tractor are close to 50 km/h;
- *Exhaust system*: aerodynamic-type broadband noise at low frequencies;
- *Fan*: Aerodynamic random noise.

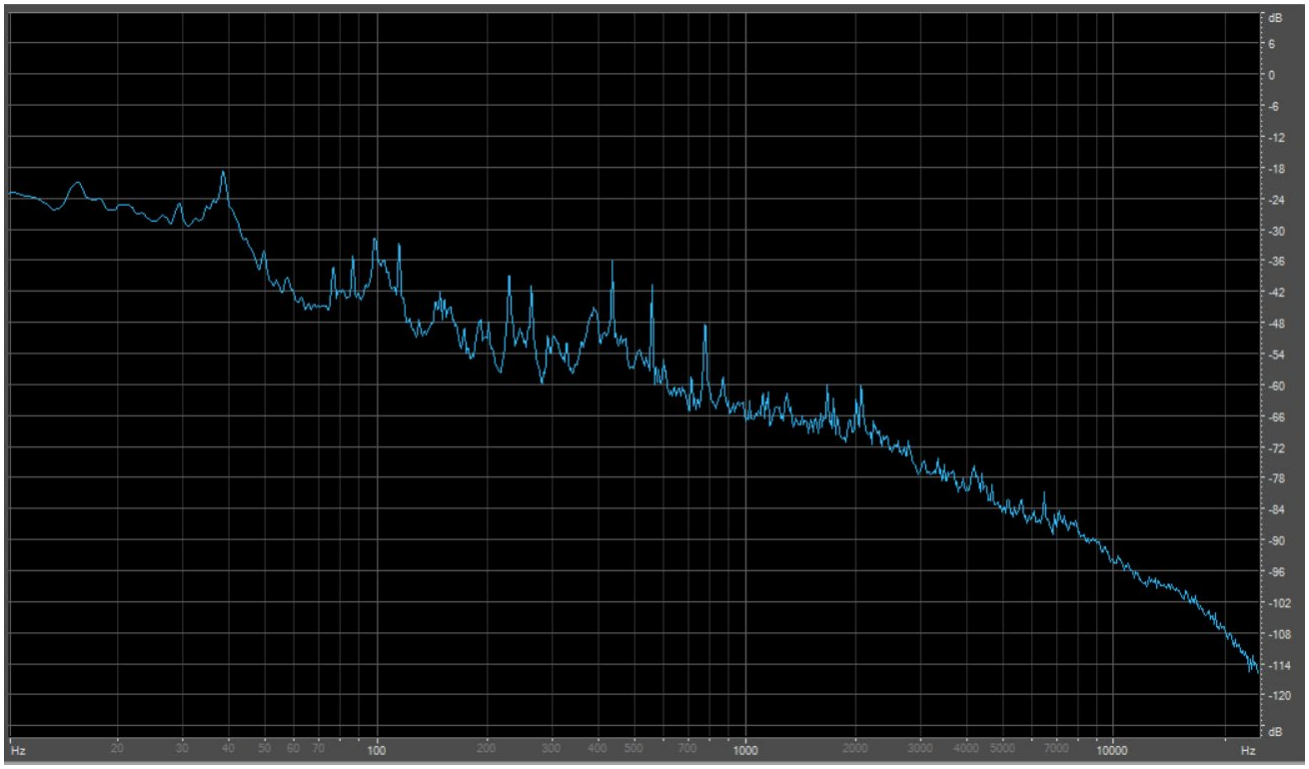

Figure 1.1: Tractor driver's ear noise spectrum at 40 km/h and 1700-rpm engine speed.

1.2 Noise Control Approaches

After having outlined the main characteristics of the acoustic field present in the cab of a tractor, it is necessary to describe the strategies available today for the reduction of noise on board motorized vehicles, which apply to both air-

borne and structure-borne noise. These techniques can be divided into two categories: passive and active.
Passive techniques are those traditionally used and can be listed as follows:

• Reduction at the source;

• Use of silencers;

• Acoustic insulation (*sound barrier*);

• Acoustic absorption;

• Vibration damping;

Among the active techniques, the main one is *Active Noise Cancellation* (ANC) object of this thesis.
As seen above, the acoustic field of a vehicle, generated by the set of mechanical and aerodynamic sources, is characterized by a spectrum that develops over a wide range of frequencies. For this reason, all the techniques listed above must work in synergy since each control method is more effective on a narrow range of noise frequencies.

1.2.1 Noise Control Passive Approaches

Among the passive noise control techniques, we can identify two categories, namely the noise reduction techniques at the source and those that involve the use of specific materials for the reduction of sound energy in the cabin.

By *source reduction* we mean all those methods essentially related to the good design of the devices that constitute a source of noise. In fact, the bad design of a device can be the cause of noise due for example to unbalance of rotating parts or to any other mechanical defect. Another typical noise problem can be related to the bad combustion cycle of the engine. Ultimately, a method to reduce the noise emitted can be the choice of devices, which make up the tractor, of good quality from the design point of view.

A particular case concerns the noise emitted by the engine exhaust system. In this case, the traditional reduction technique involves the insertion of *silencers* along the exhaust duct, consisting of elements such as expansion chambers, quarter-wave resonators or Helmholtz resonators. These elements cause a loss of sound pressure along the duct that goes from the engine to the outlet of the fumes in the external environment.

Sound barrier materials reduce the transmission of noise that propagates by air (air-borne noise) from one environment to another. Therefore, they can be used as a barrier between the cabin and the outside. The sound insulating materials can be of different nature depending on the sector or application in question. The basic rule, however, is that the denser the material, the less sound transmission is. The ideal material is identifiable in the form of a dense, non-resonant sheet (sometimes described as "*limp mass*"). The classic examples of these materials are rubber, lead, steel, marble, solid wood, glass etc. A sound insulation strategy also consists in placing a layer of light spongy material (in practice a material that would individually be sound absorbing) between two rigid layers. In practice, the multilayer that is created constitutes a *mass-spring-mass* system. In general, a solution of this type attenuates the holes of the soundproofing power at the coincidence and resonance frequencies of the two neighbouring surfaces. It is clearly deducible that a soundproofing barrier must be positioned along the direct path between the source and the noise reduction point and that it can be interposed between other materials without losing its insulating capacity.

Sound absorption consists in using materials to reduce reflected noise and therefore to avoid the phenomenon of reverberant build-up in closed environments. Porous and fibrous materials, such as foam or fiberglass, are used to absorb noise inside tractor cabs and in similar applications. Absorbing materials are more efficient near sound sources and are not effective for reducing transmission, i.e. they should not be used as soundproofing barriers. Unlike sound insulation, absorbent materials must directly receive the acoustic energy by air and for this reason, they must be installed as an external covering not covered by other continuous layers of material.

Vibration damping refers to the process of removing vibration energy from rigid surfaces such as sheet metal or plastics. Noise is reduced by applying, by adhesion, sheets of damping material at selected locations. To underline the need for the best possible adhesion between the vibrating rigid surface and the damping panel. The damping sheets can also be coupled to one or two thin layers of rigid material, such as aluminium, to create a composite panel with increased damping capabilities. This technique is commonly called "*constrained layer*" damping

1.2.2 Active Noise Cancellation (ANC)

Traditional passive mitigation methods, which involve the use of sound-absorbing and sound-insulating materials, are very efficient at broadband control of medium to high frequency noise but may not be very effective in controlling low-frequency components. *Active Noise Cancellation* (ANC) method, mentioned for the first time in a patent from 1936 [6], is based on the emission, through a dedicated loudspeaker, of an acoustic signal, usually referred to as "anti-noise" of equal amplitude and opposite phase with respect to the disturbing noise. Ideally, these two audio signals overlap each other destructively, thus obtaining perfect silence in the point of space where they are incident (Figure 1.2). The ANC technique is effective in controlling low frequency noise where traditional passive methods have limitations. The cancellation speaker, also called *secondary source*, is driven by an electronic system whose operation is based on an adaptive system essentially consisting of a digital filter whose coefficients are updated in real time by an adaptive algorithm. The term "adaptive" means a system that follows the variations of the noise to be cancelled by updating its characteristics. Adaptive systems will be treated with greater precision in Chapter 2.There are various architectures to develop an ANC system of which an excellent general discussion was conducted by Kuo and Morgan [7]. Control systems for ANC applications are essentially divided into two main categories: *feedforward* and *feedback* controllers. The feedforward controllers use reference signals from sensors placed in correspondence with the noise sources. Furthermore, they also use the error signal which provides an estimate of the cancellation actually obtained. The feedback controllers only use the error signal as input for the calculation of the anti-noise.

Since the late 1980s, the first studies on ANC for noise mitigation within car cabins have been carried out by Elliot et al [8]. Inspired by the results in the automotive field, ANC studies have been then carried out in the field of tractors and other agricultural machinery, like that by Gulyas et al. [9].

Currently the ANC technology is applied on some industrial products. For several years, headphones have been available that effectively reduce external noise, such as, first of all, those produced by Bose [10]. In the automotive field, the ANC technology has been particularly developed by Hyundai [11] in the *Road Active Noise Cancellation* (RANC) version. The goal of the RANC systems is the cancellation of noise due to the interaction of the tires with the asphalt. The cancellation of this type of noise will prove to be important with

the advent of electric cars since by failing the source due to the engine, the rolling noise of the tires will probably become the predominant noise source.

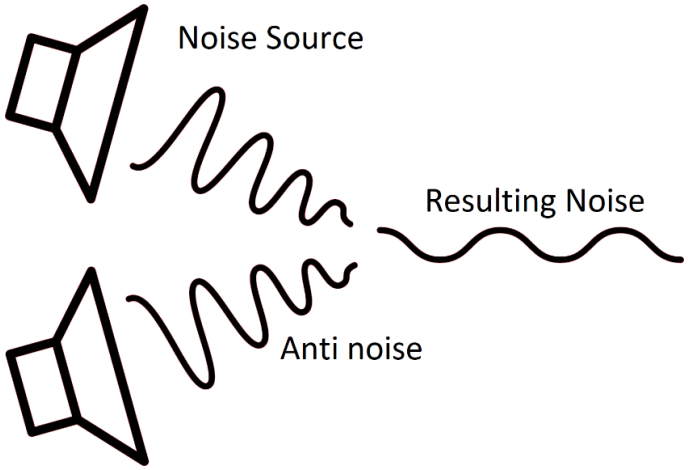

Figure 1.2: Active Noise Cancellation

1.3 Thesis Objectives and Structure

At the beginning of the research process, at the basis of this work, some objective characteristics were set that the ANC system should have respected:

• The system sought had to focus on the reduction of the noise propagated through the tractor structure or the so-called *structure-borne* component of the noise;

• The control system architecture had to be of the *feedforward* type with the acquisition of at least two reference signals in the proximity of the main structure-borne noise sources present on the tractor;

• The system had to be *Parallel Single Input Single Output* (SISO) type. In other words, two ANC systems would be developed in parallel, not interfering with each other, each consisting of a loudspeaker that would take care of the cancellation at one of the driver's ears in the cabin. So it was decided to obtain two cancellations, separately, respectively in correspondence of the left ear and right ear of the occupant in the cabin;

• The hardware components of the system had to be for the most part *general-purpose*, without the need of expensive and hard-to-program Digital Signal Processing (DSP) devices;

• The software control of the system had to be managed using models created in the MATLAB/Simulink environment in order to make the programming process more accessible even to the less experienced users;

The general objective of the project was to obtain a reduction in the noise level at the occupant's head of the tractor cabin but also a reduction of the annoying tonal noise generated by some sources in order to improve the *sound quality* on board the tractor.
The study was mainly carried out on an isolated cabin solicited by electromagnetic shakers. However, the solutions adopted, especially from the hardware point of view, allow the installation of the prototype resulting from this work on a real vehicle running without adaptation problems.

This thesis work is organized as follows.

Chapter 2 will illustrate the theoretical foundations on adaptive algorithms that underlie the operation of the control of an Active Noise Cancellation system. Particular attention will be given to feedforward control which today is practically the only one used in the automotive field.

Chapter 3 will describe all the experimental tests and the analysis of the results aimed at characterizing the acoustic field on board the cabin of a real tractor. In particular, the goal was to identify the sources that most affect the noise that reaches the driver's ear. For this purpose, the coherence analysis between the acoustic field in the cabin and the signals acquired near the various sources will be important.

Chapter 4 discusses the hardware and software implementation process of the ANC system. In particular, the various devices used to assemble the system will be listed and the Simulink models implemented to check its operation will be described.

Chapter 5 will describe the tests carried out first in the form of off-line simulation and then on board a tractor cabin mounted on electromagnetic shakers. The results of these tests will be discussed.

In Chapter 6, the final considerations on the results of the research will be presented and the possible developments that may derive from it will be evaluated.

Chapter 2: Active Noise Cancellation Basic Understanding

In this chapter, the theoretical bases regarding *Active Noise Cancellation* systems will be proposed. The adaptive *Least-Mean Square* (LMS) algorithm, which underlies all system identification and active system control problems, will be described in its original form and in its *Filtered-x LMS* variant. The latter, conceived for the control of ANC *feedforward* systems, involves the use of an estimate of the transfer function of the acoustic path between the speaker and the cancellation position. The chapter will end with the description of the method used to estimate this transfer function, usually called *Secondary Path Transfer Function*.

2.1 Adaptive Algorithms

In the context of analog or digital signal processing, *filtering* means that process of selective alteration of the spectral content of a signal. The instrument that allows this operation is called *filter* and if the input signal is made up of discrete samples, the filter is called *digital* or *numerical filter*. Each filter is characterized by parameters, such as bandwidth, which can be constant or variable over time. When these parameters are not constant but adapt according to the variations of the input signal, the filters are defined as *adaptive*. Compared to conventional filters, the time-invariance hypothesis is lacking. The updating of the filter coefficients is controlled by an algorithm, called *adaptive*, which detects the variable input signal and acts accordingly by recalculating the new coefficients to be supplied to the filter. The set of adaptive filter and algorithm constitute the so-called *adaptive system*. Figure 2.1 shows the basic block diagram of an adaptive system where signals represented are named as follows:

- *x(k)*: *reference* input signal;
- *d(k)*: *primary* or *desired* signal;
- *y(k)*: *output* signal from the digital filter, result of the adaptive filtering of *x(k)*;
- *e(k)*: *error signal*, obtained as the difference between *d(k)* and *y(k)*.

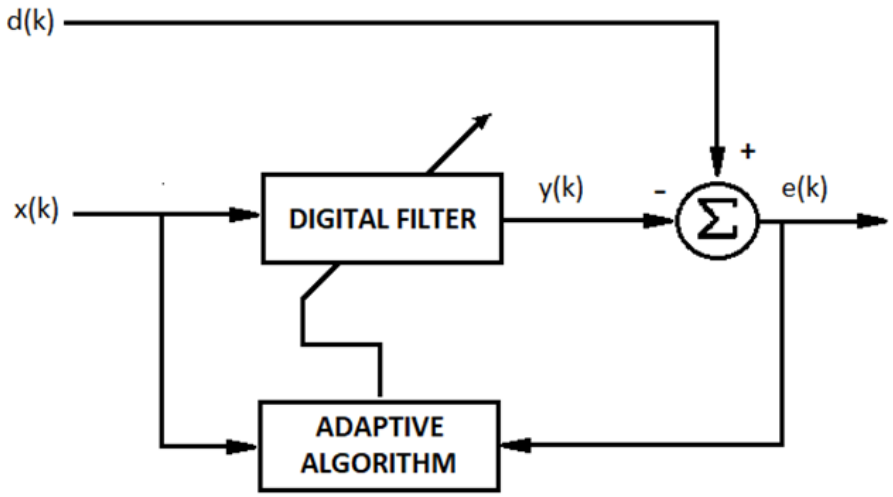

Figure 2.1: Block diagram of an adaptive filter

It is immediately deduced that the output of the filter *y(k)* will strictly depend on the input signal *x(k)* and on the error signal *e(k)* therefore indirectly from *d(k)*.

The goal of adaptive algorithms, such as those described in this chapter, is to minimize the error signal *e(k)*, ideally reaching $e(k) \approx 0$, updating the filter coefficients. To measure the performance of the entire process, *the mean square error* (*MSE*) is used, defined as:

$$J(k) = E[e^2(k)] \qquad (2.1)$$

Where the *E* operator indicates the expected value of the function in square brackets. In a generic *Finite Impulse Response* (FIR) filter, MSE is a quadratic function of the weights that can be represented as a convex hyperbolic surface. In order to minimize the error, the algorithm must adjust the filter coefficients by traveling the surface downwards until it reaches the minimum point of the function in which the weight vector will have its optimum. In other words, the algorithm will iteratively estimate the MSE gradient and, subsequently, perform an incremental downward movement. In choosing the type of algorithm, among the various available, the determining factors are essentially:

- Speed of convergence;
- Computational complexity.

In nonlinear programming and optimization problems, the basic iterative technique used to find the solution that minimizes an objective function is that of the *gradient method*. It is based on successive corrections of the filter

weights vector $\boldsymbol{w(k)}$ in the direction of the maximum negative gradient of the convex error surface. Upon reaching $J(k_m) = J_{min}$, where $J(k)$ is the objective function and k_m is the instant of reaching the minimum value J_{min}, the weights vector reaches its optimal value.

Taking on:

- $J(0)$: MSE value at the initial instant k=0;

- $\boldsymbol{w(0)}$: value of the weight vector $\boldsymbol{w(k)}$ at instant $k=0$.

The gradient method is mathematically expressed with the following expression:

$$\boldsymbol{w}(k+1) = \boldsymbol{w}(k) - \frac{\mu}{2}\boldsymbol{\nabla} J(k) \qquad (2.2)$$

The parameter μ is called *step-size* and controls the stability and the speed of convergence of the algorithm. The vector $\boldsymbol{\nabla J(k)}$ represents the gradient of the objective function and the - sign indicates the increment from $\boldsymbol{w(k)}$ to $\boldsymbol{w(k+1)}$ in the direction of the negative gradient, following approximately the fastest descent path in the surface representing the mean square error.

2.1.1 Least-mean Square Algorithm (LMS)

In many applications, it is not possible to use the gradient method directly since the statistics of the input signals $x(k)$ and $d(k)$ are not known and therefore it is not possible to calculate $J(k)$ as defined in (2.1). A solution to this drawback is to use an estimate of the mean square error represented by the instantaneous square error $e^2(k)$:

$$\hat{J}(k) = e^2(k) \qquad (2.3)$$

This approximation is used in the algorithm, derived from the gradient method, which is called *Least-mean Square Algorithm (LMS)*. From the definition in (2.3), it follows that the instantaneous gradient of the quadratic error to the sample k:

$$\boldsymbol{\nabla}\hat{J}(k) = 2[\boldsymbol{\nabla} e(k)]e(k) \qquad (2.4)$$

The error signal $e(k)$ can be mathematically expressed as:

$$e(k) = d(k) - y(k) = d(k) - \boldsymbol{w^T}(k)\boldsymbol{x}(k) \qquad (2.5)$$

If we define L the order of the filter, or the length of the vector of the coefficients $\boldsymbol{w}(k)$:

$$\boldsymbol{x}(k) = [x(k), x(k-1), x(k-2), \dots, x(k-L+1)]^T \qquad (2.6)$$

$$\boldsymbol{w}(k) = [w_1(k), w_2(k), \dots, w_L(k)] \qquad (2.7)$$

it is demonstrated that:

$$\boldsymbol{\nabla} e(k) = -\boldsymbol{x}(k) \qquad (2.8)$$

$$\boldsymbol{\nabla} \hat{J}(k) = -2\boldsymbol{x}(k)e(k) \qquad (2.9)$$

By substituting (2.7) in (2.9) we obtain the mathematical expression of the LMS algorithm:

$$\boldsymbol{w}(k+1) = \boldsymbol{w}(k) + \mu \mathbf{x}(k)e(k) \qquad (2.10)$$

Observing the expression (2.10), we note that the LMS algorithm is simple and inexpensive for the computer since it does not require squaring, averaging or differentiation operations. For the LMS algorithm to work, it is necessary to choose a priori the values of the parameters L and μ and the initial conditions intended as vector $\boldsymbol{w}(0)$ of the filter weights at time k=0.

Defined $w_i(k)$ the value of the i-th term of the vector $\boldsymbol{w}(k)$ (with i = 0, 1, 2, ..., L-1), the output of the adaptive filter at instant k will be mathematically expressed by:

$$y(k) = \sum_{i=0}^{L-1} w_i(k)x(k-i) \qquad (2.11)$$

The error signal $e(k)$, obtained from the difference of $d(k)$ and $y(k)$, will be acquired by the adaptive algorithm which updates the terms $w_i(k)$ of the filter weights vector to the subsequent values $w_i(k+1)$:

$$w_i(k+1) = w_i(k) + \mu x(k-i)e(k) \qquad con \;\; i = 0, 1, 2, \dots, L-1 \qquad (2.12)$$

A fundamental choice for the functioning of the LMS algorithm is that of the parameter μ. Kuo and Morgan [12] have shown that for the stable convergence of the average of the weights, the step-size μ must be chosen in the interval:

$$0 < \mu < \frac{2}{LP_x} \qquad (2.13)$$

P_x represents the power of the input signal *x(k)*. For the convergence of the variance of the weights, or the mean square error (MSE), the condition is even more stringent. In fact, assuming a Gaussian signal, the range of choice of the step-size value must be:

$$0 < \mu < \frac{2}{3LP_x} \qquad (2.14)$$

From conditions (2.13) and (2.14) it can be deduced that, for the purposes of convergence, a small value of μ must be preferred when dealing with high filters order *L* and high power P_x of the signal. In these cases, a compromise value must be found between convergence speed (high step-size) and algorithm stability (reduced step-size). It is conventional to use a value included in the range proposed by [12]:

$$\frac{0.01}{LP_x} < \mu < \frac{0.1}{LP_x} \qquad (2.15)$$

The LMS algorithm is the most used in practical applications, especially in the variants derived from it in order to improve its intrinsic characteristics. Stability and convergence time depend on the step-size. As seen previously, the power of the input signal affects the choice of the parameter μ. In order to optimize the convergence speed regardless of the power of the input signal, a variant of the original algorithm called *Normalized LMS Algorithm (NLMS)* is used, whose mathematical expression is expressed as:

$$\boldsymbol{w}(k+1) = \boldsymbol{w}(k) + \mu(k)\mathbf{x}(k)e(k) \qquad (2.16)$$

The adaptive parameter *μ(k)* is defined:

$$\mu(k) = \frac{\alpha}{L\hat{P}_x(k)} \qquad (2.17)$$

In expression (2.17):

- α is defined normalized step and 0 <α <2;
- $\widehat{P_x}(k)$ represents the estimate of the power of the input signal at instant *k*.

In order to have a good estimate of the input power, the calculation using a movable window of length *M* is used:

$$\widehat{P_x}(n) = \frac{1}{m}\sum_{m=0}^{M-1} x^2(n-m)$$
$$= \widehat{P_x}(n-1) + \frac{x^2(n) - x^2(n-m)}{M} \qquad (2.18)$$

If we assume $M = L$, from expressions (2.6) and (2.18) we get that:

$$\widehat{P_x}(k) = \frac{\boldsymbol{x^T}(k)\boldsymbol{x}(k)}{M} \qquad (2.19)$$

Consequently, substituting (2.19) in (2.17), the adaptive step-size is expressed as:

$$\mu(k) = \frac{\alpha}{\boldsymbol{x^T}(k)\boldsymbol{x}(k)} \qquad (2.20)$$

In using the NLMS algorithm, it is advisable to adopt some implementation measures [12]. The first is the choice of the initial value $\widehat{P_x}(0)$ as the best a priori estimate of the power of the input signal. The second is to impose a software constraint on the algorithm such that

$$\widehat{P_x}(k) = max\{\widehat{P_x}(k), P_{min}\}$$

where P_{min} represents an arbitrary lower limit value that the estimated power must respect. This constraint is advisable since it is not desirable that, in the absence of the input signal for prolonged periods, $\widehat{P_x}(k) \approx 0$. This would cause $\mu(k)$ to grow indefinitely. With this device, the expression of the adaptive step-size becomes:

$$\mu(k) = \frac{\alpha}{L \cdot max\{\widehat{P_x}(k), P_{min}\}} \qquad (2.21)$$

A second variant of the LMS algorithm is the one called *Leaky LMS*. The practical occurrence in which there is insufficient spectral stress of the input signal is considered, as in the case of a non-noisy input sinusoid. Without tricks, the original LMS algorithm would lead to an uncontrolled growth of the vector of the coefficients of the adaptive filter. The solution is to introduce a loss by means of a factor γ between the values 0 and 1. The mathematical expression (2.10) of the LMS algorithm in this case is transformed into:

$$\boldsymbol{w}(k+1) = \gamma \boldsymbol{w}(k) + \mu \mathbf{x}(k) e(k) \qquad con\ 0 < \gamma \leq 1 \qquad (2.22)$$

The use of a Leaky algorithm, with the introduction of a loss factor γ, leads to a degradation of the performance of the adaptive system. It is necessary to find a value of γ as a compromise between robustness and performance on an experimental basis.

2.1.2 Application Fields of Adaptive Filters

As can be deduced, adaptive systems are a very powerful tool in the fields of signal processing and control. The characteristic researched in adaptive filters is the ability to operate in systems with unknown behaviour by following the temporal variations of both the input signals and the systems in which they operate. The application areas of the adaptive systems described are essentially four:

- System Identification problems;
- Adaptive (or active) Noise Cancellation;
- Inverse Modelling;
- Prediction.

In this work, only the first two types of problem will be considered, including the one concerning the adaptive identification of a system that can also be considered the basis of noise cancellation. By *identification* of a system, we mean the reconstruction of the model of the system starting from collected data. In other words, known signals are supplied to the system and the model of the system is reconstructed from the collected response. The process can be *off-line* or *on-line*. In the first case, the identification takes place downstream of the collection of all data leaving the system. In the case of on-line identification, the process is simultaneous with the data collection: the model is identified and updated for each sample k of the signal collected at the output. It is in the latter case that adaptive filters and algorithms are used, in fact we also speak of *adaptive identification*. Figure 2.2 shows the block diagram of an adaptive identification problem. The system is seen as a “black box” of which only inputs and outputs are known. We define *P(z)* as the transfer function of the unknown system. *W(z)* represents the transfer function of the filter used to model *P(z)*. The same digital input *x(k)* of the system is supplied to the filter. At the output we have the desired signal *d(k)* and the response of the filter *y(k)*. The goal is that *W(z)* converges to *P(z)*: the adaptive algorithm has the purpose

of minimizing the error *e(k)* between the outputs by updating the filter coefficients until *W(z)* ≈*P(z)*. Upon reaching convergence, *W(z)* provides an initially unknown model of *P(z)*.

Another application of adaptive systems is the *Active Noise Cancellation (ANC)*. Let us consider a generic acoustic system where noise is generated by a source positioned at a point in the system. We want to cancel or reduce this noise when it reaches another position in the system from the source. The effect of the path between the two points on the acoustic signal can be modelled using a transfer function *P(z)*. Also in active noise cancellation, the *W(z)* transfer function of the adaptive filter is used to model the incognito acoustic system. In this case, the signal is processed by two different sensors (Figure 2.3). The reference sensor captures the noise signal *x(k)* near its source. The primary sensor acquires the signal *d(k)* which represents the noise in the position of the system where cancellation is to be obtained. This is given by the sum of the component *x'(k)*, which departed from the source and passed through the system, and the component *s(k)* which represents noise not generated by the source of the reference signal. By hypothesis we neglect the component *s(k)*: we assume *d(k) = x'(k)*, since the ANC system focuses only on the component related to *x(k)*.

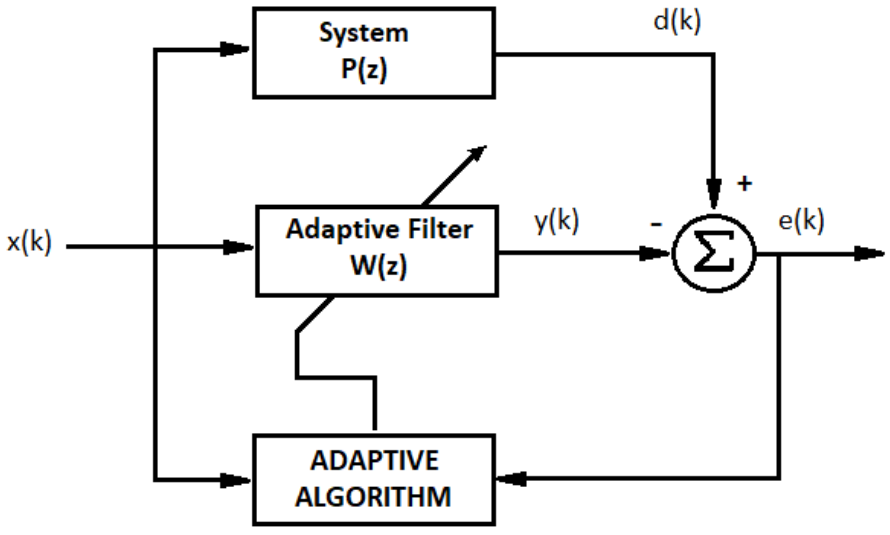

Figure 2.2: System Adaptive Identification block diagram

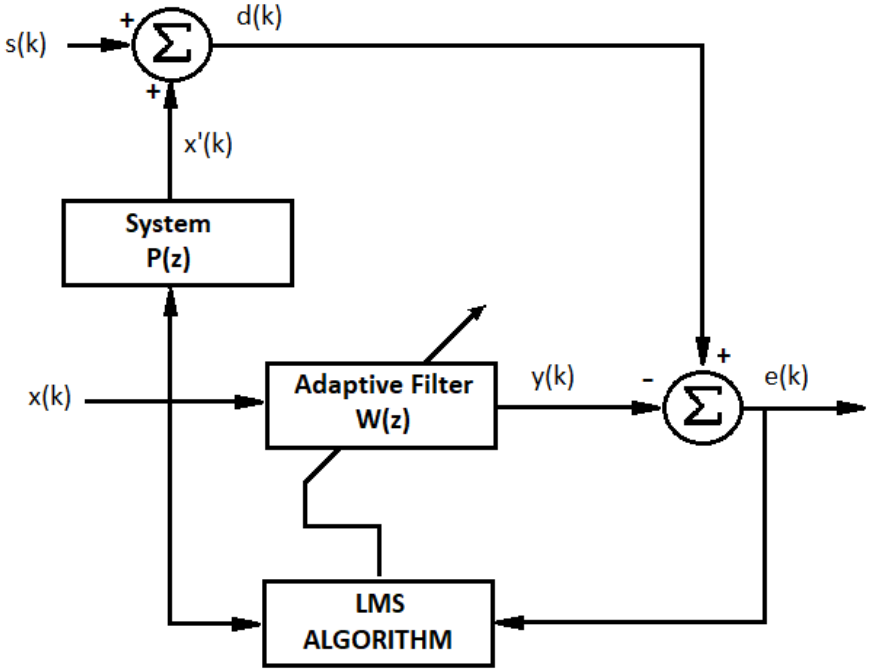

Figure 2.3: Active Noise Cancellation block diagram

Also in this case the adaptive system, consisting of filter and algorithm, works with the aim of making the function *W(z)* converge to the unknown transfer function *P(z)* of the system by minimizing the residual error *e(k)*. At convergence the output *y(k)*, transformed into an acoustic signal, approximates *x'(t)* and the cancellation is obtained from their acoustic sum.

2.2 Feedforward ANC

In the area of signal processing and system control, there are essentially two types of control:

- *Feedforward* or *open chain* controls;
- *Feedback* or *closed chain* controls.

In this paragraph, ANC systems with so-called *feedforward* (FF) control will be discussed in which disturbances (reference signals) affecting the system are measured and used by the controller algorithms to generate a compensation action. Figure 2.4 shows the pattern of a simple ANC system consisting of a duct in which at one end there is a source of noise while at the other end the cancellation of the noise, which has passed through the duct, is required. Near the source, there is a reference sensor while in the position in which the

cancellation is sought there is a sensor that acquires the error signal. The control is implemented with a secondary source driven by a controller, which acquires the reference signals *x(k)* and error *e(k)*, by means of an adaptive algorithm, generates the control signal *y(k)*. The two acquisition transducers can be microphones or accelerometers which transform acoustic or vibratory signals into electrical signals which are subsequently sampled in *x(k)* and *e(k)*. The secondary source is usually a loudspeaker, which after a digital /analog (D/A) conversion of *y(k)*, generates the cancellation acoustic signal.

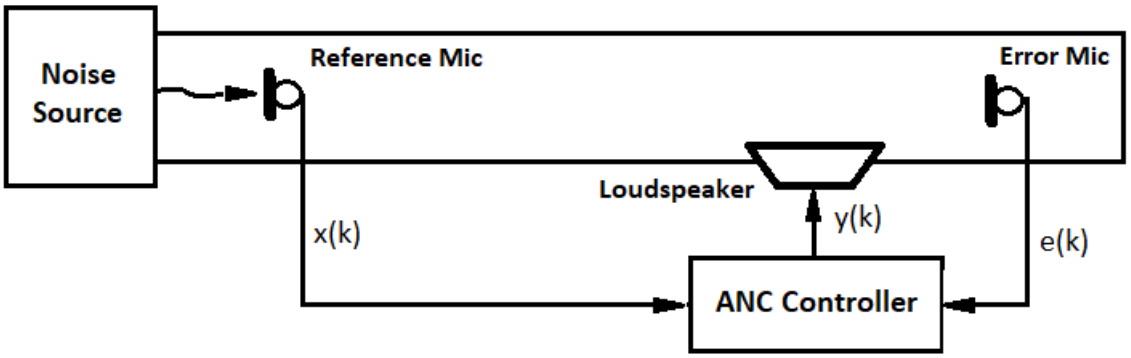

Figure 2.4: Single Input Single Output (SISO) feedforward ANC system

Such a system is ideally capable of cancelling random noise with a broadband spectrum. The first fundamental requirement, for the achievement of the cancellation objective, is that the process, consisting of acquisition of the reference signal *x(t)* (by the adaptive filter) and calculation of the output y(t), takes place before the noise from the source arrives at the cancellation position through the duct. In other words, an important parameter in ANC systems is the value of the set of all delays, hardware and software, of the control system. As anticipated in paragraph 2.1, the problem of adaptive noise cancellation is attributable to a system identification problem. Figure 2.5 shows a first simplified block diagram of active noise control operation. The transfer function *W(z)* of the filter is used for estimating the unknown system *P(z)*. The purpose is pursued by minimizing the residual error *e(k)*. In fact, defined:

- *D(z)* the z-transform of the primary noise signal *d(k)*;
- *X(z)* the z-transform of the reference signal *x(k)*;
- *Y(z)* the z-transform of the filter output *y(k)*;
- *E(z)* the z-transform of the error signal *e(k)*.

We have:

$$E(z) = D(z) - Y(z) = P(z)X(z) - W(z)X(z) \qquad (2.23)$$

If, after the convergence of the filter, $E(z) \approx 0$, with the assumption that $X(z) \neq 0$, from (2.23) results that:

$$W(z) = P(z) \qquad (2.24)$$

If equation (2.24) is verified, $y(k) = d(k)$ that is

$$e(k) = d(k) - y(k) = 0. \qquad (2.25)$$

From a theoretical point of view, (2.25) is the condition sought in the use of an adaptive filter with LMS algorithm to obtain the cancellation of the primary noise d(k). From a practical point of view, however, it must be considered that the cancellation system works between two domains that interact with each other:

• Electrical-digital domain of acquisition, processing and generation of signals;

• Acoustic domain of noise and anti-noise propagation.

In particular, in the acoustic domain, it is important to consider the path that the anti-noise, generated by the loudspeaker, travels to reach the position where the cancellation is sought. This path, called *Secondary Path* (SP), affects the anti-noise signal that actually arrives in the cancellation position by introducing, in the simplest of cases, a delay due to the distance between the cancellation speaker and the error microphone. This influence and the changes that must be made to the LMS algorithm to compensate for the effect of the secondary path will be described in the following paragraph.

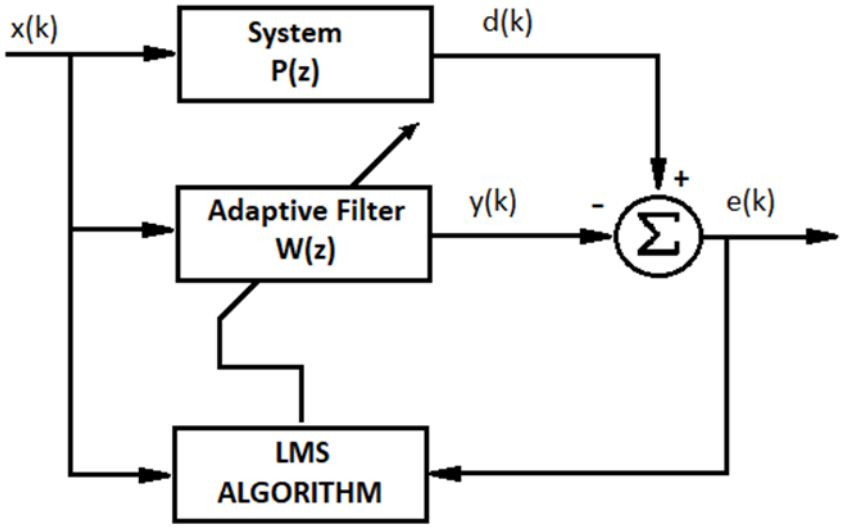

Figure 2.5: Simplified ANC system block diagram

2.2.1 Secondary Path Effect and FxLMS Algorithm

Until now, the problem of adaptive noise cancellation by an adaptive filter has been addressed from a purely theoretical point of view. The practical application of the principles set out involves some complications. As anticipated and deducible from Figure 2.4, the cancellation system works between two domains, the acoustic one and the electrical/digital one, interfaced by transducers like microphones or loudspeakers. Error and reference microphones convert acoustic signals into electrical signals. The dynamic behaviour of the microphones must therefore be considered in our models. The speaker then transforms an electrical signal, generated by the adaptive filter, into the acoustic cancellation signal, which subsequently has to travel through the secondary path to reach the position where the error microphone is located. Since the LMS algorithm, in its form seen so far, assumes that the error signal is available as the difference between the primary disturbance *d(k)* and the output of the filter *y(k)*, it is necessary to modify the model in Figure 2.5 introducing the effects of the dynamic behaviour of the sensors, by means of a transfer function *R(z)*, and the effect of the secondary path on the anti-noise signal, by means of the transfer function *S'(z)*. Figure 2.6 shows the blocks representing these transfer functions and the summing node represents the

superposition, in the acoustic domain, of the cancellation signal produced by the loudspeaker with the primary noise at the position of the error microphone.

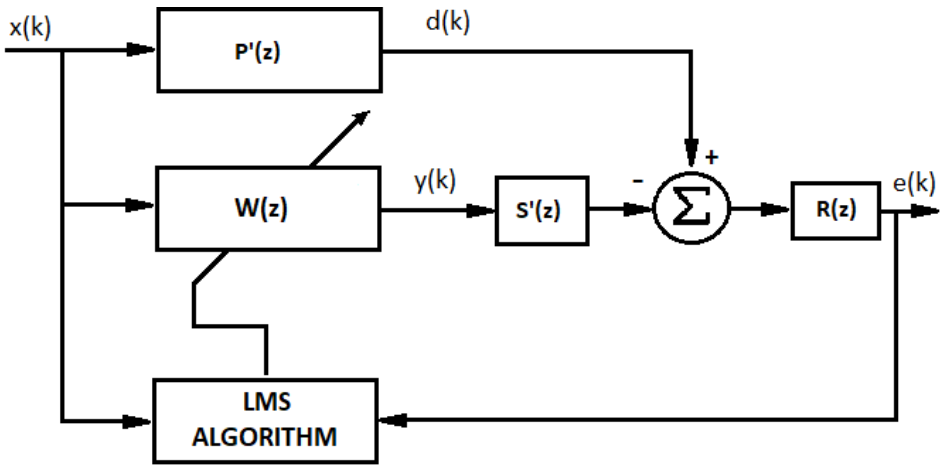

Figure 2.6: Block diagram of ANC system with insertion of the Secondary Path transfer function

S'(z) represents the secondary transfer function from the adaptive filter output to the adder block. It models the system that includes the D/A converter, any amplifier, speaker and the space between speaker and error microphone. *R(z)* represents the transfer function residual from the adder block to the error signal. It provides a model of the system consisting of an error microphone, A/D converter and any other devices before the error signal is entered into the LMS algorithm. *P'(z)* represents the transfer function of the vibro-acoustic system of the reference microphone, near the source of the noise, to the error microphone. With the latest changes, the expression (2.23) becomes:

$$E(z) = R(z)\big(P'(z)X(z) - S'(z)W(z)X(z)\big) =$$

$$= R(z)P'(Z)X(z) - R(z)S'(z)W(z)X(z) \qquad (2.24).$$

We can define

$$S(z) = R(z)S'(z)$$

$$P(z) = R(z)P'(z)$$

substituting in (2.24) we obtain

$$E(z) = P(z)X(z) - S(z)W(z)X(z) \qquad (2.25).$$

The scheme in Figure 2.6, with the use of *P(z)* and S(z) instead of *P'(z)* and *S'(z)*, is transformed into its equivalent in Figure 2.7 where the adder block is brought into the electric domain from the acoustic one. Assuming that *X(z)* is always non-zero, the adaptive cancellation algorithm updates *W(z)* of the adaptive filter to minimize *E(z)*. If *E(z)* ≈0 the relation (2.25) becomes:

$$P(z)X(z) - S(z)W(z)X(z) = 0 \rightarrow W_{opt}(z) = \frac{P(z)}{S(z)} \qquad (2.26).$$

At the convergence of the algorithm, the adaptive filter *W(z)* models *P(z)* directly and inversely *S(z)*.

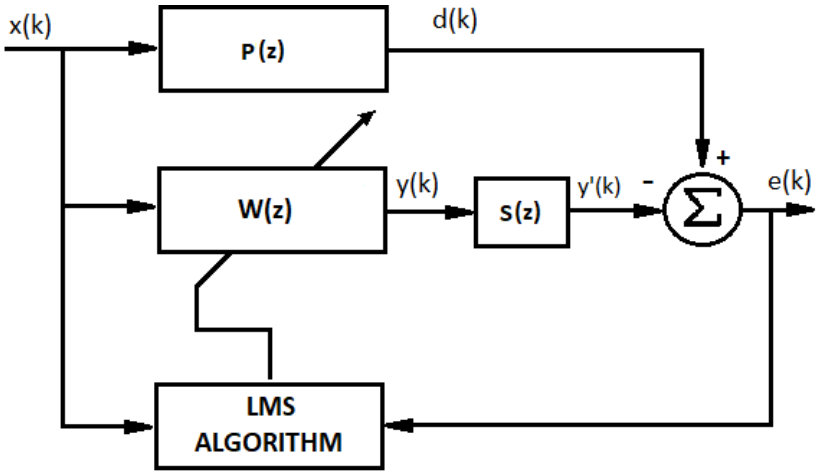

Figure 2.7: Simplified block diagram of ANC system with insertion of the SP transfer function

The adaptive filter must reverse the transfer function of the secondary path and this can lead to the instability of the vector of the filter coefficients for a value of the pulsation ω such that $S(e^{j\omega}) = 0$. In the case, like the one in Figure 2.7, the secondary path transfer function is downstream of the adaptive filter, the LMS algorithm needs a modification in order to compensate for the effect of adding the *S(z)* function. There are essentially two solutions to this problem:

- Place an inverse filter *1/S (z)* in series with *S(z)* in order to compensate for its effects;
- Place a filter with a transfer function equal to *S(z)* on the path of the reference signal *x(k)* in input to the LMS algorithm.

The second option is preferable to the first since it does not require the inversion of the transfer function *S(z)* with, therefore, a reduction in the computational load. However, this solution requires the condition of time invariance or slow

variation of *W(z)*. This hypothesis can be considered verified in most of the real vibro-acoustic systems and will therefore be assumed in the present work. The modified LMS algorithm, by placing the secondary path transfer function on the path of input reference signal, is called *Filtered-x LMS algorithm (FxLMS).*

From Figure 2.7 it is possible to deduce that the residual error signal can be expressed as

$$\begin{aligned} e(k) &= d(k) - y'(k) \\ &= d(k) - [s * y](k) = \\ &= d(k) - [s * (\boldsymbol{w}^T \cdot \boldsymbol{x})](k) \end{aligned} \qquad (2.27)$$

were s(k) is the secondary path impulse response at the instant k and the symbol $*$ is the convolution operator. The vector of the signal $\boldsymbol{x}(k)$ at instant k and that of the coefficients of the adaptive filter $\boldsymbol{w}(k)$ were previously defined by the relations (2.6) and (2.7) for a filter of order L.

Recall that the goal of the LMS algorithm is to minimize the instantaneous quadratic error $\hat{J}(k) = e^2(k)$ by updating the vector of the coefficients of the adaptive filter in the direction of the negative gradient with speed dictated by the convergence factor μ. The method is mathematically explained by the expression

$$\boldsymbol{w}(k+1) = \boldsymbol{w}(k) - \frac{\mu}{2}\boldsymbol{\nabla}\hat{J}(k) \qquad (2.28)$$

$\boldsymbol{\nabla}\hat{J}(k)$ represents the instantaneous estimate of the gradient of the mean square error and can be expressed as:

$$\boldsymbol{\nabla}\hat{J}(k) = \boldsymbol{\nabla}\mathrm{e}^2(k) = 2[\boldsymbol{\nabla}e(k)]e(k) \qquad (2.29)$$

From (2.27):

$$\boldsymbol{\nabla}e(k) = -[\mathrm{s} * \mathbf{x}](\mathrm{k}) = -\mathbf{x}'(\mathrm{k}) \qquad (2.30)$$

where

$$\boldsymbol{x}'(k) = [x'(k), x'(k-1), x'(k-2), \ldots, x'(k-L+1)]^T$$

and

$$x'(k) = [s * x](k) \qquad (2.31).$$

By substituting (2.30) in expression (2.29) we obtain the estimate of the instantaneous gradient as:

$$\boldsymbol{\nabla}\hat{J}(k) = -2\boldsymbol{x}'(k)e(k) \qquad (2.32).$$

At the end we get the mathematical expression of the FxLMS algorithm:

$$\boldsymbol{w}(k+1) = \boldsymbol{w}(k) + \mu\, \boldsymbol{x}'(k)e(k) \qquad (2.33).$$

The result shows that when a transfer function, such as *S(k)*, is present downstream of the adaptive filter, it must also be inserted in the reference signal path.

Usually the transfer function *S(k)* is not directly determinable in a precise way. For this reason, an estimate $\widehat{S}\,(z)$ must be used in the FxLMS algorithm. In this case the definition of $\mathrm{x}'(\mathrm{k})$ changes:

$$x'(k) = [\hat{s} * x](k) \qquad (2.34)$$

where $\hat{s}(\mathrm{k})$ is the estimation of the secondary path impulse response.

The fundamental problem of Secondary Path estimation will be addressed in the next paragraph. Figure 2.8 shows the block diagram of the ANC system with FxLMS algorithm and use of the secondary path estimation. An interesting aspect of the diagram of Figure 2.8 is that it is easily extendable to an ANC system with multiple reference signals to simultaneously capture multiple noise sources, multiple loudspeakers and multiple error microphones to control cancellation in different positions.

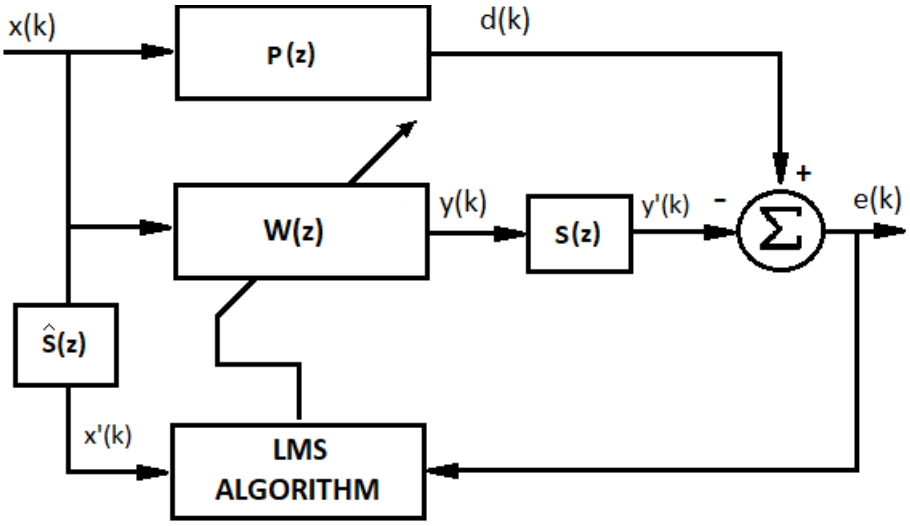

Figure 2.8: Block diagram of ANC system with SP transfer function estimation

2.2.2 Secondary Path Estimation

As already anticipated, *S(z)* represents the transfer function between the source of the anti-noise signal (the cancellation loudspeaker) and the position where cancellation is to be obtained, i.e. where the error microphone is positioned. In other words, *S(z)* provides information on the transformations that the environment applies to the noise cancellation signal emitted before being perceived by a microphone in the cancellation position. It provides a measure of:

- The time delay (called *fly time*) between emission and acquisition due to the distance between the speaker and the error microphone
- The presence of reverberations due to the acoustic reflections of the internal surfaces of the environment;
- The frequencies of the noise spectrum amplified due to the internal modes of the cavity.

In practical applications of ANC systems it is not possible to accurately determine this transfer function, however, it is evident the importance of inserting a good estimate $\hat{S}(z)$ in the FxLMS algorithm for the purposes of the performance of the noise cancellation system. In the literature, several adaptive algorithms have been proposed for SP estimation, e.g., by employing LMS algorithm with white noise as input and reference signal [13]. In this work, the SP have been estimated by employing the *Exponential Sine Sweep* (ESS) method proposed by Farina [14]. The rationale behind this algorithm is to play, from the loudspeakers used for the anti-noises emission, a known signal *x(t)*,

i.e., the *exponential sine sweep*, and to record, by the error microphones, the received audio signal *r(t)*. An exponential sine sweep signal is a sine wave whose frequency grows exponentially over time between two fixed values. After evaluating the so-called inverse filter $x^{-1}(t)$, it is possible to retrieve the considered secondary path by convolving *r(t)* with the inverse signal. In Figure 2.9, an example of exponential sine sweep signal *x(t)* and its spectrogram are shown. In Figure 2.10 the inverse signal $x^{-1}(t)$, with the corresponding spectrogram, is represented. Figure 2.11 shows an example of impulse response $\hat{s}(k)$ estimated with the method just described for the secondary path inside the cab of a tractor. It is possible to notice immediately some characteristic parts of all impulse responses in closed environments. The initial horizontal section represents, in samples, an estimate of the flight time or the time taken by the sound to reach the measurement position after being emitted by the loudspeaker. The corresponding t_v value in seconds depends on the sampling frequency f_s of the processed signals, using the formula:

$$t_v = \frac{C_v}{f_s} \quad [s] \qquad (2.33)$$

where C_v represents the length in samples of the initial horizontal section. If we indicate with c the speed of sound, usually equal to 343 m/s, from the flight time it is also possible to derive the distance between speaker and error microphone with the formula:

$$SP = t_v \cdot c = \frac{C_v}{f_s} \cdot c \quad [\text{m}] \qquad (2.34)$$

The value calculated with (2.34) can be compared with the actual distance measured in the system to evaluate the goodness of the result of the secondary path estimation method. Looking again at Figure 2.11, the first peak represents the direct sound arriving at the microphone while the subsequent ones indicate the reflections of the interior surfaces of the enclosure which provide an estimate of the reverberation entity.

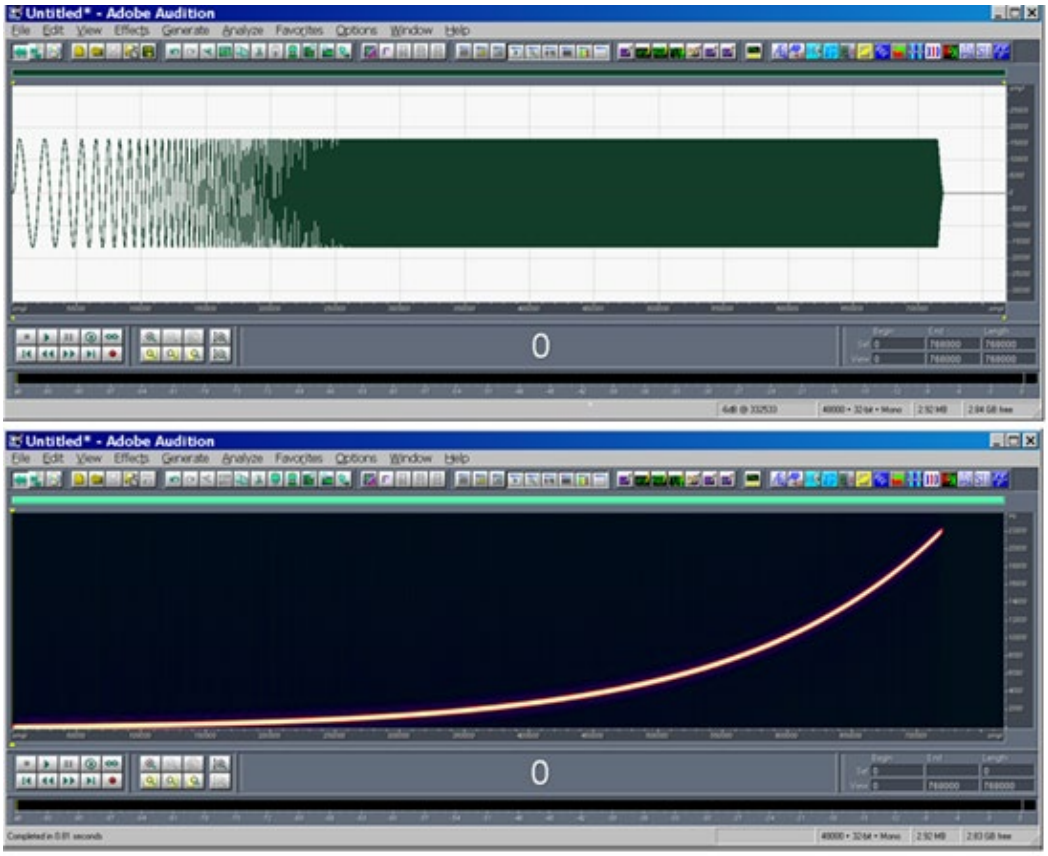

Figure 2.9: Exponential Sine Sweep (top) and its spectrogram (below)

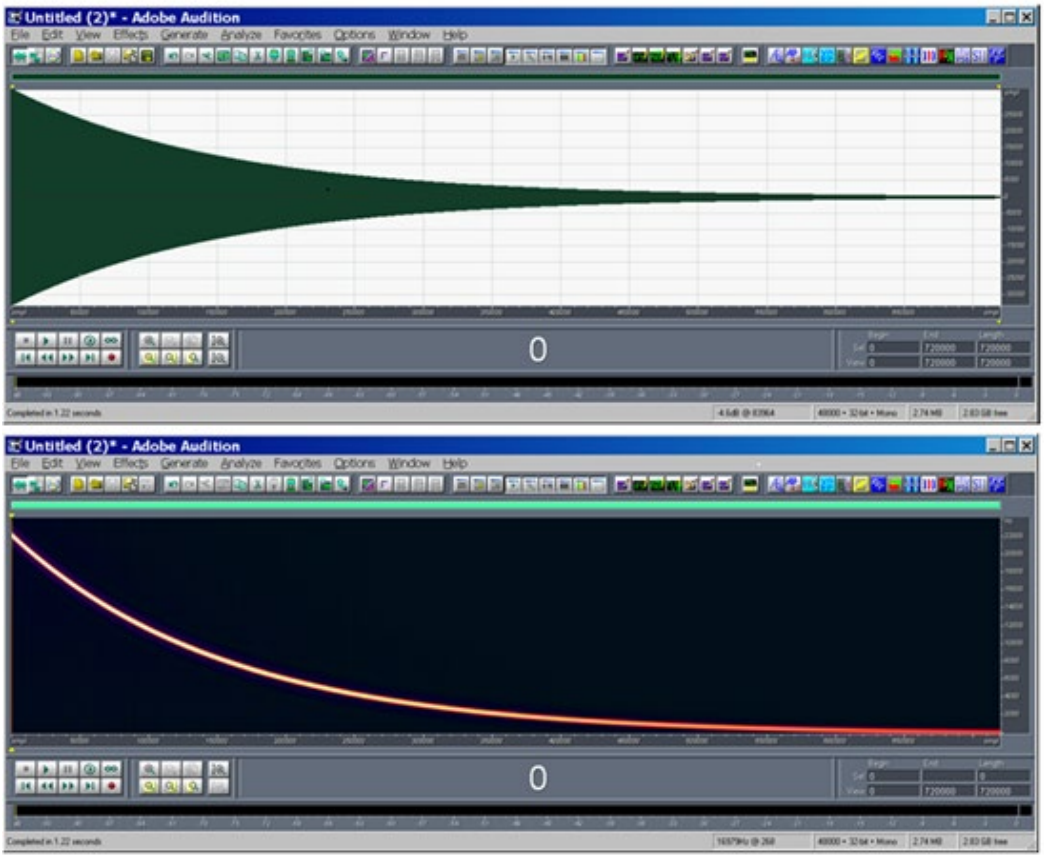

Figure 2.10: Inverse Sine Sweep (top) and its spectrogram (below)

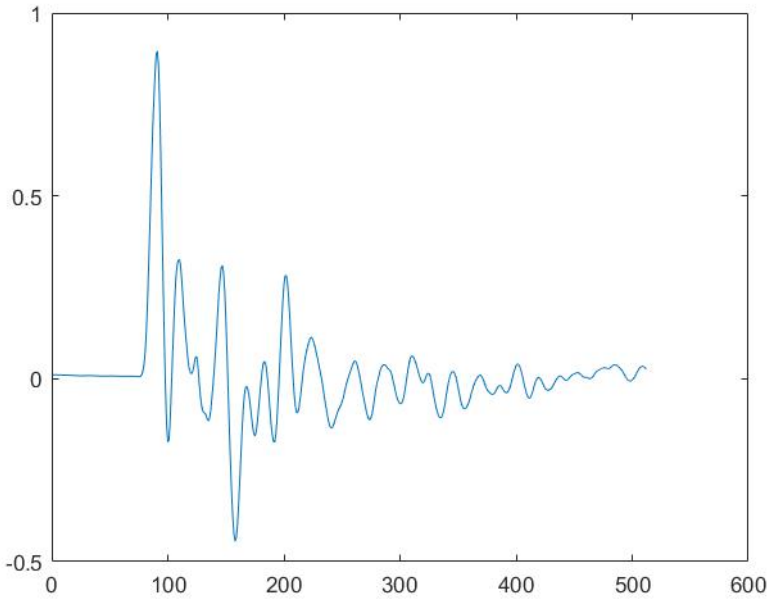

Figure 2.11: An example of estimated secondary path impulse response

Chapter 3: Experimental Characterization of Tractor Cabin Sound Field

As anticipated in the previous chapters, the basis of the realization of a performing ANC system is the analysis of the sources on the vehicle that affect the acoustic field inside the cabin. In fact, the latter is composed of the combination of effects due to various causes that must be correctly catalogued in order to identify, then, those that have the greatest impact on sound levels and acoustic comfort in the driver's position. As explained in Chapter 2, the ANC algorithms are strongly dependent on the reference signals supplied to the controller and the general hardware and software characteristics of the system must be chosen based on the target components of the sound field to be attenuated. It should be remembered that the design of the ANC system has focused on reducing the noise propagated through the structure of the tractor (*structure-borne*) which can be modelled through appropriate accelerometric measurements on the structures of the tractor itself. This chapter describes the various *NVH* tests performed on the tractor model under study, in order to characterize the sources and the acoustic field in the cab on the basis of which to implement the ANC system. For this purpose, the signals obtained during these tests were analysed in order to obtain useful information.

3.1 Preliminary Vibroacoustic Measurements on Real Tractor

Chapter 1 lists what are usually the mechanical sources that affect the acoustic field on board the cab of a tractor. They are briefly shown below indicating, in brackets, the type of noise generated in terms of spectrum:

• Engine (tonal);

• Distribution pumps group (tonal);

• Rear wheel transmission reducer (tonal);

• Ground-tire interaction (low-frequency noise, broadband rolling noise);

• Exhaust (random broadband aerodynamic);

• Fan (random broadband aerodynamic).

Although the fixed objective of the ANC system to be implemented was to act more on tonal components, as can be seen, non-tonal sources were also considered, for the following two reasons: (i) not to exclude a priori the possibility of a broadband cancellation system (if necessary or more efficient) and (ii) being able to know all the main noise sources that make up the mix in the cabin, in order to possibly exclude them from the analysis.

For the purpose of the vibro-acoustic study of the tractor system, in the measurement sessions sensors were positioned near the sources listed above and acquisitions of the various signals were performed in correspondence with predefined operating conditions of the vehicle.

The positioning of the sensors took into account the following requirements:

- Acquire, for each source, at least one reference signal that could be a candidate to be effectively used also in the implementation phase of the ANC system and not only in the vibro-acoustic diagnosis phase;
- Acquire at least one microphone signal in the cabin in a position where it was actually possible to install the error sensor in the prototype phase;
- Acquire the signals "in the ears" of the driver in the cabin, from which it is possible to evaluate the effectiveness of the cancellation system.

With regard to the last point, a clarification is necessary. The active noise cancellation systems allow, using the speakers, to generate an "anti-noise" that adds up in phase opposition to that detected by the error microphone. The systems therefore do not actually perform the cancellation in correspondence with the ears, unless the error microphones are placed right in correspondence with them. The sound field in which the cancellation is effective is not punctual, but fortunately it corresponds to a bubble whose radius is a function of the cancelled frequency (the bubble decreases as the frequency increases). To have an effective cancellation, it is sufficient that the ears are positioned inside the aforementioned bubble. Therefore, having an error microphone close to the ears always remains a desirable condition, since it allows you to increase (upwards) the erasable frequency range.

During the research process, object of this work, two sessions of vibro-acoustic measurements were performed. The first with the aim of characterizing the tractor system in a general way in terms of sound sources. From the analysis of the data obtained from the first, a second session aimed to study in more detail the noise sources that have proved to be of interest in the development of the ANC system. This paragraph will describe the first preliminary characterization

session with the analysis of the results obtained. The second session, aimed at perfecting and confirming the results of the first, will be described in a subsequent paragraph.

The characterization of the noise sources required the simultaneous use of a large number of sensors. In fact, in measurements of this type, primary sensors that characterize the "cause", that is the source of the noise, and secondary sensors, that measure the "effect", that is the noise in the cabin following the propagation. The secondary sensors in the cabin are essentially microphones, while the primary sensors can be of various kinds: microphones, accelerometers or digital signals. The hardware setup of sensors and DAQ acquisition systems used in the first test session will be described below.

To begin with, six Brüel & Kjær (B&K) microphones, with nominal sensitivity 36 mV/ Pa (Figure 3.1), were placed in the cab on the perimeter of the cab ceiling positioned in relation to the driver as follows: *FrontLeft*, *FrontRight*, *CenterLeft*, *CenterRight*, *RearLeft* and *RearRight*. To these were added two binaural microphones (Figure 3.2) worn by the driver: it is a pair of microphones each placed inside an in-ear headset. This feature makes them the best error microphone in existence, but also obviously impractical. However, they allow for an excellent evaluation of performance, as they provide information right to the ears.

Figure 3.1: B&K measurement microphone with 4188 capsule and 2671 preamplifier

Figure 3.2: Roland CS-10EM binaural headphones

On the tractor structure, on the other hand, the following sensors were used:

- Two B&K measurement microphones: for picking up the noise emitted by the fan (Figure 3.3a) and exhaust mouth (Figure 3.3b);

- Four triaxial accelerometers were used to capture the vibrations generated by the engine, pumps, transmission and wheel unit. It should be noted that vibrations are the cause of noise and are even more important than acoustic sources: vibrations can in fact propagate structurally and generate noise even at a great distance from the source. The accelerometers used are Brüel & Kjær or PCB, both with power supply in ICP format (Figure 3.4) and having different sensitivities (10 mV/ g, 100 mV/g or 500 mV/g) to adapt them to the source to be measured. The fixing to the structure is done by gluing, with quick-setting cyano-acrylate adhesive (Fig. 3.5 for an example of fixing), after having treated the surface with degreaser and abrasive paper. Figure 3.6 shows the actual arrangement of the accelerometers on the group formed by the engine support, transmission and rear axle.

- Two phonic wheels acquired the digital signals about the speeds of the rear *Power Take Off* (PTO) and the rear tyres. From the transmission ratios between the various organs it is possible to obtain the information necessary for cancellation, without the use of any analog sensor: it is the best possible scenario of course. Compared to accelerometers, the phonic wheels do not give any amplitude information (how strong the vibration will be) but an almost perfect phase information.

Figure 3.3: Microphones that acquire signals at the fan (a) and the exhaust mouth (b) equipped with a windproof ball

Figure 3.4: ICP accelerometer (PCB)

Figure 3.5: Accelerometer glued to the structure

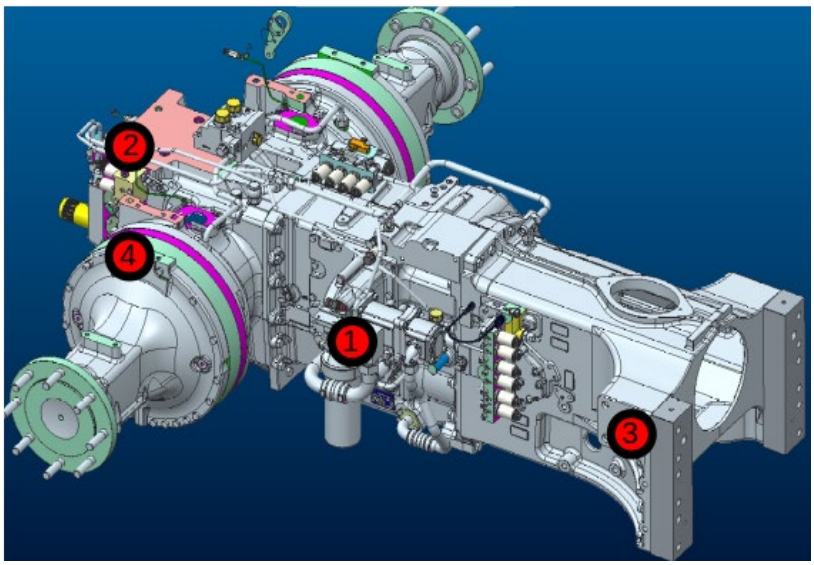

Figure 3.6: Installation of accelerometers for vibro-acoustic evaluation of the system: positioning

Inside the cabin, it was decided to also place a multi-channel spherical probe: the *Eigenmike32* (Figure 3.7). It is a microphone array consisting of 32 capsules arranged on a sphere of 84 mm in diameter: thanks to it, it is also possible to

acquire the spatial information of the sound field and then study the main sources of origin. For example, it allows us to understand if the sound enters for the most part from the glass, from the door seals that make poor sealing or from a structural one and is then generated inside the cabin by the floor panels.

Figure 3.7: Eigenmike32

The *Eigenmike* was positioned on a tripod in the center of the cabin, between the driver and the steering wheel and in such a way as not to obstruct the view and prevent safe maneuvers. To view the acoustic mapping correctly, it must be superimposed on a 360 ° background photo (Figure 3.8) of the mapped environment, taken in the same position in which the microphone array will then be positioned (i.e. keeping the optical and acoustic centers coincident). In this case, the panoramic camera used is a Samsung Gear 360 (Figure 3.9).

Figure 3.8: Samsung Gear 360.

Figure 3.9: Panoramic background for noise mapping

Four sound cards were used for the acquisition of all these sensors:

- Roland Studio Capture (Figure 3.10): 12 microphone and 4 line inputs, USB connection. Two of the 12 microphone inputs are high impedance (Hi-Z) and allow the acquisition of digital signals from the tone wheels. Two of the four line inputs are used for the acquisition of binaural headphone signals. To properly power the 10 microphone channels with the 48V phantom power supply, it was decided to disable the latter and use a specially designed external interface;

Figure 3.10: Roland Studio-Capture

- MetricHalo 2882 (Figure 3.11) 8 microphone inputs, FireWire connection;

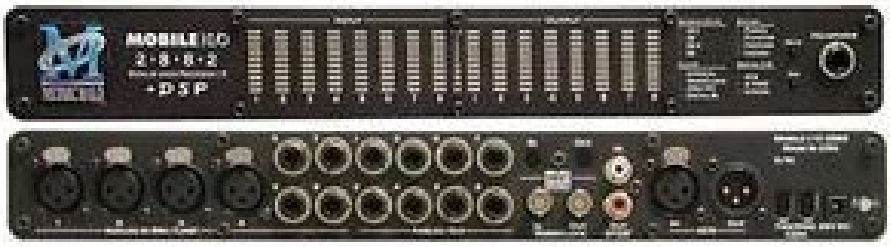

Figure 3.11: MetricHalo 2882

- Emib (Figure 3.12): interface for Eigenmike, FireWire connection;

Figure 3.12: interfaccia digitale Emib per Eigenmike32

- Zoom H4n (Figure 3.13): four microphone inputs and equipped with PiP power supply (*plug-in-power*), it allows powering the binaural microphones.

Figure 3.13: Zoom H4n

All cards have been set to the standard sampling frequency (f_s) for the audio band 20Hz-20kHz, i.e. fs = 48kHz. In order to consistently analyse the acquisitions of multiple sound cards working in parallel, these must also be clocked together, ensuring that they share the same f_s (master clock). To this end, the MetricHalo board has been set as the master. It shares the clock via digital SPDIF with Roland Studio Capture and via WordClock with the Emib.

Since two of the cards used have a FireWire connection, it was decided to use an Apple computer that has this interface. The MetricHalo and the Emib have been daisy chained as the FireWire link allows this. The native Apple audio driver allows you to simultaneously acquire the signals of multiple sound cards, creating a so-called "*aggregate device*": the three connected cards become a single virtual unit having the sum of the input and output channels of the units that compose it.

The final system (Figure 3.14) is therefore equipped with 12 accelerometric inputs (4 triaxial accelerometers), 6 B&K measurement microphones and two binaural microphones, 2 digital signals from the phonic wheels plus the 32 channels of the spherical array, for a total of 54 channels operating at 48kHz, 24 bit. The computer was equipped with SSD to be able to handle the huge real-time data flow. The acquisition software used is Plogue Bidule.

Figure 3.14: Complete acquisition system

The tests carried out, for each noise source subject to testing, will now be listed, describing the characteristic operating conditions of each test:

ENGINE:

- Measure 1: constant speed 40 km/h, fan ON;
- Measure 2: constant speed 50 km/h, fan ON.

WHEEL REDUCER (right side):

- Measure 1: constant speed 40 km/h, fan OFF, gear 5.6;
- Measure 2: constant speed 50 km/h, fan OFF, gear 5.6;
- Measure 3: constant speed 40 km/h, fan ON, gear 5.6;
- Measure 4: constant speed 50 km/h, fan ON, gear 5.6.

DISTIBUTION PUMPS GROUP:

- Series 1: stationary tractor, minimum flow:
  - Measure 1: engine revolutions 850 rpm;
  - Measure 2: engine revolutions 1250 rpm;
  - Measure 3: engine revolutions 1750 rpm;
  - Measure 4: engine revolutions 2250 rpm.

- Series 2: stationary tractor, standard flow
  - Measure 1: engine revolutions 850 rpm;
  - Measure 2: engine revolutions 1950 rpm;

- Measure 3: engine revolutions 2250 rpm.

TRANSMISSION:

- Measure 1: rear-wheel drive, constant speed 40 km/h, fan OFF;
- Measure 2: rear-wheel drive, constant speed 50 km/h, fan OFF;
- Measure 3: rear-wheel drive, constant speed 40 km/h, fan ON;
- Measure 4: rear-wheel drive, constant speed 50 km/h, fan ON;
- Measure 5: four-wheel drive (4WD), constant speed 40 km/h, fan OFF;
- Measure 6: 4WD, constant speed 50 km/h, fan OFF;
- Size 7: 4WD, constant speed 40 km/h, fan ON;
- Size 8: 4WD, constant speed 40 km/h, fan ON.

FAN:

- Series 1: Stationary tractor, maximum fan speed
  - Measure 1: engine revolutions 850 rpm;
  - Measure 2: engine revolutions 1250 rpm;
  - Measure 3: engine revolutions 1750 rpm;
  - Measure 4: engine revolutions 2250 rpm.

EXAUST PORT:

- Series 1: Stationary tractor, fan maximum speed
  - Measure 1: engine revolutions 850 rpm;
  - Measure 2: engine revolutions 1250 rpm;
  - Measure 3: engine revolutions 1750 rpm;
  - Measure 4: engine revolutions 2250 rpm.

After having described the setup and the series of tests carried out, we are now going to expose the results of an initial analysis of the collected data. In particular operating conditions of the system, which will be specified from time to time, the frequency analysis of the six microphone signals in the cabin was performed. The resulting spectra are reported. In addition, the corresponding noise maps obtained through the signals acquired by Eigenmike will be reported in order to try to map the acoustic sources.

- **Operating Conditions [1]: Tractor speed 40 Km/h, gear 5.6, fan ON:**

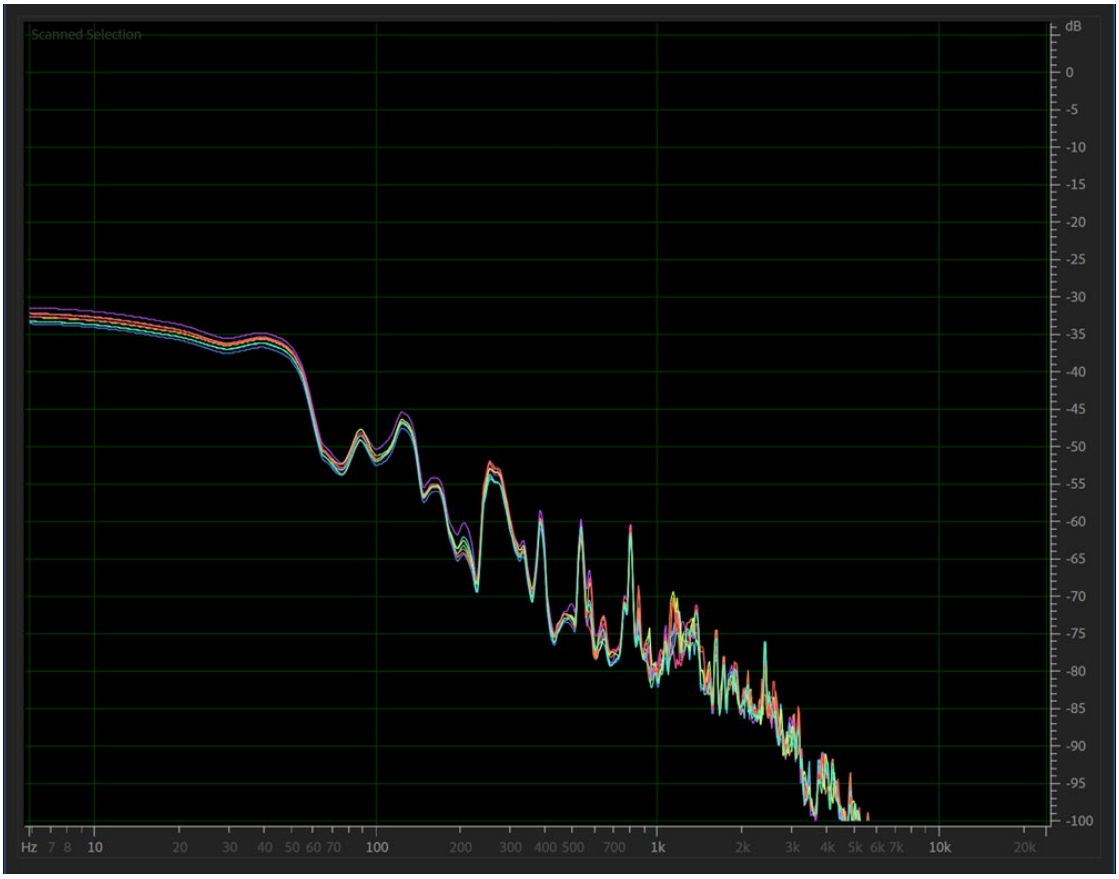

Figure 3.15: Spectra of microphone signals in the cabin, operating condition [1]

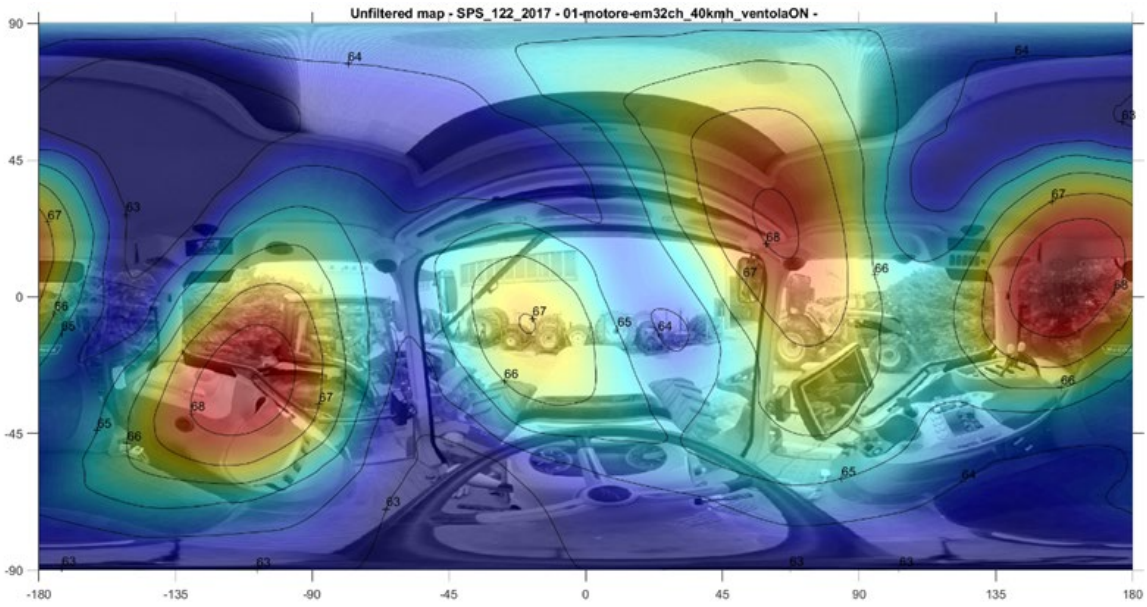

Figure 3.16: Unfiltered Acoustic Map, operating condition [1]

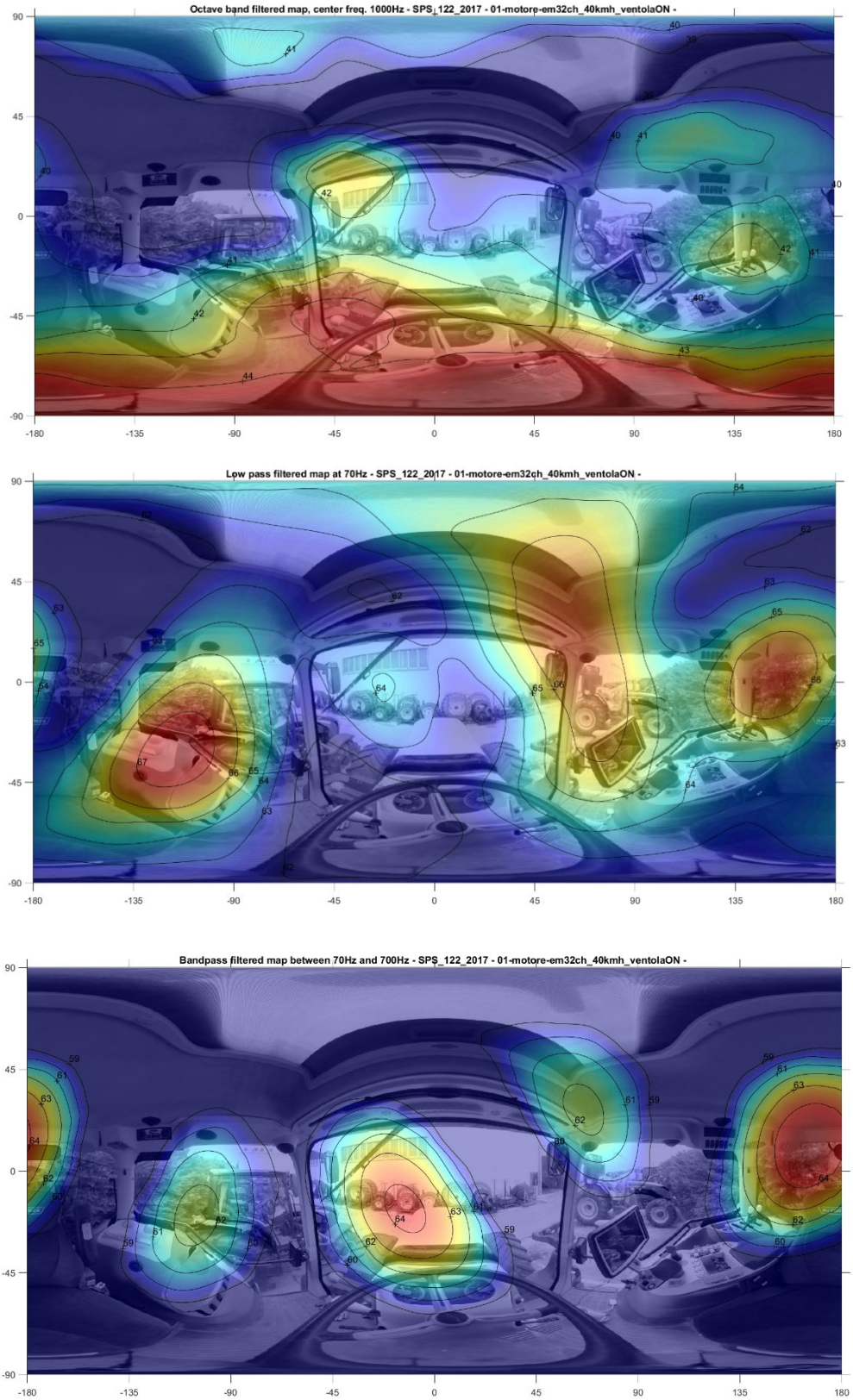

Figure 3.17: Operating conditions [1]: (from top to bottom) 1000 Hz center frequency octave band filtered map, low-pass 70 Hz filtered map and bandpass 70-700 Hz filtered map

➢ Operating Conditions [2]: Tractor speed 50 Km/h, gear 5.6, fan ON

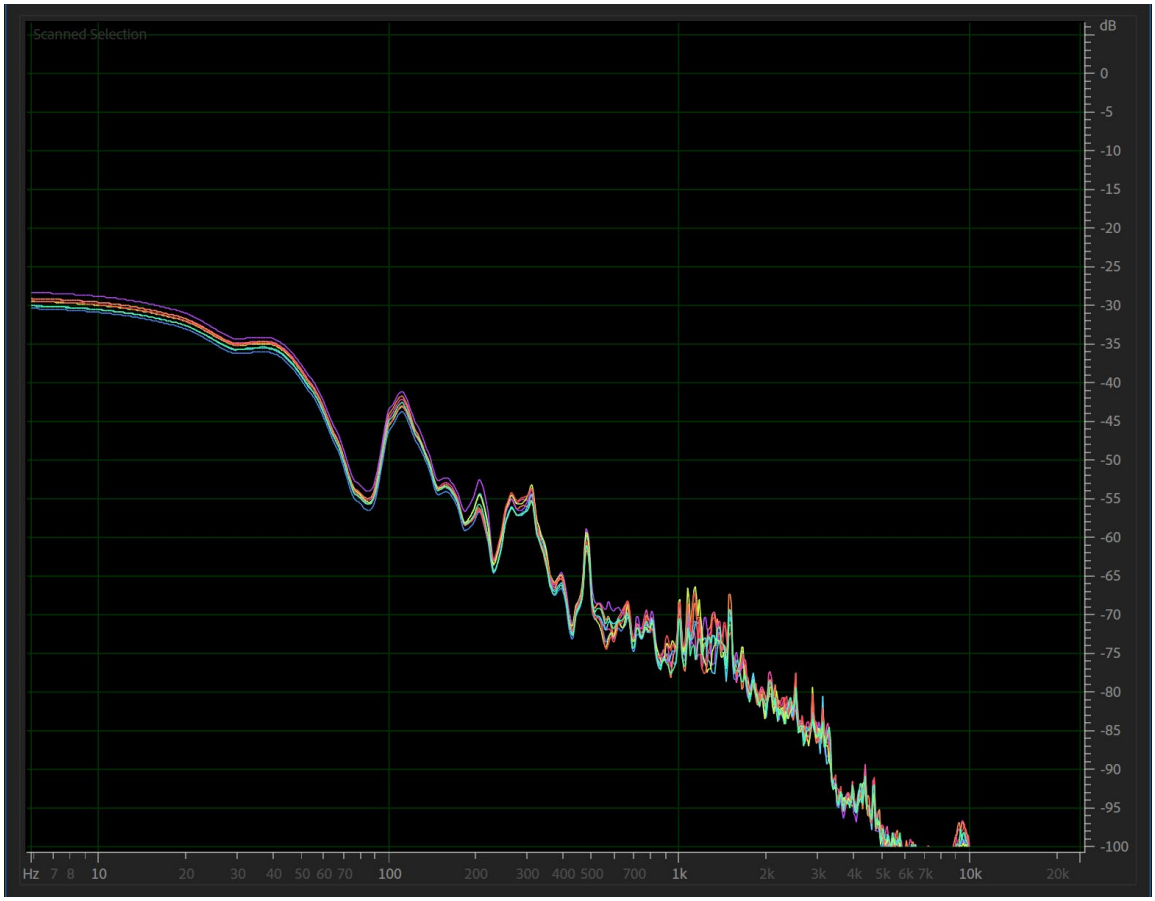

Figure 3.18: Spectra of microphone signals in the cabin, operating condition [2]

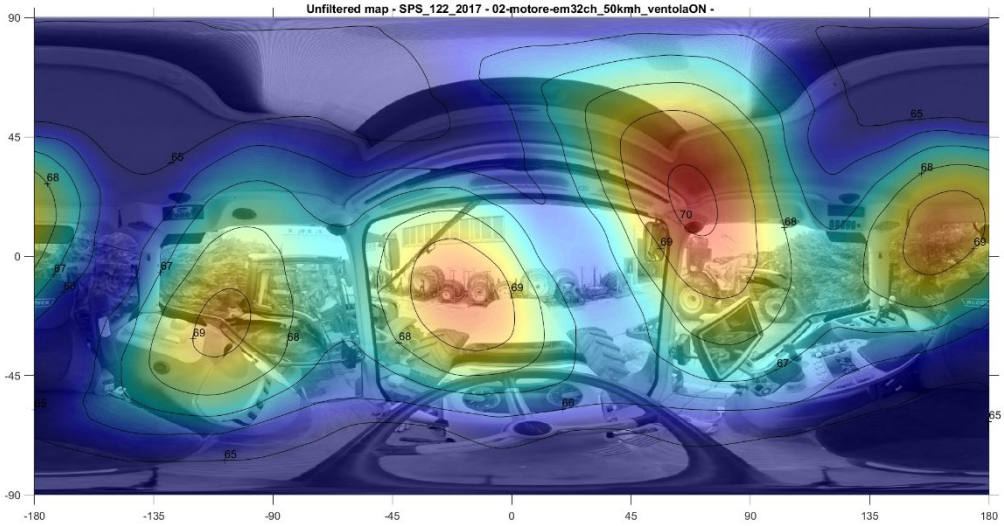

Figure 3.19: Unfiltered Acoustic Map, operating condition [2]

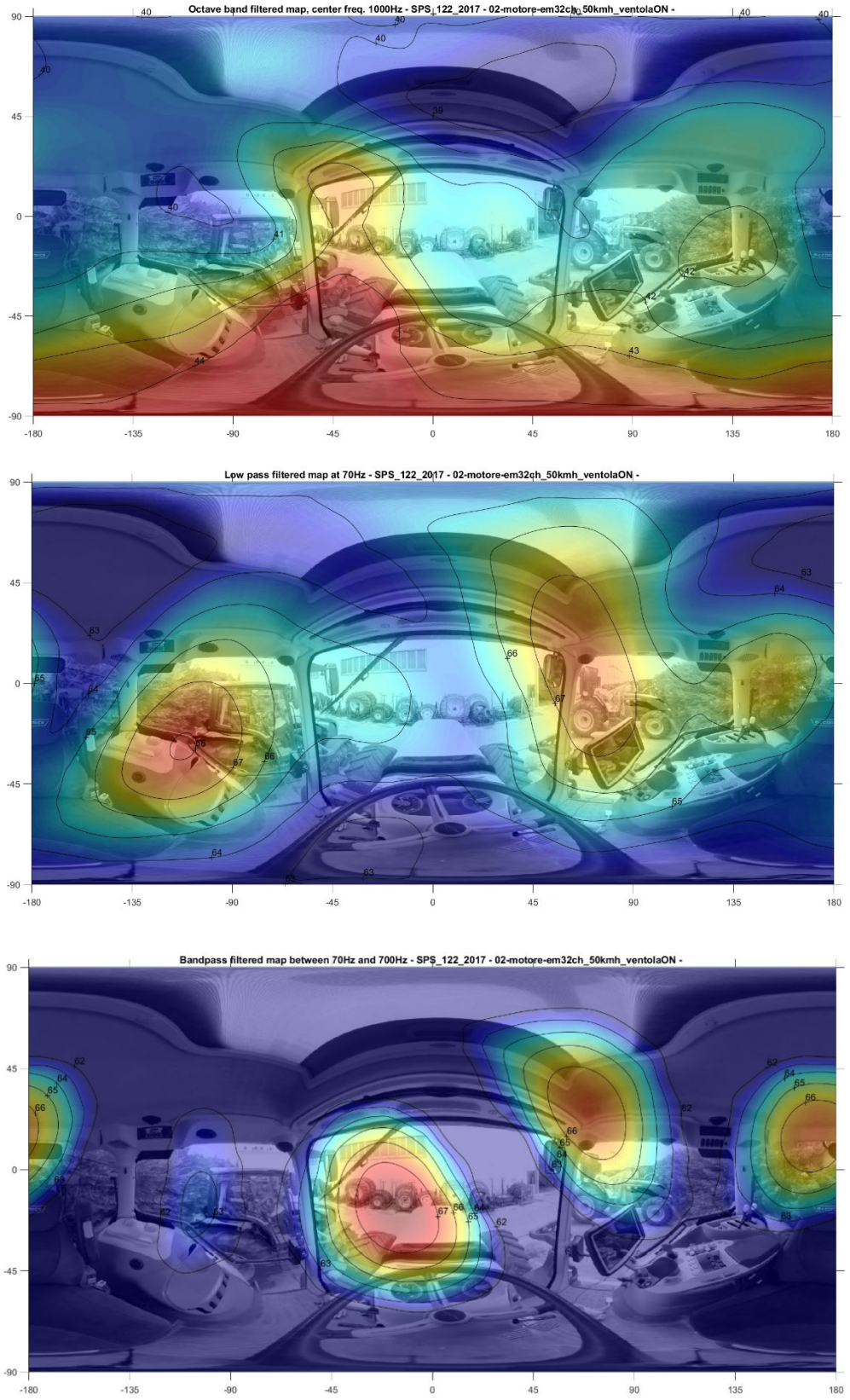

Figure 3.20: Operating conditions [2]: (from top to bottom) 1000 Hz center frequency octave band filtered map, low-pass 70 Hz filtered map, bandpass 70-700 Hz filtered map

- **Operating Conditions [3]: Stationary tractor, minimum pump flow, engine 850 rpm speed**

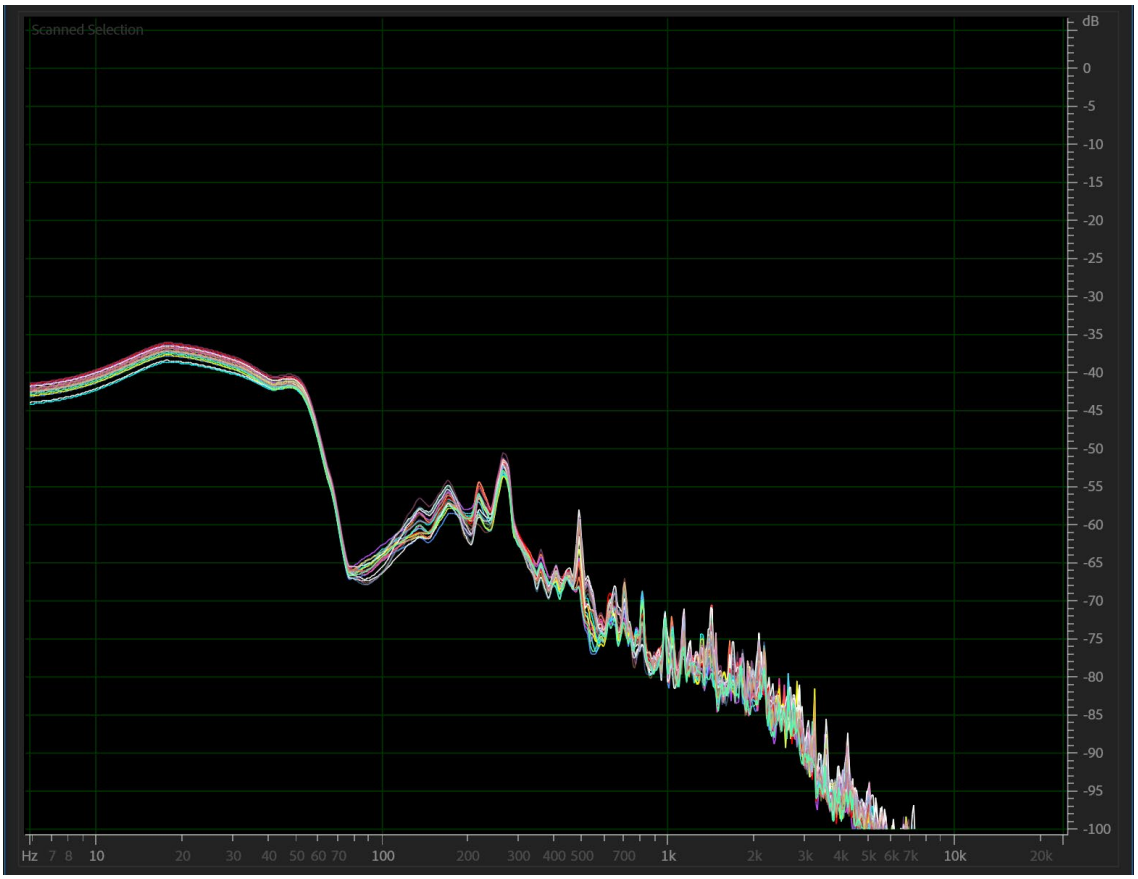

Figure 3.21: Spectra of microphone signals in the cabin, operating condition [3]

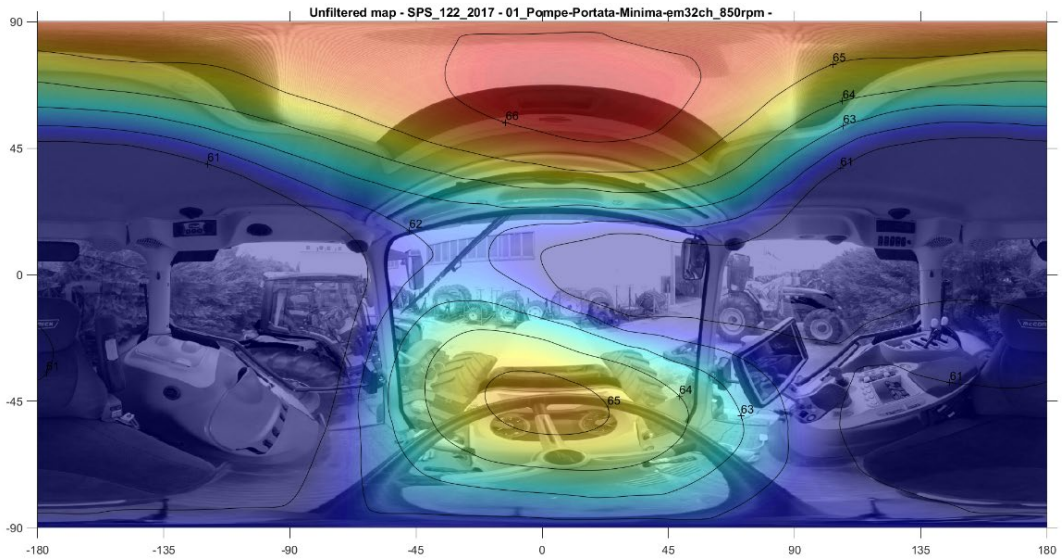

Figure 3.22: Unfiltered Acoustic Map, operating condition [3]

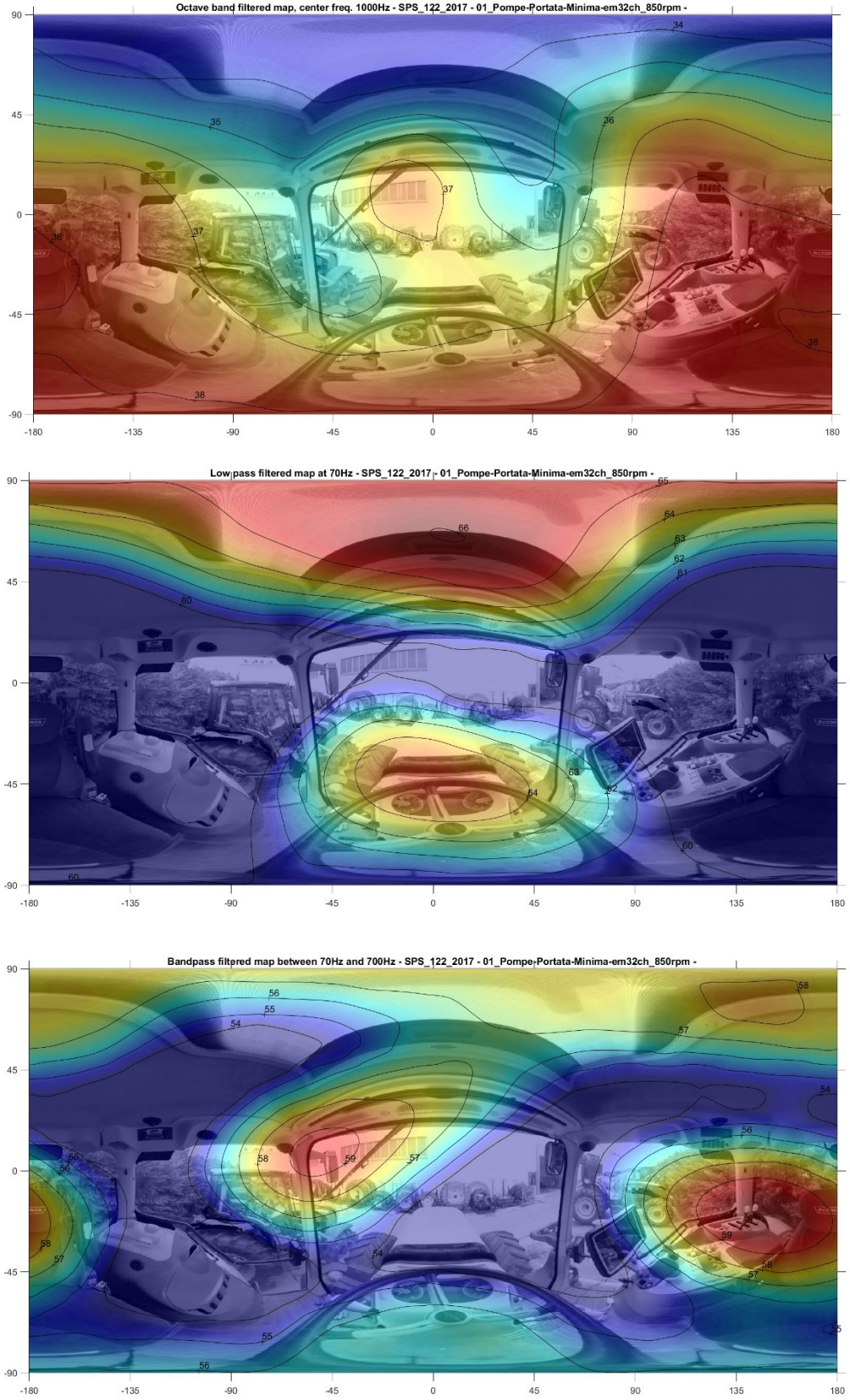

Figure 3.23: Operating conditions [3]: (from top to bottom) 1000 Hz center frequency octave band filtered map, low-pass 70 Hz filtered map, bandpass 70-700 Hz filtered map

- **Operating Conditions [4]: Stationary tractor, minimum pump flow, engine 2250 rpm speed**

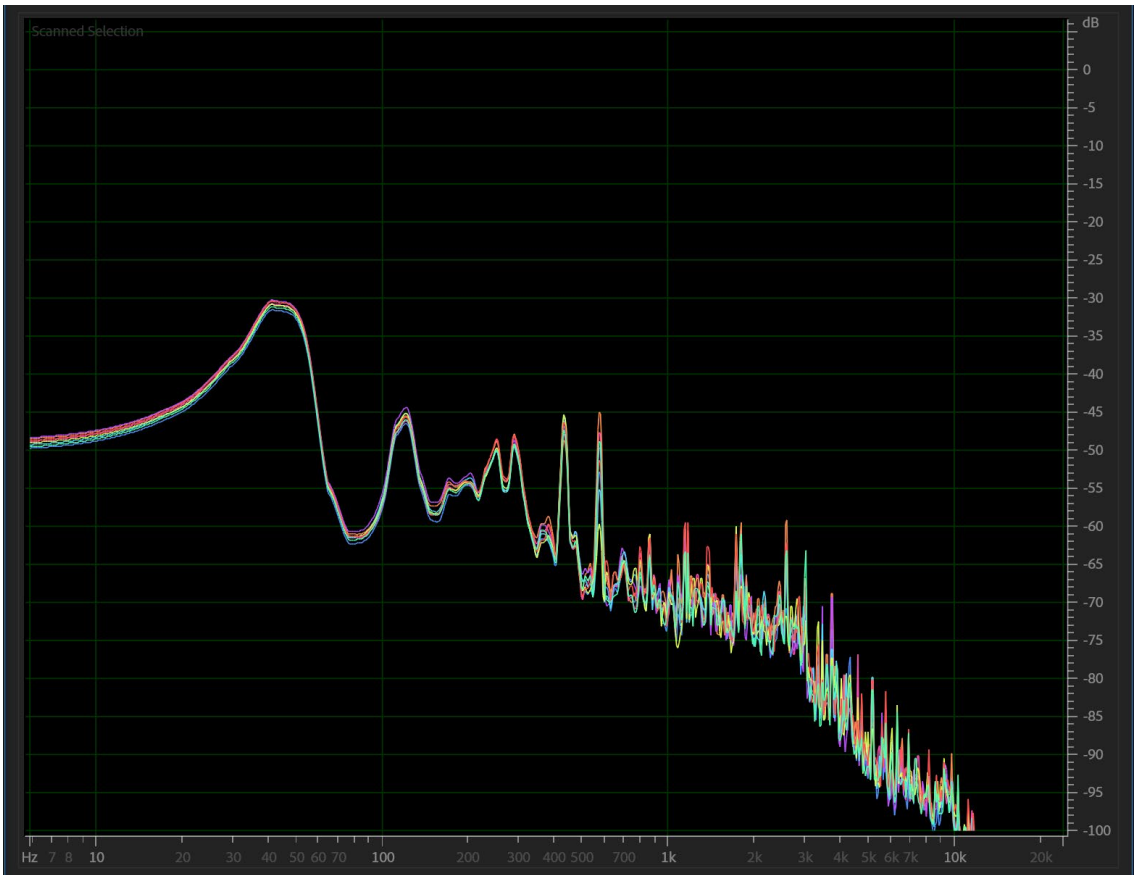

Figure 3.24: Spectra of microphone signals in the cabin, operating condition [4]

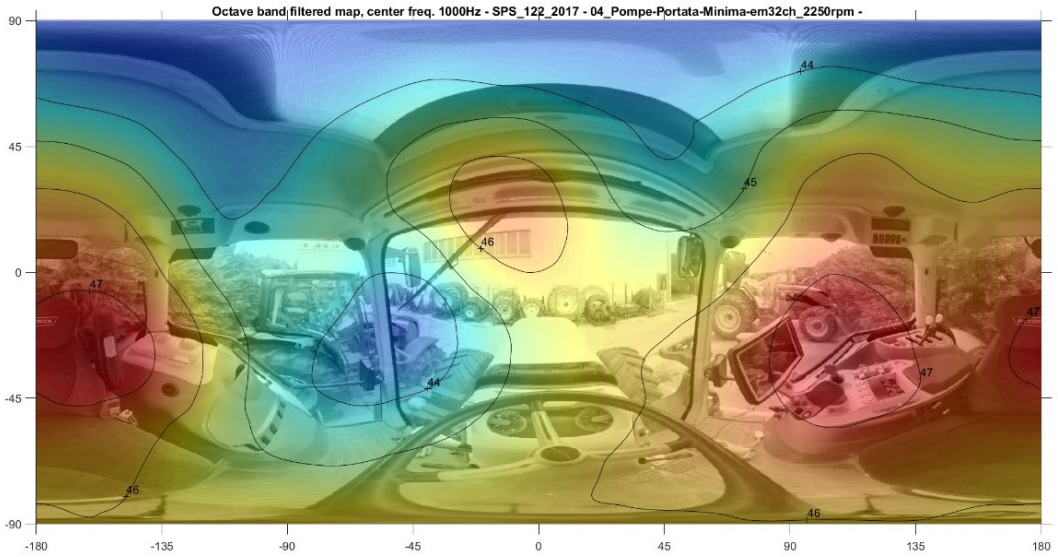

Figure 3.25: Unfiltered Acoustic Map, operating condition [4]

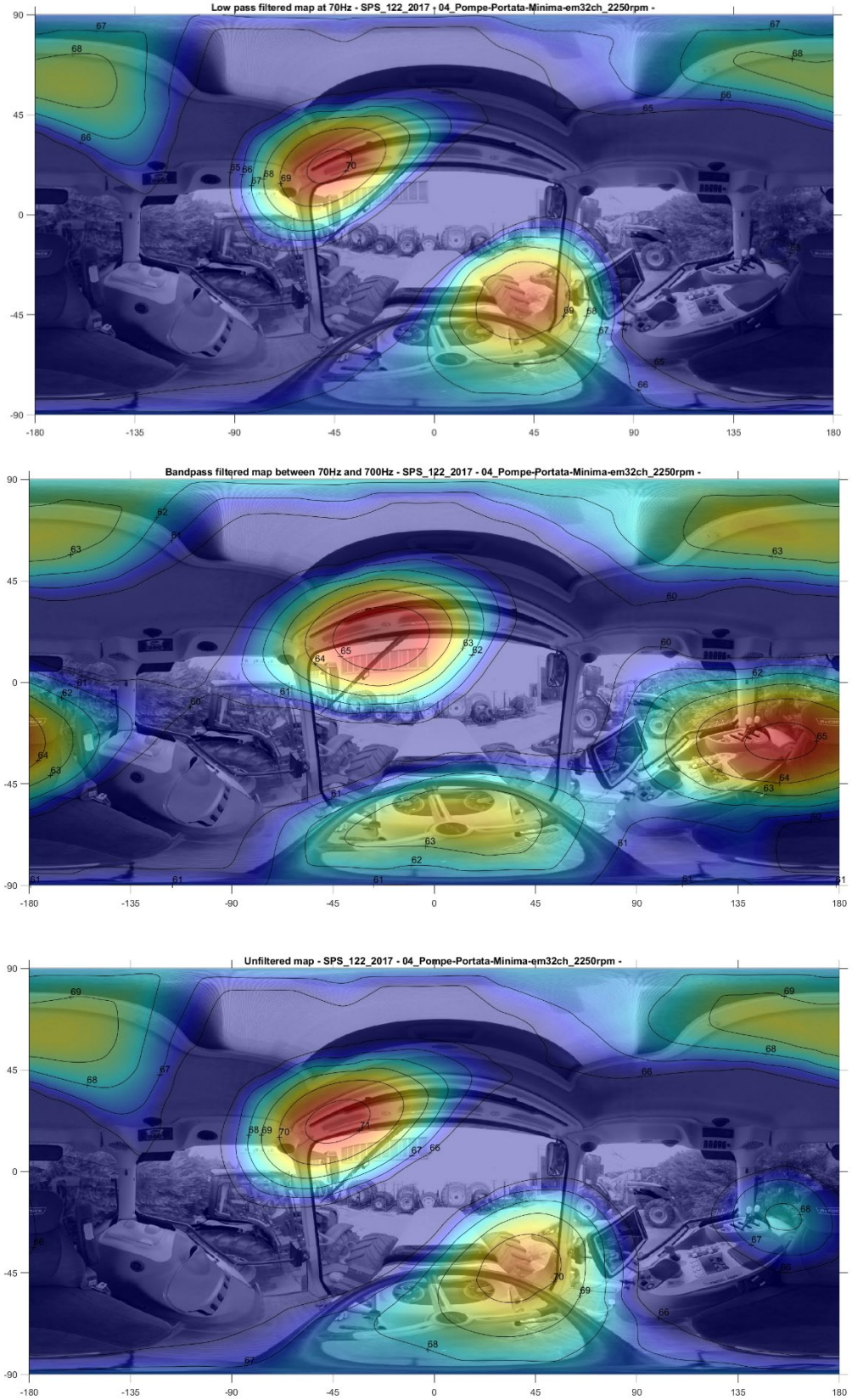

Figure 3.26: Operating conditions [4]: (from top to bottom) 1000 Hz center frequency octave band filtered map, low-pass 70 Hz filtered map, bandpass 70-700 Hz filtered map

- **Operating Conditions [5]: Stationary tractor, standard pump flow, engine 2250 rpm speed**

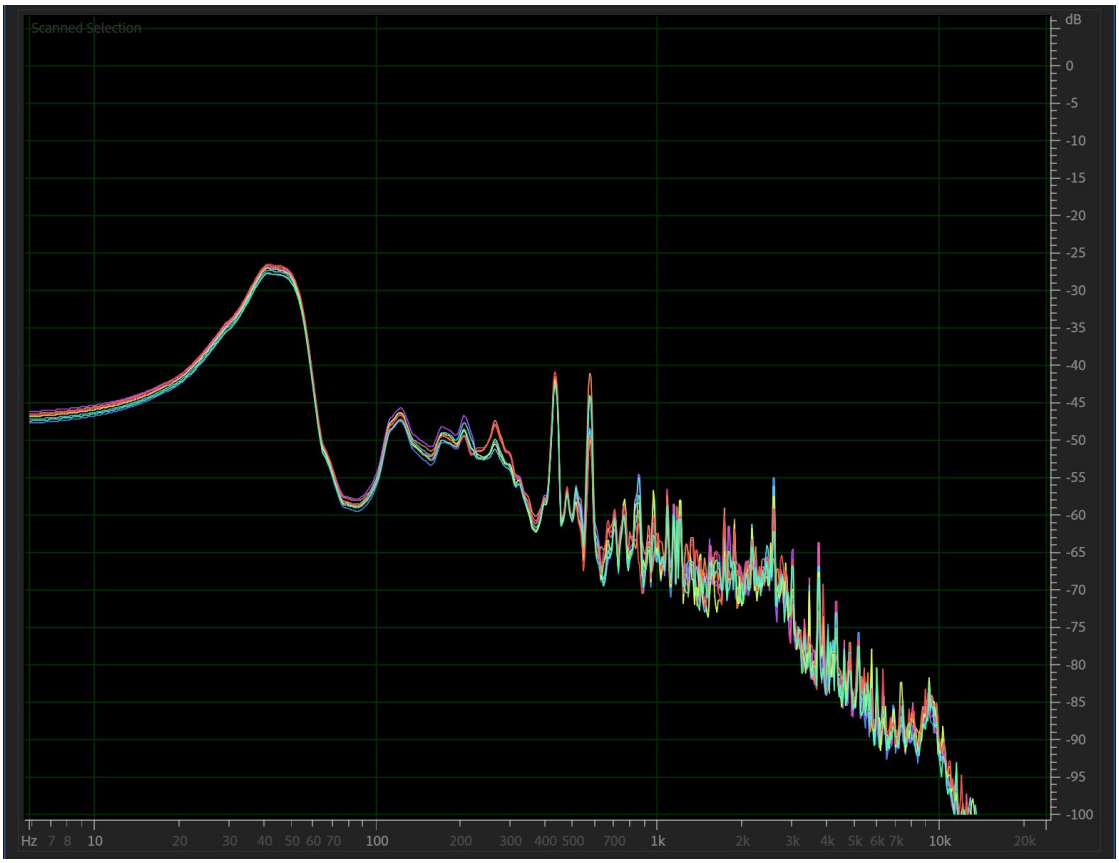

Figure 3.27: Spectra of microphone signals in the cabin, operating condition [5]

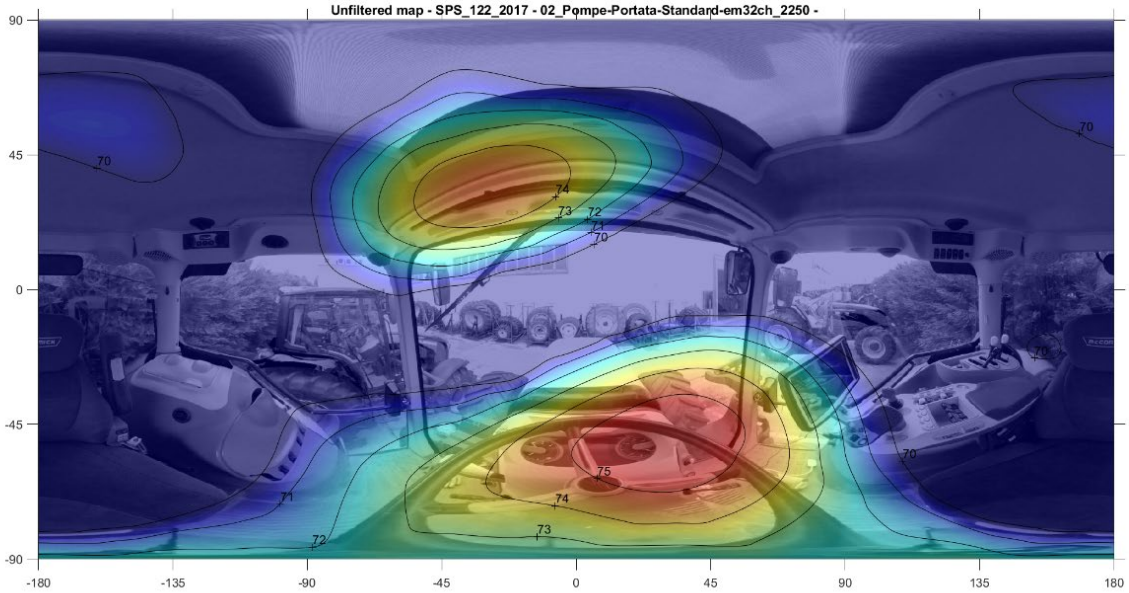

Figure 3.28: Unfiltered Acoustic Map, operating condition [5]

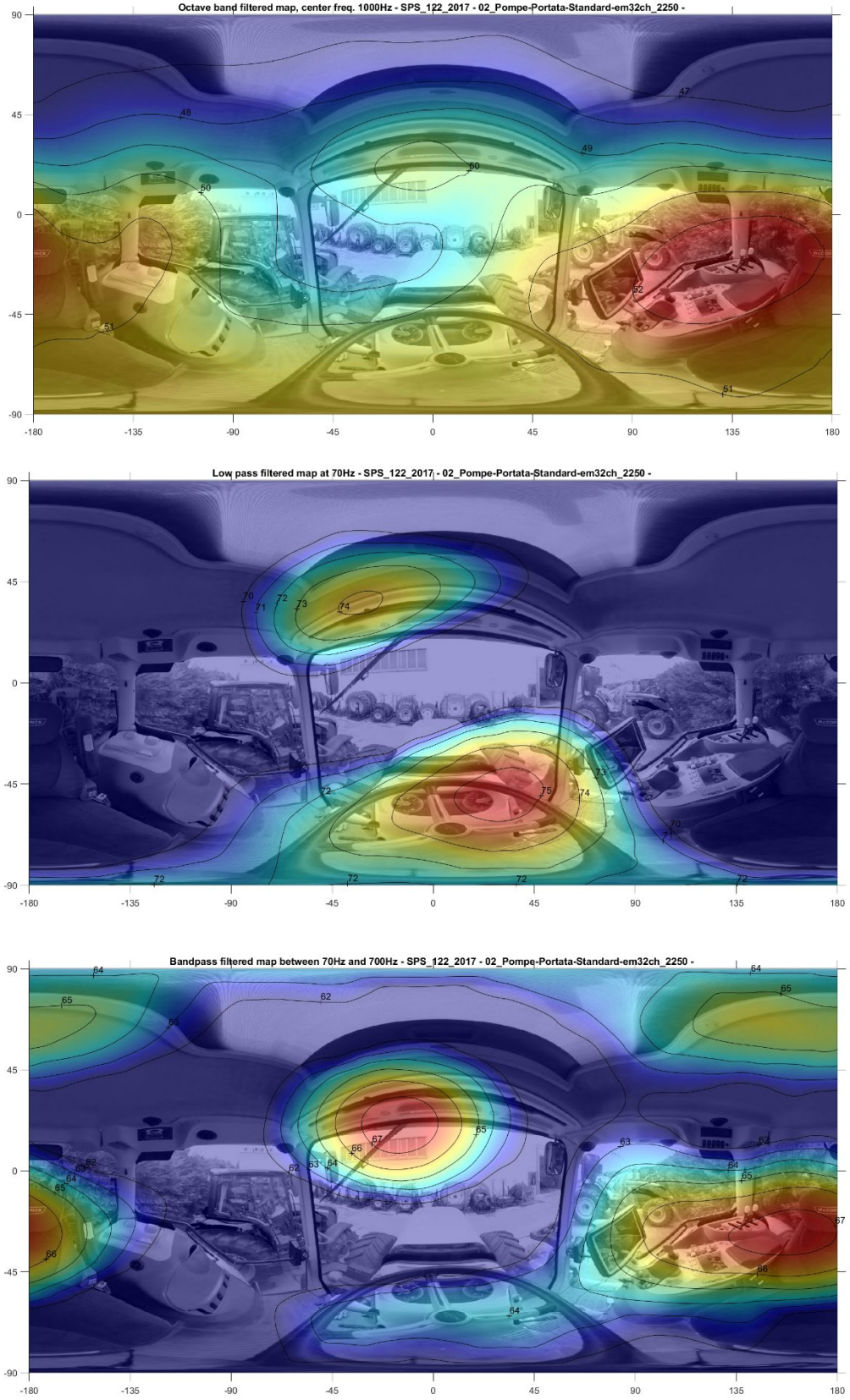

Figure 3.29: Operating conditions [5]: (from top to bottom) 1000 Hz center frequency octave band filtered map, low-pass 70 Hz filtered map, bandpass 70-700 Hz filtered map

3.1.1 Engine and Hydraulic System Impact.

In the setup described above, two phonic wheels measured the rotation speed of two specific mechanical parts of the tractor. A first wheel measured the speed of rotation of tires but it will not be analysed later in this work. The other wheel measured the rotation speed of the *Power Take Off* (PTO), that is, the coupling present in the rear part of the tractor where the tools (for example a seeder) are hooked. This information was collected by fixing a sensor to the side of the tractor PTO. The sensor considered for this operation is a *Hall effect* sensor which detects the variation of the magnetic field flux when a body made of ferro-magnetic material (metallic protrusion) approaches and moves away. In this case, the sensor measures the variation in the magnetic field created by the teeth or voids present in the PTO, which normally has six teeth. From the PTO rotation speed, it is possible to obtain the engine rotation speed by means of a simple proportionality formula, through a constant transmission ratio value.The knowledge of the rotation speed at which the engine is operating is important as many mechanical parts, which cause significant vibrations, are integral with the transmission. In addition, the engine rotations can be linked to the vibration frequencies (fundamental and harmonics) due to engine bursts according to the following relationship:

$$f_{k,burst} = k \cdot 3\frac{RPM}{60} = k \cdot 3 f_{engine} \qquad k = 1,2,\ldots. \qquad (3.1)$$

where *RPM* is the speed of rotation of the crankshaft in revolutions per minute, $f_{engine} = RPM / 60$ is the frequency of rotation of the engine and the factor 3 is due to the fact that the engine of the tractor is six cylinders which burst in groups of two at a time. For example, at 850 rpm engine speed correspond to f_{engine} = 14.17 Hz and $f_{1,\,burst}$ = 42.5 Hz.

The magnetic field modulation created by the teeth / voids in the PTO made it possible to measure the signal (over time) shown in Figure 3.31(a) for an example scenario where the engine rotated at 2250 rpm. It is possible to observe that the signal collected has a periodicity that is directly proportional to the number of revolutions of the engine since the PTO is directly connected to the main crankshaft. The proportionality factor is defined by the reductions that connect the shaft with the power take-off itself. In particular, the following relationship can be written between the rotation frequency of the engine f_{engine} and the rotation frequency of the PTO f_{PTO}:

$$f_{engine} = f_{PTO} \cdot K_{conv} \qquad (3.2)$$

where K_{conv} is the scaling factor sought. To empirically identify the value of the Kconv scale factor, a frequency analysis of the signal acquired on the PTO was conducted, considering the signal periodogram, as shown in Figure 3.31 (b). In this figure, the frequency at which the greatest peak is present corresponds to the PTO rotation frequency, while the other (lower) peaks correspond to its harmonics. Therefore, by analysing the periodogram for signals acquired for different constant *RPM* values, it is therefore possible to empirically derive this ratio, which is invariant to *RPM*. The values calculated for different RPM values are summarized in Table 3.1. Considering the average between the experimentally calculated values for each experiment, we obtain a conversion factor in (3.2) equal to *Kconv* = 0.1847.

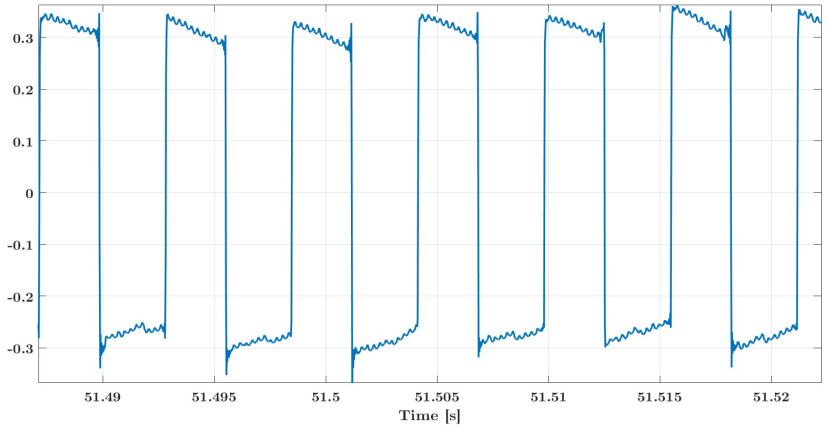

(a)

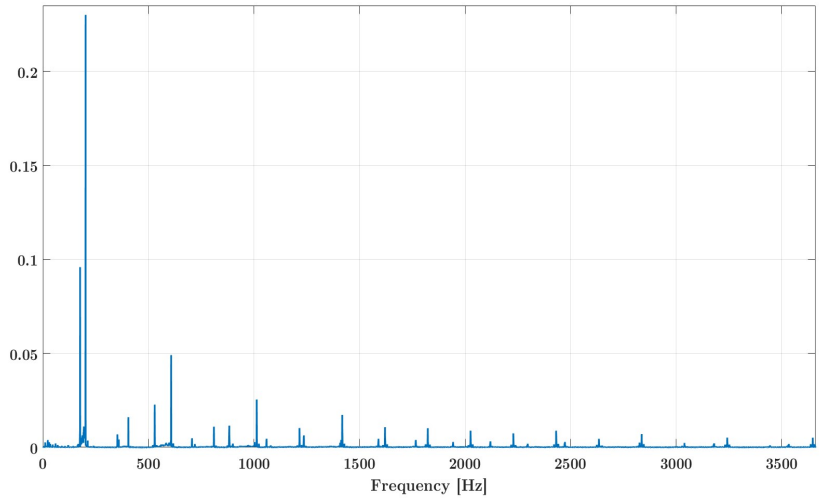

(b)

Figure 3.31: Signal measured by the Hall Effect sensor on the PTO for a scenario in which the engine is running at 2250 RPM: (a) signal over time and (b) its periodogram.

RPM [rpm]	f_{engine} [Hz]	f_{PTO} [Hz]	*Kconv*
850	14.666	76.5	0.1852
1250	20.833	113	0.1844
1750	19.166	158.1	0.1845
2250	37.5	202.9	0.1848

Table 3.1: Conversion factor for different RPM values.

Let us now consider the measures relating to the impact on noise in the cabin of the hydraulic distribution pump group, consisting of a Bosch axial piston pump and two rotary pumps (Bosch G Rotor).

In detail, the pump group is solidly connected to the transmission shaft through a reduction ratio K_{rid} = 1.2564 and is composed of a series of two rotary pumps with twelve teeth and a N_{pist}=9 pistons pump. The flow rate of this pump is regulated by a disc valve and, in the tests carried out, the pump was at both the minimum and standard flow rates. The frequencies (fundamental and harmonics) at which this pump should vibrate can be linked to the corresponding engine frequencies, and consequently to RPM, through the following relationship:

$$f_{pump} = K_{rid} \cdot N_{pist} \cdot f_{engine} = 11.3076 \cdot f_{engine} \qquad (3.3)$$

For example, at 850 rpm we have $f_{pump} \cong 160.19$ Hz.

After calculating the values of the fundamental and harmonic frequencies of vibration of the hydraulic system and of the engine bursts, it is possible to compare these values with the noise spectrum acquired in the cabin. This makes it possible to make the first connections between the noise sources on the tractor and the tonal peaks visible in the noise spectrum in the cab.

To obtain the spectrum of the noise signals recorded in the cabin, the following operating steps were applied:

• A signal pre-filtering has been applied using a *Butterworth* band-pass filter which filters the signals in the band between 10 Hz and 1 kHz. This filtering allows you to eliminate all those (potentially noisy) components well beyond the operating limits of the ANC system under development;

• FFT transforms have been calculated with $n_{FFT} = 215 = 32728$ points. Since the acquired audio signals were sampled at the frequency f_s = 48 kHz, it results

that the spectral resolution of the analysis is equal to f_s / n_{FFT} = 1,465 Hz as the periodograms are calculated only on the positive axis of the frequencies;

• *Welch's superimposed mean periodogram* method [15] is applied with (i) Hanning windowing, (ii) long signal segments $L = n_{FFT}$ samples, and (iii) overlapping windows with sliding equal to $n_{overlap} = n_{FFT} / 4$;

• The audio spectrum (in logarithmic scale) is further band-pass filtered to simulate the psychophysical signals processing by the human auditory system. This filtering is known as *A-filtering* and progressively decreases frequencies below 500 Hz. The frequency response of this filter is shown in Figure 3.32 and the corresponding spectrum is measured in dB_A.

• All results will be shown in the range between 80 Hz and 500 Hz, where the speakers are able to cancel well the noise highlighted in the audio signal.

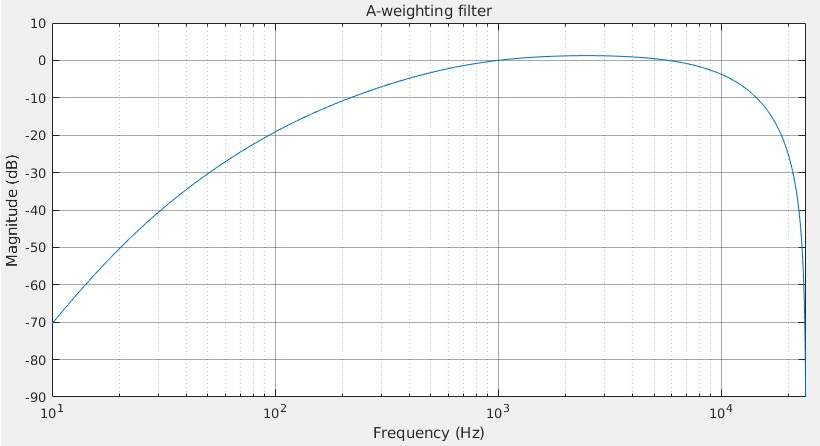

Figure 3.32: Frequency response of A-filtering.

As a preliminary analysis, let us now evaluate the spectrum of the audio signal for the two channels acquired in the binaural microphones during tests at different engine rpm values. The goal is to see if the engine burst and pump vibration frequencies, respectively predicted by the analytical expressions (3.1) and (3.3), are actually found in the audio signal. In Figure 3.33, these curves are shown for the different engine rpm values.

a)

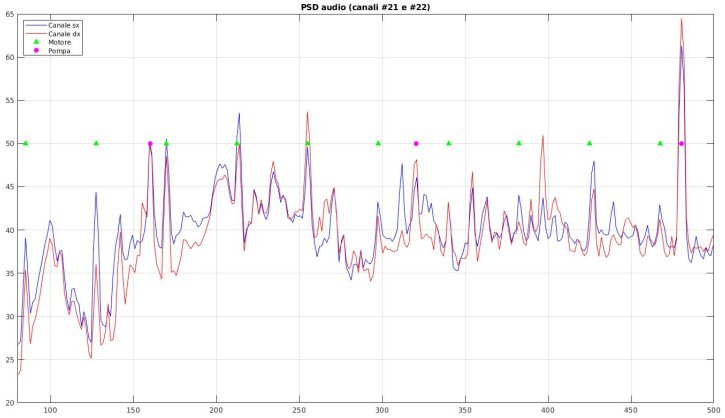

b)

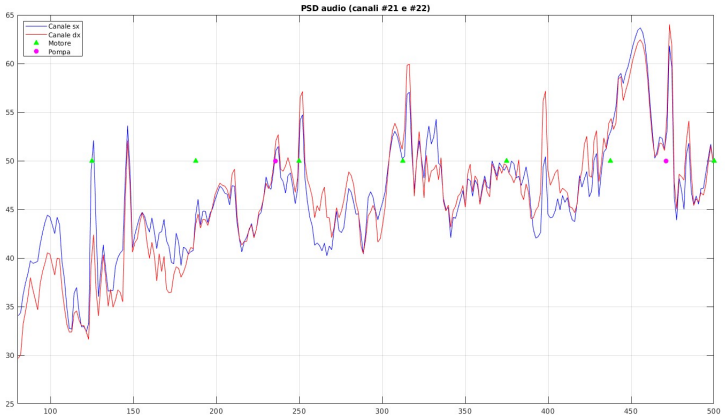

c)

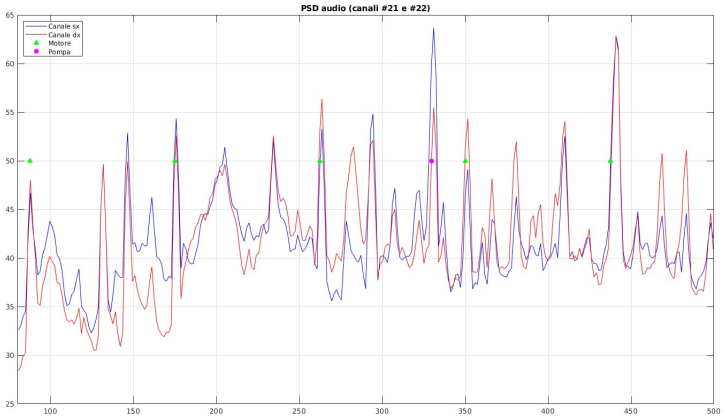

d)

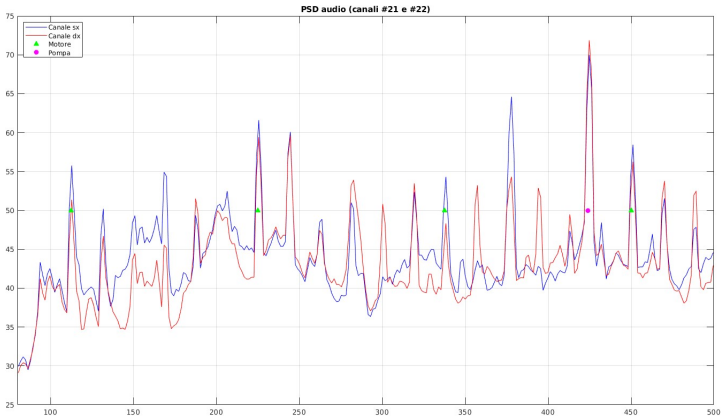

Figure 3.33: Spectrum of the audio signal for the two channels acquired in the binaural microphones during the tests at different rpm values: (a) 850 rpm, (b) 1250 rpm, (c) 1750 rpm and (d) 2250 rpm. As a comparison, the analytically calculated engine burst and pump vibration frequencies are shown.

First, it can be noted that in both channels the audio signal presents some significant power peaks at certain frequencies. It can also be seen how many of the peaks present in the audio signal can be traced back to the theoretically predicted frequencies for engine and pump. This would lead to the design of a tonal (*narrow-band*) ANC system, which operates in a very small neighbourhood of certain frequencies. However, the design of a tonal algorithm requires a very precise and stable phase reference over time, which is why the final choice fell on a *wide-band* ANC system, in which the cancellation is attempted on a wide band regardless of the presence or absence of tonal sound peaks. This system is more robust and versatile even in the presence of narrow band noise.

3.1.2 Coherence Analysis of Tractor Noise Sources

The objective of this paragraph is the derivation of vibro-acoustic indicators useful for identifying the correlation between vibrational sources and the sound level perceived in the cabin.

An acoustic system (such as a tractor cab) can be modelled as a linear time-invariant system which, given a number J of input signals $x_1(t)$, $x_2(t)$, ..., $x_J(t)$ (associated with the vibrations produced by mechanical parts and each measurable with an accelerometer), produces an output $y(t)$ (the noise perceived in the cabin) according to the relation

$$y(t) = \sum_{i=1}^{J} \mathcal{L}_i[x_i(t)] = \sum_{i=1}^{J} h_i(t) \otimes x_i(t)$$

Where $£i[\cdot]$ is the system's response to input $x_i(t)$ which can be characterized through its impulse response $h_i(t)$, being $\otimes$ the convolution operator.

Since in the environment of interest the noise signal $y(t)$ is obtained from the stimulus of different vibrational sources, it is of interest to understand how much this signal is related to a specific set of input signals $x(t)$, defined as:

$$\boldsymbol{x}(t) = [x_1(t), x_2(t), \ldots, x_J(t)]^T$$

where T is the transposition operator of a vector. *The (multiple) spectral coherence* between the input vector and the output can therefore be defined as [16] [17]:

$$C_{\boldsymbol{x}y}(f) = \frac{P_{\boldsymbol{x}y}(f)^{\dagger} P_{\boldsymbol{x}}(f)^{-1} P_{\boldsymbol{x}y}(f)}{P_y(f)} \tag{3.4}$$

where † denotes the Hermitian operator and

$$\begin{aligned} P_{\boldsymbol{x}y}(f) &= [P_{x_1,y}(t), P_{x_2,y}(t), \ldots, P_{x_J,y}(t)]^T \\ P_{\boldsymbol{x}}(f) &= \begin{bmatrix} P_{x_1x_1}(f) & P_{x_1x_2}(f) & \cdots & P_{x_1x_J}(f) \\ P_{x_2x_1}(f) & P_{x_2x_2}(f) & \cdots & P_{x_2x_J}(f) \\ \vdots & \vdots & \ddots & \vdots \\ P_{x_Jx_1}(f) & P_{x_Jx_2}(f) & \cdots & P_{x_Jx_J}(f) \end{bmatrix} \end{aligned}$$

In other words, $P_{xy}(f)$ represents the vector (of dimension J) having as elements the *Cross Power Spectral Density* (CPSD) between the generic component of the input vector and the output, while $P_x(f)$ is the matrix (of dimensions $J \times J$) having as a generic element the CPSD between pairs of components of the input vector. In particular, $P_x(f)$ contains on the diagonal the *Power Spectral Density* (PSD) of the input signals. For $J = 1$, equation (3.4) is reduced to the coherence between a generic input signal and the output:

$$C_{xy}(f) = \frac{|P_{xy}(f)|^2}{P_x(f) P_y(f)}$$

Coherence is a function of the frequency that can assume values in the interval [0,1]. In particular, $C_{xy}(f) = 0$ when the input vector is not correlated with the output.

In the case of high coherence, however, the output is determined by the input vector, so $C_{xy}(f) = 1$. Finally, the intermediate values $0<C_{xy}(f)<1$ are representatives of the following possible situations: (i) measurements are subject to noise; (ii) the function between inputs and output is not linear; (iii) the output signal also depends on other input signals.

The coherence of a linear system can be interpreted as the fractional part of the output signal power produced by the inputs at that frequency. We can also visualize the quantity $1 - C_{xy}(f)$ as an estimate of the percentage of the output signal power that is not deterministically caused by the inputs at frequency f. For this reason, it is possible to define the maximum cancellation theoretically obtainable by generating a signal perfectly in counter-phase at frequency f as follows:

$$\eta(f) = -10\log_{10}\left[1 - C_{\boldsymbol{x}y}(f)\right]$$

Since definition (3.4) is evaluated, dealing with signals of finite length, by calculating periodograms (which are estimates of the PSD), the coherence can be approximated by Welch's superimposed mean periodogram method [15]for discrete signals. In particular, this frequency estimate is based on the following method:

• The signal for which to calculate the PSD / CPSD is divided into long segments L samples;

• An appropriate window is applied to each segment to reduce edge effects;

• The segments are superimposed by an amount equal to $n_{overlap}$ samples, with typical $n_{overlap}$ values ranging from 50% to 75% of L;

• For each segment the Fourier transform is calculated by means of an L-point Fast Fourier Transform (FFT) algorithm (with L corresponding to a power of 2);

• The final periodogram is obtained as the average of those obtained for each segment.

The insight behind Welch's method consists in the fact that the PSD / CPSD of complex signals is sufficiently time-invariant to ensure that its estimates on partially overlapping segments of L samples are representative of the same "average" PSD / CPSD.

At this point, however, it is necessary to find out if the peaks to which the theoretical frequencies of the engine and pump (fundamental frequency and harmonics) can also be found in some accelerometric signal. This analysis allows us to understand if these peaks are actually due to the cause highlighted (engine or pump) and if the possible use of an accelerometer for the generation of an input signal to an ANC algorithm could be of interest: the analysis of illustrated consistency can help. In particular, an automatic method was sought that allows characterizing the coherence for all the possible recorded accelerometric channels. For this purpose, we can consider the coherent spectrum, defined as the product between the coherence function and the PSD of the audio signal (in dB_A), i.e:

$$\tilde{C}_{xy}(f) = C_{xy}(f)\left[P_y(f)\right]_{\mathrm{dBA}}$$

This definition allows emphasizing the coherence peaks where the PSD of the audio signal is high and, consequently, where it is theoretically possible to cancel a large amount of "noise". On the contrary, in $\tilde{C}_{xy}(f)$ the coherence peaks where there is little sound power to be canceled and the power peaks that can be cancelled but not coherent with the accelerometric signal are eliminated.

This quantity is shown for all the accelerometric channels considered from Figure 3.34 to Figure 3.37 for various configurations considered. For each accelerometric channel and frequency, a colour scale returns information on the intensity of the coherent spectrum, ranging from yellow (not very coherent spectrum) to red (very coherent spectrum). It can be seen that, in all cases, the spectrum is very coherent only at a few frequencies and most of them can be predicted from the theoretical frequencies (main and harmonics) of engine and pump. Furthermore, the use of 1-2 accelerometers allows you to identify the remaining frequencies that are not multiple of the fundamental frequency of engine and pump. In particular, the best positions for these sensors should be those labelled 1 and 2 in the tests analysed here. These positions correspond to the pump itself and under the cab at the rear right. The latter is close to the pump group and solidly connected to it. In any case, the accelerometer 4 seems to provide a signal that is much uncorrelated with the acquired audio signal.

Observe how, based on the previous considerations, the main frequencies with high noise power to be cancelled and high coherence with the analysed accelerometers could be automatically extracted. For this purpose it is sufficient to extract from the coherent spectrum, the frequencies at which the coherence is sufficiently high, that is, the frequencies for which $\tilde{C}_{xy}(f) > \tau$, being τ an appropriate threshold.

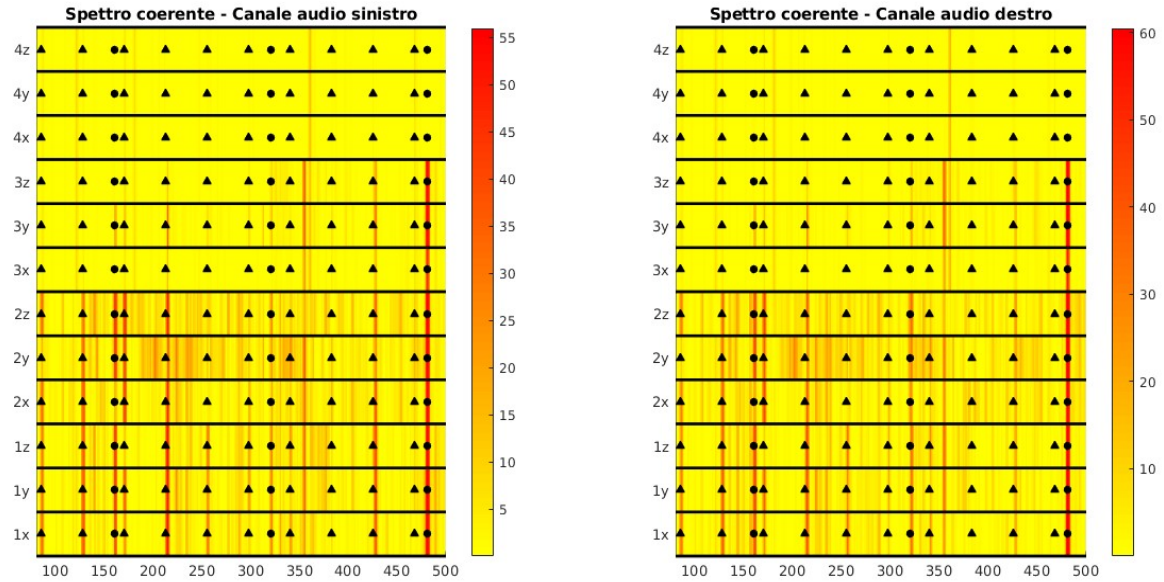

Figure 3.34: Coherent spectrum for the two channels acquired by the binaural microphones during the tests at 850 rpm. As a comparison, the engine burst (triangles) and pump vibration (squares) frequencies, analytically calculated, are shown.

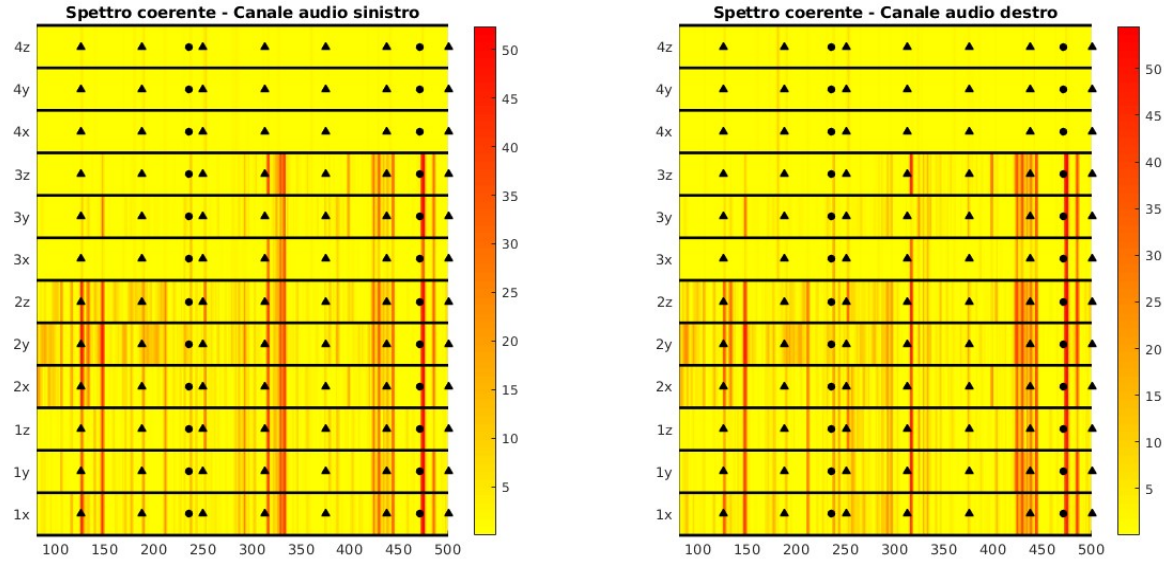

Figure 3.35: Coherent spectrum for the two channels acquired by the binaural microphones during the tests at 1250 rpm. As a comparison, the engine burst (triangles) and pump vibration (squares) frequencies, analytically calculated, are shown.

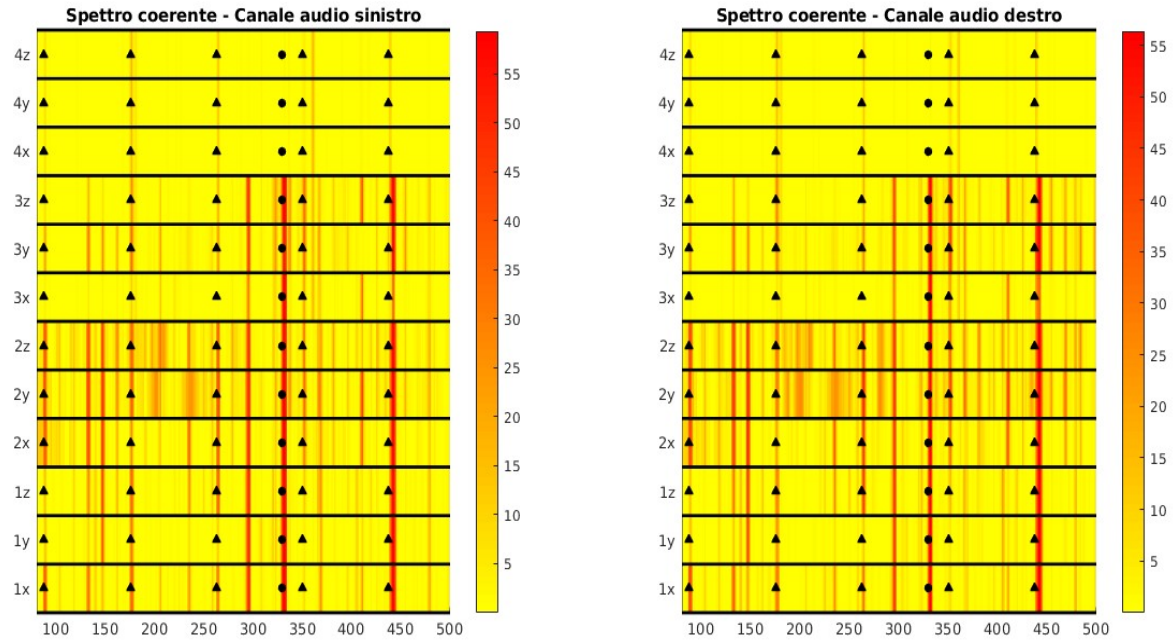

Figure 3.36: Coherent spectrum for the two channels acquired by the binaural microphones during the tests at 1750 rpm. As a comparison, the engine burst (triangles) and pump vibration (squares) frequencies, analytically calculated, are shown.

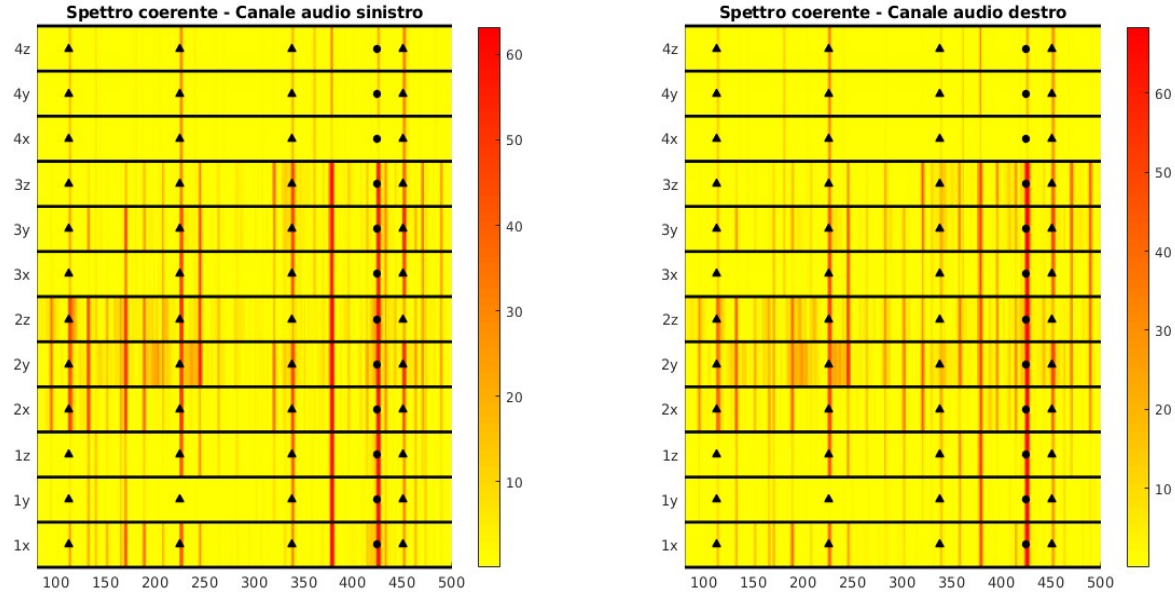

Figure 3.37: Coherent spectrum for the two channels acquired by the binaural microphones during the tests at 2250 rpm. As a comparison, the engine burst (triangles) and pump vibration (squares) frequencies, analytically calculated, are shown.

3.2 Targeted Vibro-acoustic Measurements on Real Tractor

From the results of the analysis conducted downstream of the first general session of vibro-acoustic measurements, a second series of acquisitions was planned on board a real tractor with the aim of studying in a more targeted way the noise sources that have proved to be more suitable to guide the development and performance analysis of the ANC system. From the analysis described in the previous chapter, it was established that the cancellation algorithm must operate in broadband mode, trying to cancel mainly the harmonics produced by the engine, the hydraulic system and the transmission reducer to the rear wheel. The accelerometric signals at the sources, acquired during the measurement session, will then be used in the test phase, described in Chapter 5, of the ANC system.
Compared to the first session, the number of acquired signals has been reduced by arranging the sensors only in the ideal positions for cancellation deduced from the previous analysis. Three series of measurements were carried out on a straight stretch of road (800m) with smooth asphalt:

• Series 1: Constant speed 25 km/h, gear 4.4;

• Series 2: Constant speed 40 km/h, gear 5.4;

• Series 3: Constant speed 50 km / h, 6.4 gear.

For each series of measurements, four consecutive repetitions were carried out, acquiring only the stretch at constant speed and thus excluding the acceleration and braking transients. In this way it is possible to have for each series a single track lasting about 120 seconds, sufficient to send the cancellation algorithm to convergence and carry out listening tests (first *off-line* and then *real-time*).

3.2.1 Measurement Setup

Five *B&K* 4188 type microphones with 2671 preamplifier and 31.6 mV/Pa sensitivity were used in the cabin. With these microphones, we wanted to evaluate the possible positions in which to place the error microphones of the ANC system being designed. Three microphones were arranged as follows:

- Central front position at the top (Figure 3.38): this microphone has been placed in correspondence with the microphone of the *Bluetooth* hands-free communication system already integrated in the current cabin. The position is the least favourable as it is the farthest from the driver's ears, but it is probably the one that would have required the least engineering effort as a microphone is already present there;

- Central position above the head (Fig. 3.39): this position would have required some effort to engineer the positioning in the center of the imperial, but does not involve particular complications as the space is large and free. Therefore a compromise solution.
- Position at the bottom, in the middle, behind the head: here the microphone has been placed under the nape of the neck, in a position where it could be integrated into the headrest of the seat. This would have been the most complex solution, but it is also the one that brings the microphone as close as possible to the ears, allowing the range of frequencies in which noise can be actively cancelled to be extended upwards.

Figure 3.38: Front microphone near the Bluetooth speakerphone

Figure 3.39: Microphone in the center above the head

The binaural headphones have been replaced by a standard solution widely adopted in the automotive field: a pair of "horns" protruding towards the driver's ears and each bearing a microphone at about 50 mm from the ear. This way the microphones are close enough to the driver's ears but not too close to prevent head movement safely during manoeuvres. Thanks to this solution, the measurements are compatible with those of the other microphones. Furthermore, the positioning is fixed, separated from the oscillatory movements and rotations performed by the driver's head during the measurement. Usually these supports are fixed to the headrest, not present here. For this reason, a special support has been created with various degrees of freedom for all adjustments (Figure 3.40).

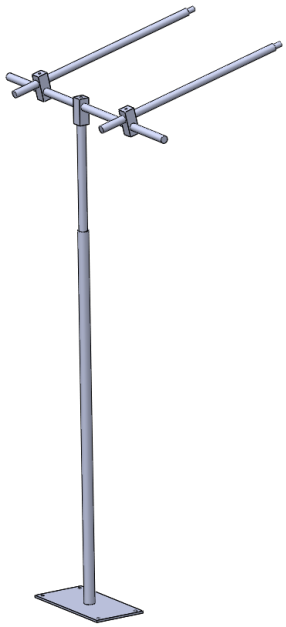

Figure 3.40: Support for cancellation evaluation microphones

For the accelerometric acquisition, three ICP triaxial accelerometers with a sensitivity of 10 mV/g were used. They, in accordance with the results of the analysis of the previous series of measures, were respectively positioned on:

- Pump group;
- Engine support;
- Planetary reduction gear of the right rear wheel.

Finally, during the recordings, the following three digital signals were also acquired:

- Hall sensor on phonic wheel 54 teeth integral with PTO;
- Optical Taco sensor on crankshaft;
- CAN bus.

In this second series of measurements, a DeweSoft SIRIUS acquisition system (Figure 3.41) was chosen in two overlapping modules of eight channels each.

Figure 3.41: 8 Channels DeweSoft Sirius

The two modules were synchronized by means of a special cable and controlled together by a PC on board the tractor,

Microphone signals were acquired with f_s =50 kHz, accelerometer signals with f_s = 25 kHz and digital signals with f_s=100 kHz.

3.2.2 Recordings Analysis

It is now important to analyse the vibro-acoustic characteristics of the acquired signals in order to properly drive the ANC system, the project of which will be described in Chapter 4. The analysis of the audio spectrum and of the coherence with the accelerometric signals will be shown below, using a methodology analysis similar to that described in the previous sections. The audio tracks are pre-processed in order to exclude any "dirty" portions that would affect the analysis.

In Figure 3.42, the average audio spectrum measured in the cabin is shown for the three speeds considered (25, 40 and 50 km/h) and the following microphones: (a) channel 1, (b) channel 2 and (c) channel 8. The three microphones indicated have been considered as channels 1 and 2 are representative of the sound spectrum to be deleted (i.e. the one in the driver's ears), while channel 8 is of potential application interest as in the same position there is already a microphone (that of the Bluetooth speakerphone) which could also be reused for ANC purposes. First, we can observe the different behaviour of the sound spectrum at the two ears; this result is due to the asymmetries of the cabin that lead to a different auditory perception on both sides. Some significant peaks at

medium-high frequencies (approximately above 200 Hz) present at all speeds can be highlighted. Being independent of this parameter, it is reasonable to think that these peaks can be linked to a specific vibration of the mechanical structure, independent of the engine speed. There is also a significant peak around 100 Hz, due to the *booming* effect in the cabin. Finally, once a speed has been set, the spectrum of channel 8 has peaks that can also be partially found in the two reference channels (1 and 2), confirming the potential usefulness of this microphone.

Let us now analyse the coherence of the audio signal with the six accelerometric signals (monoaxial) available from the measurements, focusing in particular on audio channel 1 (left binaural microphone). The theoretical cancellation η obtainable on the audio in channel 1 with the different accelerometric references is shown for the three constant speeds considered in the experiments: 25 km/h (Figure 3.43), 40 km/h (Figure 3.44) and 50 km/h (Figure 3.45). It can be observed that in all cases the references 1-3 (accelerometer on the tire reducer) provide high potential cancellations (about 6-7 dB) on the two peaks around 400 Hz. References 4-6 (accelerometer on the hydraulic system) seem to be potentially useful for the cancellation of peaks at lower frequencies (around 300 Hz). In chapter 5, these recorded accelerometric signals will be used to stimulate the cabin on which the final prototype of the ANC system will be tested through electromagnetic shakers.

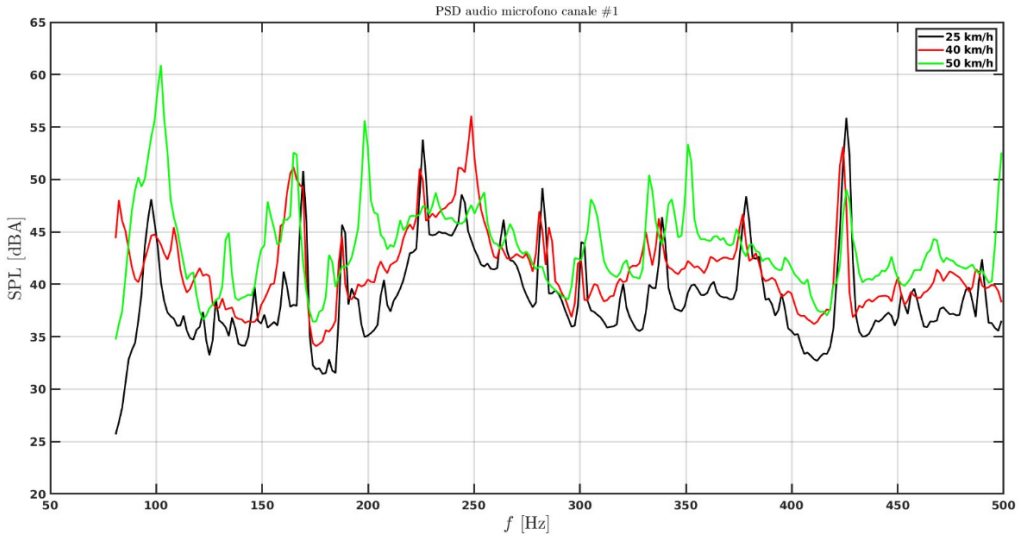

(a)

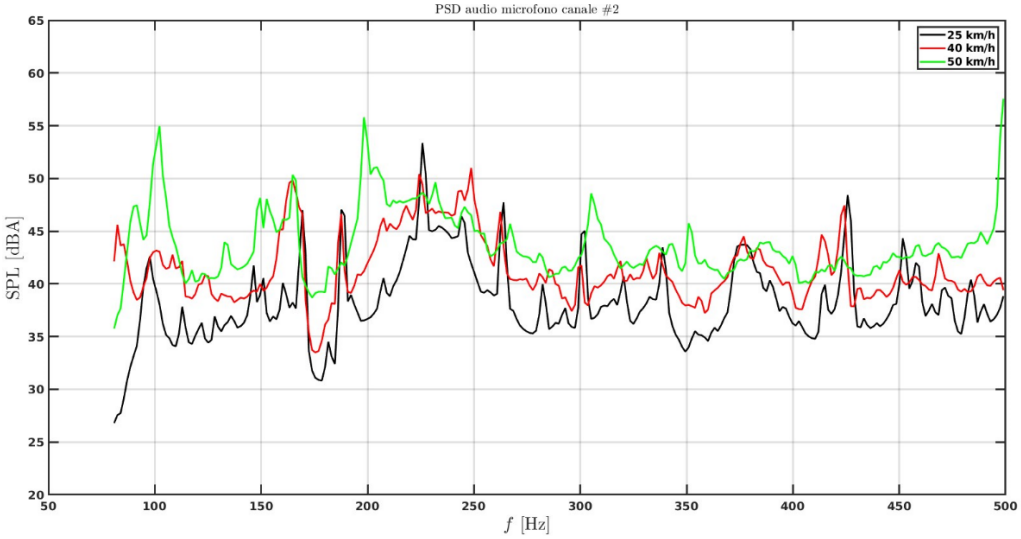

(b)

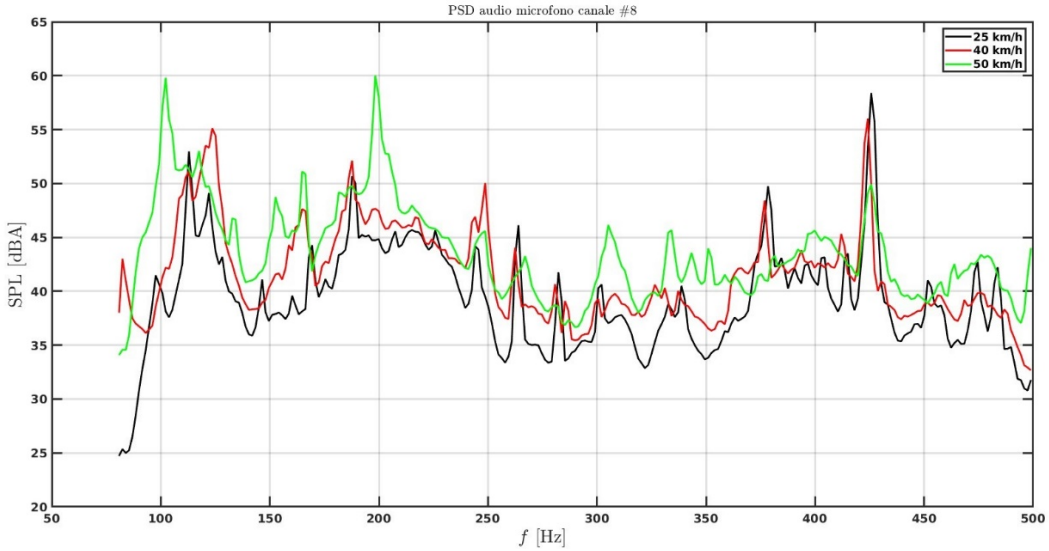

(c)

Figure 3.42: Audio spectrum for the three speeds considered (25, 40 and 50 km/h) and the following microphones: (a) channel 1, (b) channel 2 and (c) channel 8.

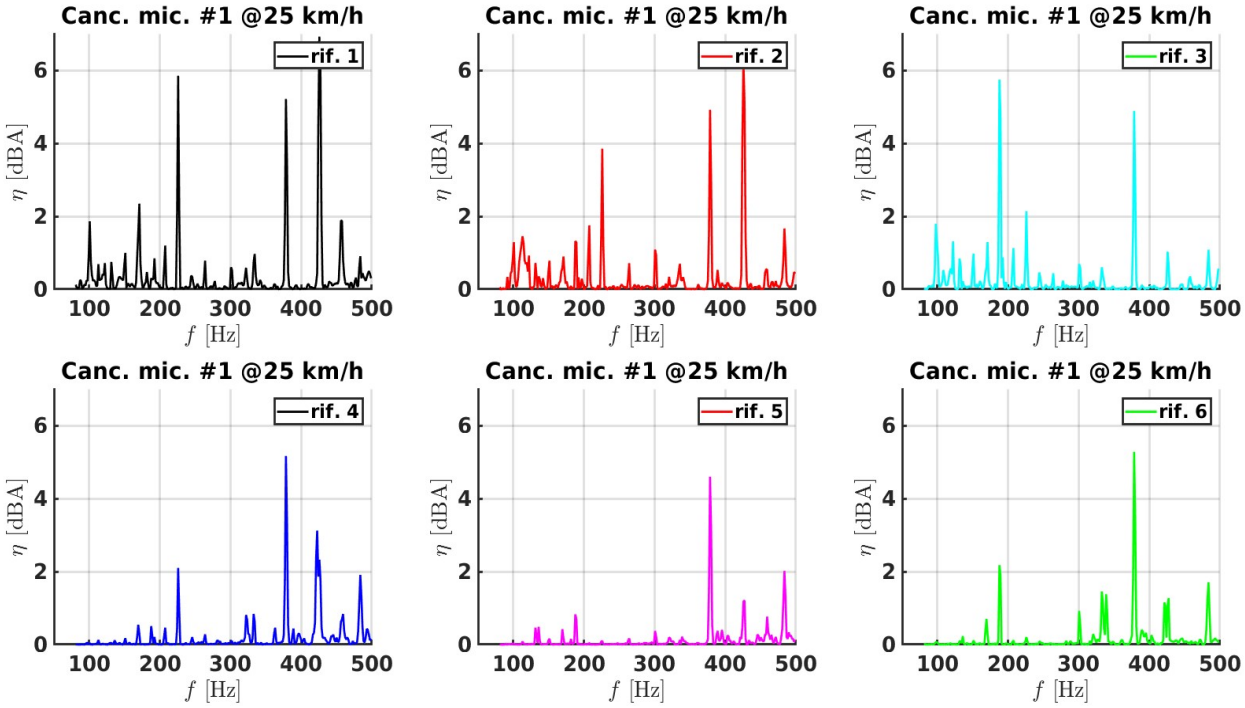

Figure 3.43: Theoretical cancellation obtainable on the audio in channel 1 with the different accelerometric references at a constant speed of 25 km/h.

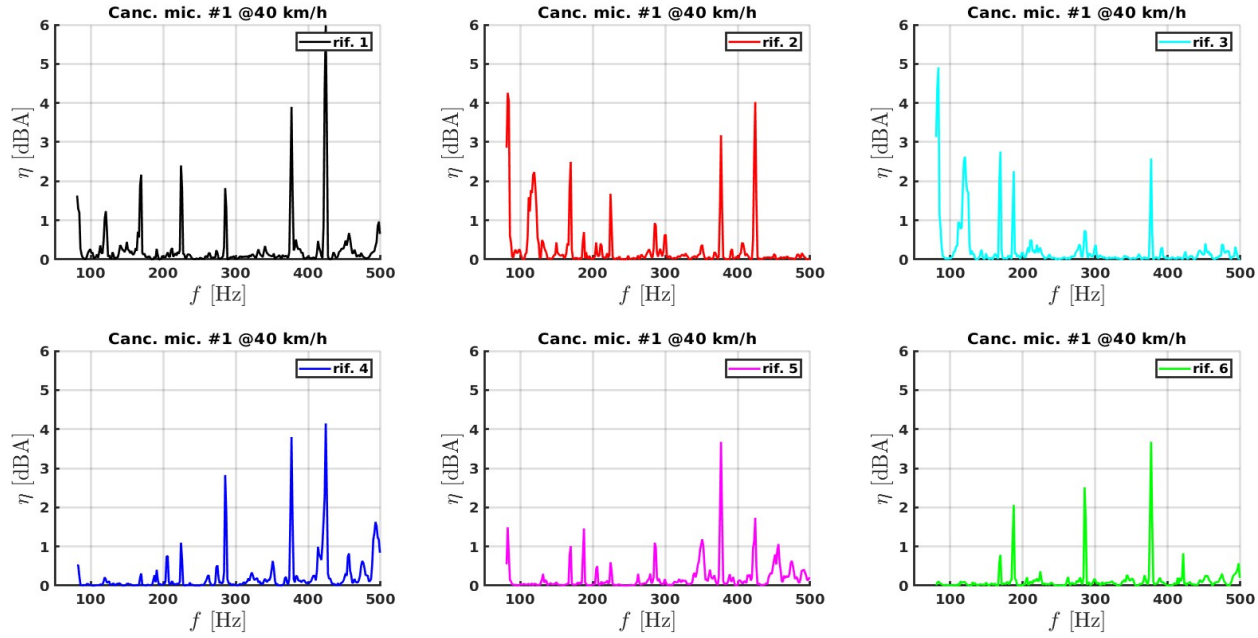

Figure 3.44: Theoretical cancellation obtainable on the audio in channel 1 with the different accelerometric references at a constant speed of 25 km/h.

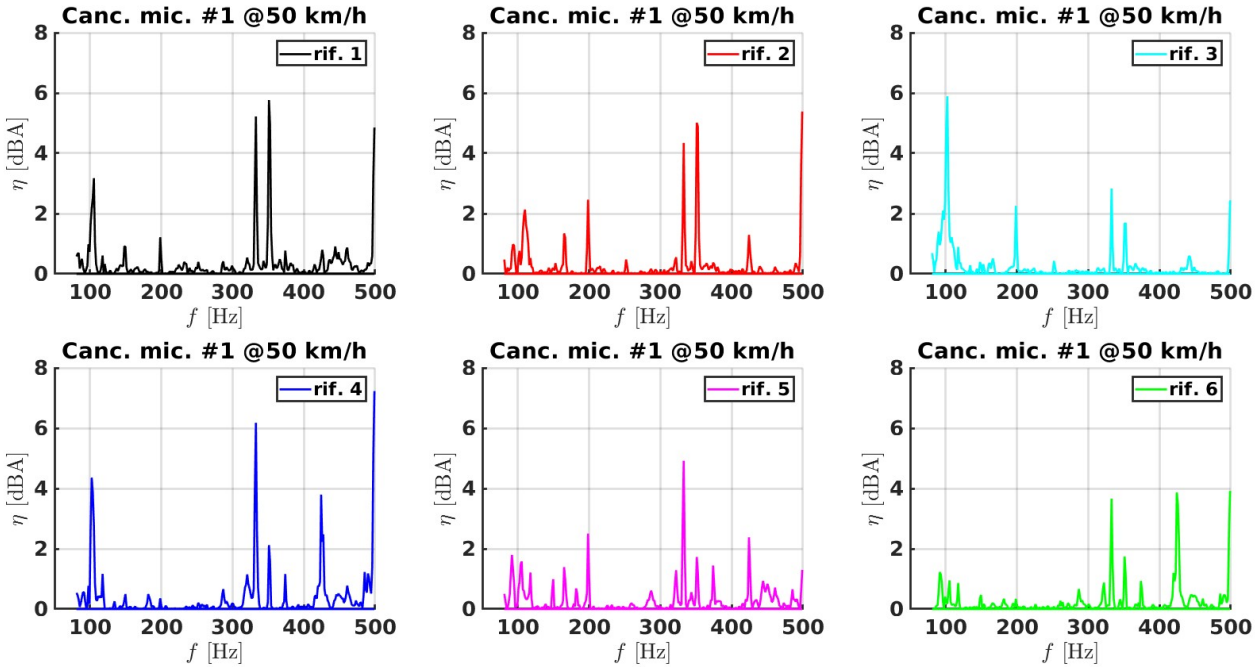

Figure 3.45: Theoretical cancellation obtainable on the audio in channel 1 with the different accelerometric references at a constant speed of 50 km/h.

Chapter 4: Active Noise Cancellation System Implementation

In this chapter, the considerations and choices that accompanied the development process of the prototype of the ANC system from the hardware and software point of view will be presented. The first prerogative sought during development was that of a good compromise between costs and performance of the hardware devices used to assemble the system. Furthermore, the use of hard-to-program Digital Signal Processing (DSP) devices was excluded. To overcome this choice, all signal processing, aimed at primary path estimation and anti-noise audio signal generation, has been performed using the software Simulink running on a commercial mini PC.

As for the type of ANC system to be developed, the choice fell from the very beginning of the research on a so-called *Parallel SISO* (Single Input Single Output) *Multireference* system. Parallel SISO designation indicates a system where there are two error microphones and two cancellation speakers. The two microphones are positioned, in the case of this study, near each of the occupant's ears. Each of the two loudspeakers takes care of the cancellation in correspondence of only one of the two error microphones or the one that is less distant. Ultimately, the system works as if it were split into two subsystems in parallel:

- Left speaker - left error microphone (Left SISO)
- Right speaker - right error microphone (Right SISO)

The term *multireference* indicates that the system uses multiple reference signals from different noise sources that affect the acoustic field in the cabin.

Let us recall again the desired characteristics of the active noise cancellation system developed in the present thesis work. The architecture of the control system sought is of the *Feedforward* type and based on an adaptive algorithm of the *FxLMS* type. Therefore, it requires the acquisition of error microphone signals and reference signals, coming from the noise sources. Furthermore, a priori knowledge of the estimation of the transfer functions of the secondary paths is necessary. Since the developed system is of the Parallel SISO type, it is also necessary to know in advance the cross-paths in order to compensate for the mutual interference of the two SISO systems.

4.1 Hardware ANC Implementation

Any Active Noise Cancellation system requires a controller that performs all the processing of the signals used, then, in order to generate the anti-noise signal. Usually a dedicated DSP card, whose programming is accessible only to expert users, represents this controller. With the aim of reducing prototyping times and costs, it was decided to base the researched system on a device that could easily integrate a Windows operating system and MATLAB / Simulink software. Programming using this software was found to be much more affordable for users with an average level of DSP knowledge. A first attempt was made with a *LattePanda* device [18], such as the one shown in Figure 4.1. This system, equipped with an Intel Atom Quad-Core 1.8 GHz processor, 2 GB of DDR3 RAM and 32 GB of SSD storage, can support a Windows operating system for a very low total cost. However, tests carried out have shown computational capabilities that are not adequate for the objectives of the project.

Figure 4.1: LattePanda board

Given the limited performance of the LattePanda systems, attention was paid to a solution based on a mini-PC, as it meets the specific requirements (Windows operating system and the possibility of working easily with MATLAB / Simulink software) with reduced dimensions and costs. , albeit larger than the LattePanda system. In particular, we opted for a solution based on Intel NUC mini PCs [19] like the one shown in Figure 4.2.

Figure 4.2: Mini PC Intel NUC.

This system was particularly interesting as it supports a power supply voltage in the range of 12-19 V in CC current as available on the tractor. The system ultimately selected is the Intel NUC8i7BEH NUC, equipped with an Intel Core™ i7-8559U processor with 32 GB of RAM (DDR4 SO-DIMM sockets) and one TB of SSD storage. The device chosen has demonstrated in the continuation of the project the computational capabilities necessary to control the cancellation system. A limitation of devices, such as those described above, is represented by the reduced performance from the point of view of processing audio signals. In addition, a device was needed that would allow the acquisition and emission of multiple signals. For these reasons, it was decided to equip the MiniPC with a good quality external sound card. The choice fell on an RME Fireface UCX card [20] with USB interface, shown in Figure 4.3.

Figure 4.3: RME Fireface UCX Audio Interface.

The selected audio interface has a total of eight inputs and eight outputs. It can be set via a software control panel accessible with the same miniPC. In this panel, also a graphic equalizer can be used to carry out part of the necessary input and output filtering directly on the audio interface. This allows lightening the computational load on the miniPC by reducing the computation latencies in the Simulink models that will

be described later. In fact, when a frequency filtering is inserted in a Simulink model (by means of the appropriate blocks) it also introduces a latency that increases as the attenuation imparted to the undesired frequency bands increases. If this mitigation is done in part by the external card, it can be assumed that the latency in the Simulink model is lower. Latency is a key performance metric of ANC systems.

This first system, consisting of audio interface and MiniPC on which to run the Simulink model of the FxLMS algorithm, represented the basis for carrying out the first *offline* tests, with headphones listening to the results, which will be described precisely in paragraph 5.1. The next steps in choosing additional hardware devices were aimed at installing and testing the ANC system on board a tractor cab. As anticipated, the developed ANC system used more error microphones and more reference signals. In particular, it was decided to use two error microphones (left ear and right ear) and at least two reference signals acquired by accelerometers. All sensors used are of ICP technology that all require an external power supply. The Fireface sound card has eight inputs, of which only two, numbered 1 and 2, are equipped with the 48 V phantom power supply necessary for the acquisition of signals with ICP sensors. To these two inputs has been chosen to connect the two error microphones, that is, the microphone in the left ear in input 1 and the microphone in the right ear in input two. Two omnidirectional measurement microphones with a sensitivity of 31.6 mV/Pa were used (Figure 4.4). The reference signals coming from ICP accelerometers would have been acquired from the inputs 3, 4 and 5 of the audio interface, which however are devoid of phantom power. For this reason, it was necessary to connect to these inputs devices for external amplification of the accelerometric signals. Initially, Behringer MIC100 Tube Ultragain [21] external pre-amplifiers (Figure 4.5) were used to connect to the necessary inputs of the sound card that do not have phantom power. These devices allow the adjustment of the gain by means of special knobs.

Figure 4.4: Microfono B&K da misura

Figure 4.5: Behringer MIC100 Tube Ultragain

These devices immediately demonstrated problems of excessive space in the cabin. In addition, they are equipped with 220 V alternating power supply therefore, in view of an installation on a real tractor, one or more inverters would have been required which, starting from the 12 V CC power supply on the vehicle, would provide 220 V alternating output. Tests carried out on a real tractor have revealed problems with the power supply stability of these amplifiers when connected, by means of an inverter, to the 12 V sockets in the cab. Furthermore, the excessive absorption of energy by these devices led to problems of overheating of the inverters and melting of fuses in the tractor's 12 V sockets. The most undesirable effect of power supply instability was found in the unacceptable distortions in the signals acquired by the reference accelerometers. To overcome these problems, the solution of using a card developed at the University of Parma was adopted (Figure 4.6). This board was specifically designed to provide amplification of signals from ICP sensors. It requires direct current power supply via a simple 18 to 30 V battery. It has three inputs with BNC connector, to which three ICP sensors can be connected, and three BNC outputs that can be connected to inputs 3, 4 and 5 of the RME sound card. This solution has solved the problems of overall dimensions and power supply with a "clean" acquisition of all the necessary signals.

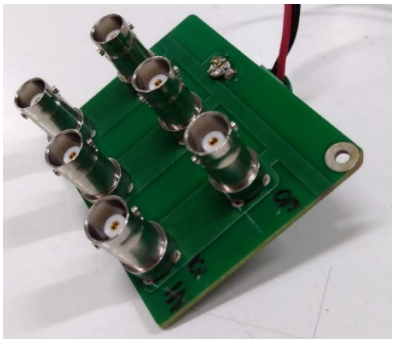

Figure 4.6: Amplification board for ICP sensors

Therefore, the hardware set up of the input signals in the ANC system is summarized. Two error signals from ICP microphones, positioned near the driver's ears in the cab, were acquired via the phantom-powered inputs of the RME sound card (1 and 2). The reference signals, from ICP accelerometers positioned near the noise sources, were acquired from inputs 3, 4 and 5 of the audio interface with the interposition of a small amplifier card. All the signals mentioned were sent to the mini PC via USB connection.

The software models developed in Simulink, for processing the input signals and for the emission of anti-noise signals, will be described below in a specific section.

Remaining in the description of the hardware devices used, the noise emission system will now be illustrated. As previously stated, a pair of speakers have been used in the Parallel SISO system, each of which takes care of cancellation at the closest error microphone position. In the various tests, two types of loudspeakers were used alternatively.

Some tests were performed using a pair of 140 mm diameter *mid-range* speakers. They were positioned behind the driver's head in the position occupied by the original series speakers in the vehicles in production (Figure 4.7). The 140mm speakers were chosen for their better low-mid frequency dynamic behaviour than the original speakers. Their characteristics make them particularly suitable for the cancellation of tonal noise components between 250 and 600 Hz. This is also determined by the reduced distance from the error microphones. The above considerations will be evident from the results of the tests described in chapter 5.

In other tests, a pair of 200 mm *woofers* was used. To optimize performance, they each need to be mounted in a 16-liter box equipped with a bass reflex. To optimize the overall dimensions in the cabin, the 32-liter box (divided in two by an airtight partition), necessary for the two woofers, was obtained by 3D printing and installed for prototype purposes in the position of the hatch on the roof of the cabin (Figure 4.8). Therefore, they were found to be positioned in front of the driver of the tractor. Figure 4.9 shows the frequency response of the speakers just described. They have proved particularly effective in cancelling frequencies close to 100 Hz.

A car audio amplifier powered both pairs of speakers used. We opted for the JVC KS-DR3004 car model (Figure 4.10), chosen for the flexibility of the power output and the ability to drive up to 4 speakers.

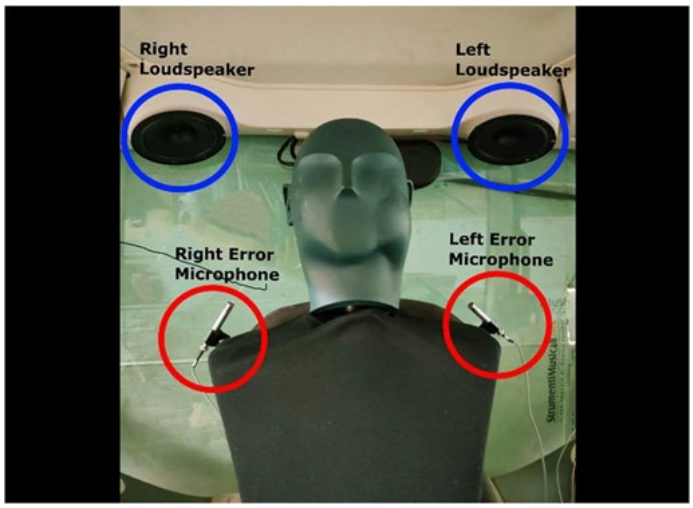

Figure 4.7: 140 mm loudspeakers and error microphones position

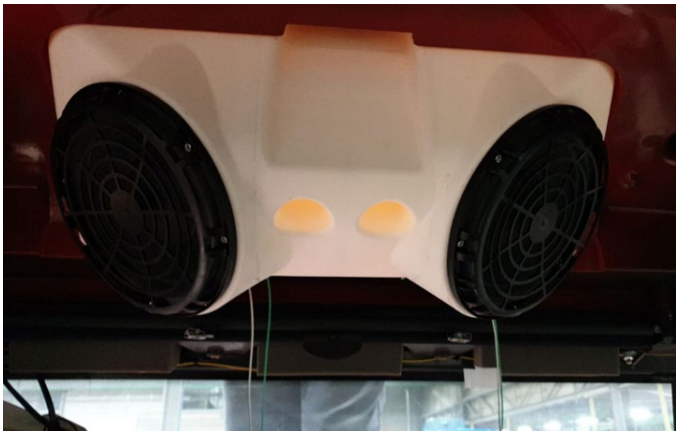

Figure 4.8: 200 mm loudspeakers

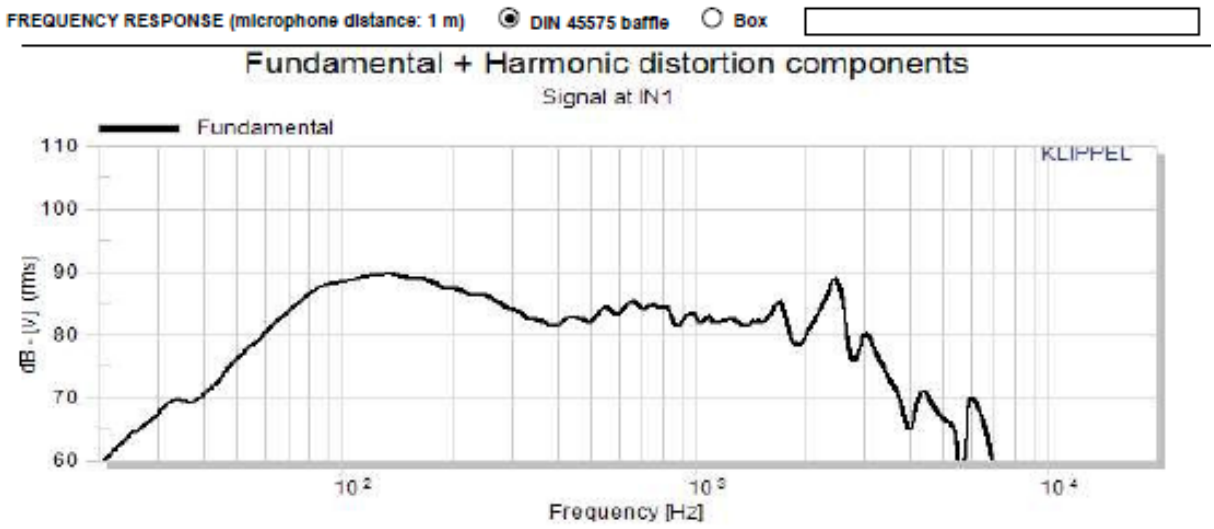

Figure 4.9: 200 mm loudspeakers frequency response

Figure 4.10: JVC car amplifier KS-DR3004

To summarize the description of the audio emission system, the two anti-noise signals generated by the miniPC are sent via the RME sound card to the two speakers after being amplified by the amplifier just described.

This concludes the description of the Parallel SISO ANC system from the hardware point of view. It should be noted that the solutions adopted were mainly tested on an isolated cabin with respect to the rest of the tractor but can be transferred without technical problems to a real running vehicle. This is because the perspective of installation on a real vehicle has always dictated the development process, so the possible adaptation problems have already been solved.

4.2 MATLAB/Simulink ANC Model Implementation

After having described the ANC system from the point of view of the hardware devices chosen for its implementation, we now move on to illustrate how the software models for controlling the operation of the ANC system have been developed. As already mentioned, the system controller consisted of a mini PC on which the Windows operating system and the MATLAB / Simulink computing environment were installed.

Recall that the system intended to be developed was of the Feedforward Parallel-SISO Multireference type based on the use of an FxLMS algorithm. As seen in Chapter 2, the FxLMS algorithm requires an estimate of the secondary path transfer function for its operation. This measure was implemented and automated by Simulink in such a way as to allow an updated measure before each session of the ANC system operation.

In the next two sections of this paragraph, we will first describe the Simulink model, which, once executed, provides the estimate of all secondary paths between speakers and error microphones. The implementation of the FxLMS adaptive system, which managed the operation of the ANC system in real time, will be described below.

4.2.1 Secondary Path Measurement

In the considered ANC Parallel-SISO system, each of the two loudspeakers takes care of cancelling the noise near the error microphone placed on the same side with respect to a seat occupant in the cabin. In other words, the speaker on the driver's left only deals with the cancellation around the driver's left ear. The same goes for the right speaker and the right error microphone. The two SISO systems in parallel must not affect each other. To achieve these objectives, it was necessary to find the transfer functions of four acoustic paths. Two represent the secondary paths between speaker and corresponding error microphone, for example left speaker and left error microphone.

Two other paths are represented by the so-called cross-paths, such as the one between left speaker and right microphone. These must be known, as will be seen below, in order to compensate for the influence of a SISO system on its parallel.

For the measurement of the secondary paths and cross-paths transfer functions, the ESS (Exponential Sine Sweep) method already described in Chapter 2 was used. To implement this method, it is necessary output the sweep signal from the loudspeakers and record it through the error microphones. This was automated using a Simulink model (Figure 4.11). Inside the model there are two special blocks belonging to the Simulink Audio Toolbox. They represent the interface between the model and the external audio interface. The first block, bearing the symbol of a loudspeaker, is called Audio Device Writer and is the one that sends the signals to a generic sound card. The second block, bearing the symbol of a microphone, is called Audio Device Reader and acquires signals from a generic sound card. The sampling frequency and the communication buffer size between the Simulink model and the audio interface are set in these blocks. The functioning of the model in Figure 4.11, when executed, can be summarized in two basic phases. In a first phase, a sweep signal is emitted from the left speaker deriving from an audio file. Simultaneously, both error microphones record the effect in the cabin. The result is two recorded tracks, one for each microphone. In a second phase, the other speaker (the right) repeats the same operations with the emission. Again, these results in a track recorded for each of the two error microphones.

For each of the speakers, an additional recorded track is obtained by placing the output of the audio interface, which feeds the speaker, in electrical loopback with a designated input port of the same card. In this way, the sweep signal is output and immediately recorded by the sound card. This signal will be used later to compensate for the calculation delays of the Simulink model just seen.

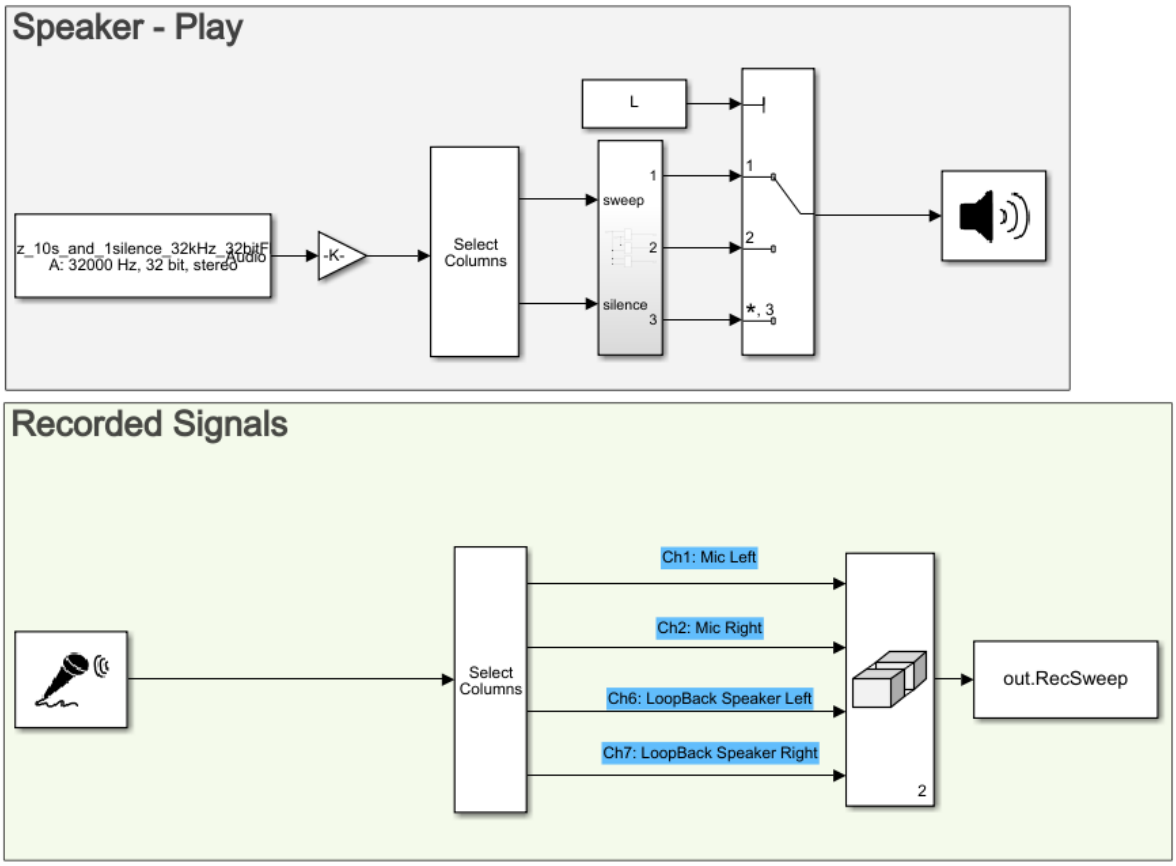

Figure2: Simulink Model for ESS recording

The output result of the process just described will be a set of six audio tracks:

• Recording from the left microphone of the sweep emitted by the left loudspeaker;

• Recording from the right microphone of the sweep emitted by the left loudspeaker;

• Loopback recording for the left speaker;

• Recording from the left microphone of the sweep emitted by the right loudspeaker;

• Recording from the right microphone of the sweep emitted by the right loudspeaker;

• Loopback recording for the right speaker.

The tracks listed above, once grouped into a single file called RecSweep, are supplied to the Simulink model that deals with the calculation of secondary and cross-paths. This model is represented in Figure 4.12.

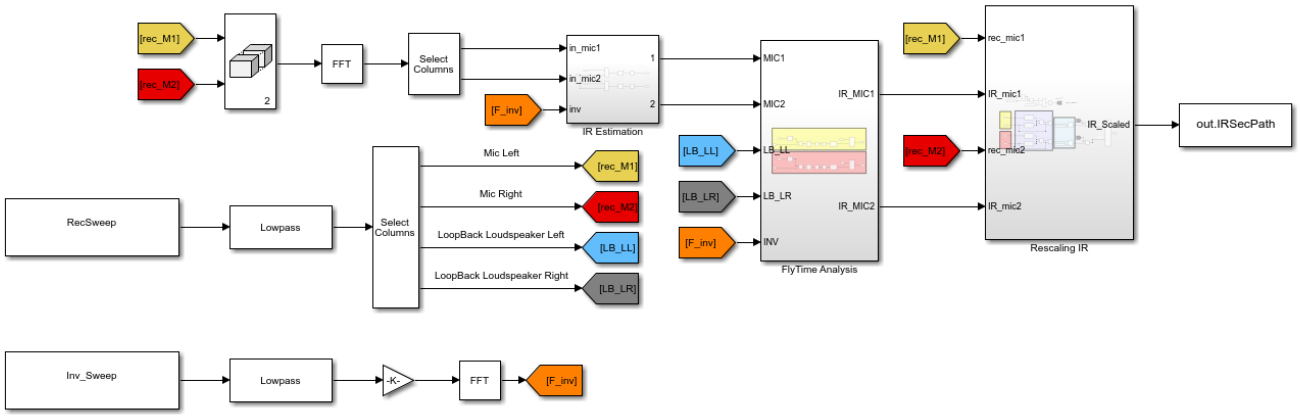

Figure 4.12: Secondary Paths Calculation Model

After an extraction of the traces from the RecSweep file, a low-pass filter with a cut-off frequency of 500 Hz filters them. This value was chosen based on the frequency range on which the ANC system will actually work, thus neglecting the rest of the spectrum.

The first fundamental operation of the model consists in calculating the fast Fourier transforms (FFT) of the previously listed recordings and of the trace that represents the inverse of the sweep signal emitted during the phase represented in Figure 4.11.

Figure 4.13 shows the contents of the IR Estimation subsystem visible in Figure 4.12. It implements the convolution of the signals recorded by the microphones with the inverse of the sweep signal, as suggested by the EES method.

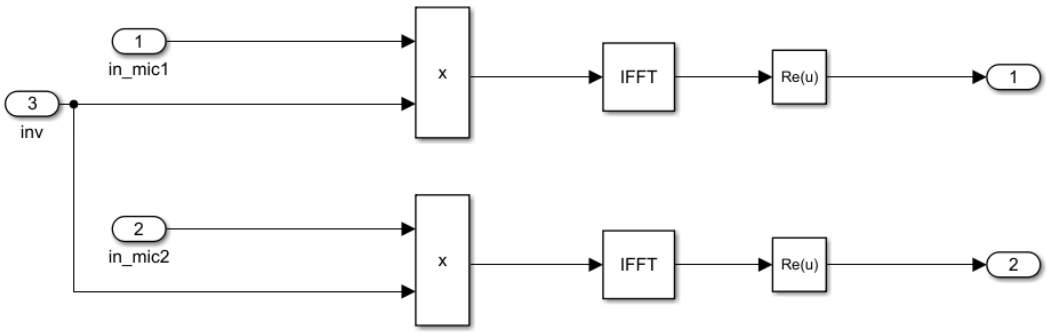

Figure 4.13: IR Estimation Block

Out of the block just described, signals are obtained that represent a first estimate of the impulse responses of all the paths between speakers and error microphones. These estimates, however, are affected by latencies inherent in the execution of the Simulink model in Figure 4.11. To clean the impulse responses from these latencies, leaving only the delay due to the flight time, the previously mentioned loopback signals are used. They were emitted and immediately recorded by the sound card without crossing the

acoustic path between speakers and microphones. Then by convolving these loopback signals with the inverse sweep, we will obtain delayed pulse signals with respect to the origin of the abscissas by an amount equal to the internal latency of the Simulink model in Figure 4.11. By removing this delay from the impulse responses obtained from the subsystem in Figure 4.13, only the flight time between speakers and microphones is preserved in the results. The operations described above are implemented in the Fly Time Analysis subsystem visible in Figure 4.12. The calculation model ends with a block that normalizes the impulse responses based on the RMS value of the recorded signals.

The result of the model described in this paragraph is the set of estimates of the responses to the impulse between the speakers and the error microphones. We can call these in the following way:

- $\hat{s}_{1,1}$: Impulse response of the secondary path between left speaker and left microphone;
- $\hat{s}_{2,2}$: Impulse response of the secondary path between right speaker and right microphone;
- $\hat{s}_{1,2}$: Impulse response of the cross-path between right speaker and left microphone;
- $\hat{s}_{2,1}$: Impulse response of the cross-path between left speaker and right microphon4;

The z-transforms of these signals can be used in the model of the FxLMS algorithm that represents the basis of the functioning of the ANC system under development.

4.2.2 FxLMS Algorithm Implementation

We will now describe the Simulink model that controls the operation of the ANC system. The active noise cancellation method based on the adaptive Filtered-x Least Mean Square (FxLMS) algorithm seen in Chapter 2 has been implemented. The error and reference signals are acquired and generated in real-time by the sensors and speakers. It is immediately understood the importance of having the minimum calculation latencies to have a correct functioning of the system. In fact, as specified in Chapter 2, it is essential that the cancellation signal is emitted and reaches the error microphone before the primary noise which from the source, passing through the vibro-acoustic system, reaches the desired cancellation position. It is therefore necessary to

optimize the parameters of the control software model in order not to exceed the computational capabilities and to avoid excessive latencies.

The Simulink control model, performed in real-time on the mini PC, interfaces, both for the acquisition and for the emission of signals, with the sound card. Model and sound card must operate at the same sampling rate, at least in the phases in which they communicate with each other. As will be seen below, signal-resampling operations will be performed within the model. However, at the interfaces between the Simulink model and the sound card, the signals must have the same sample rate on both sides. The RME Fireface UCX card allows a minimum sampling frequency of 32 kHz that represents a reduced value compared to the minimum frequency allowed by other sound cards. Commercial sound cards usually have a minimum sampling rate of 44.1 kHz. A low signal acquisition frequency allows a lower load on the computer, which is able to execute the required algorithms with greater fluidity. For this reason, the sampling frequency of the signals exchanged between the Simulink model and the audio interface has been set to the minimum value of 32 kHz.

Let us recall again the desired characteristics of the active noise cancellation system developed in the present thesis work. The architecture of the control system sought is of the feedforward type and based on an adaptive algorithm of the FxLMS type. In addition, the developed system is of the "parallel SISO" type so it is necessary to compensate for the mutual interference of the two SISO systems. Figure 4.14 shows the model developed to meet the aforementioned requirements as a whole.

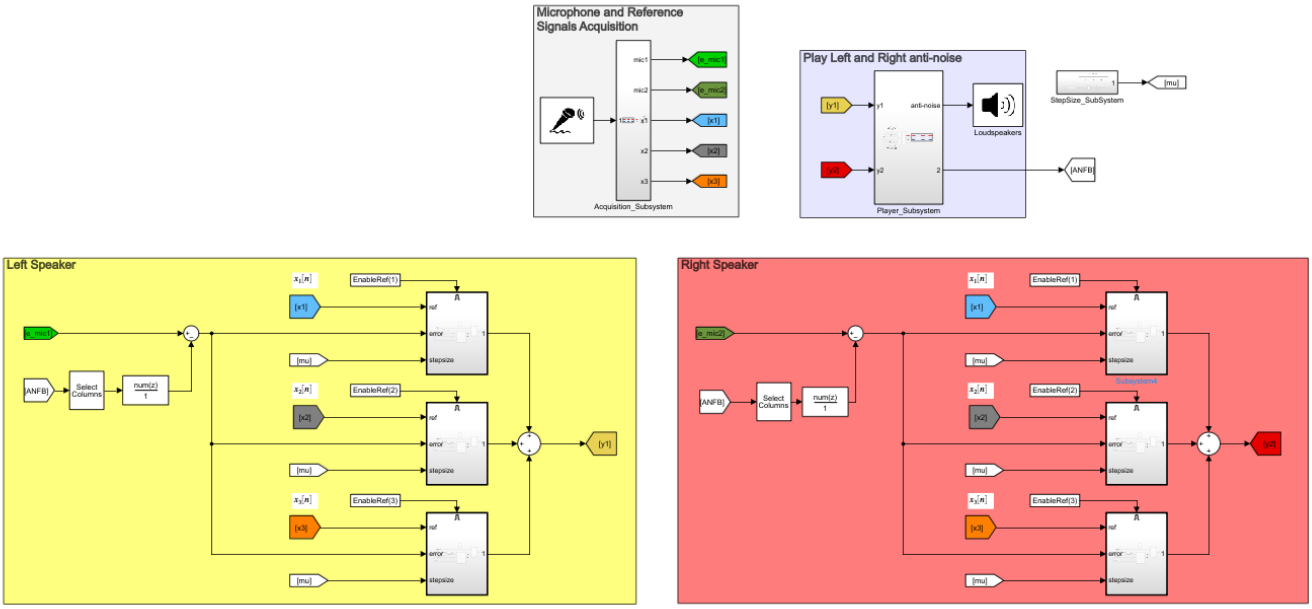

Figure 4.14: Parallel SISO Multireference ANC System: Simulink model

Figure 4.15 highlights the first part of interest of the model inherent in the acquisition of error microphone signals and reference signals. Using the Simulink Audio Device Reader block, the model acquires signals from the sound card in the form of packets of 2048 samples (buffer size). In the Acquisition Subsystem, the content of which is illustrated in Figure 4.16, the signals are subjected to subsampling from fs = 32 kHz to Fs = 4 kHz. The subsampling process includes low-pass filtering with a cut-off frequency of 600 Hz, a stopband edge frequency of 2000 Hz (equal to Fs / 2) and an attenuation of the stop band of 48 dB. This filtering restricts the operation of the model to the frequency band of interest for the ANC system (f <600 Hz) and secondly avoids aliasing problems. It should be noted that the lateral slope of the filter is deliberately kept low as this introduces less calculation latencies in the digital filtering software operation in Simulink. The down sampling just illustrated is performed to allow the next part of the model to work at a lower frequency with the aim, in this case too, of minimizing the calculation latencies. In fact, the next part of the model is the one that deals with the calculations inherent to the real adaptive cancellation algorithm. These calculations are more complex therefore, reducing the sampling frequency of the processed signals also reduces the computational load. The acquired signals finally undergo an unbuffering process since the subsequent operations of the model require the processing of one sample at a time.

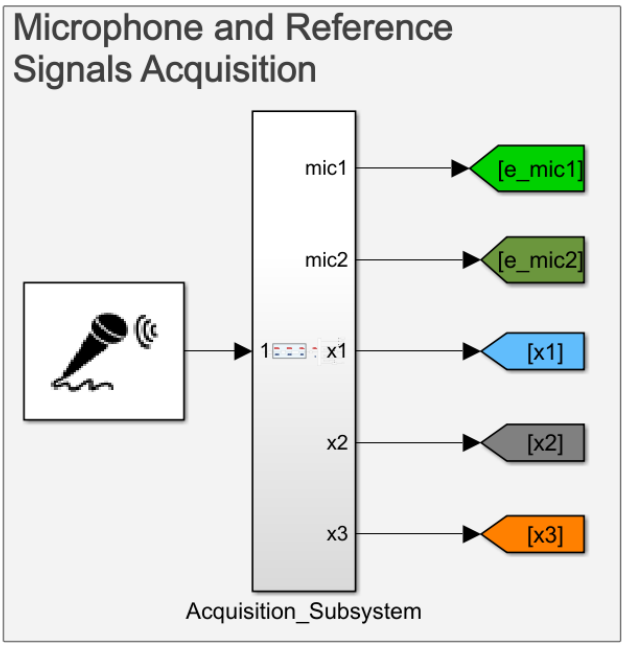

Figure 4.15: Error and reference signals acquisition

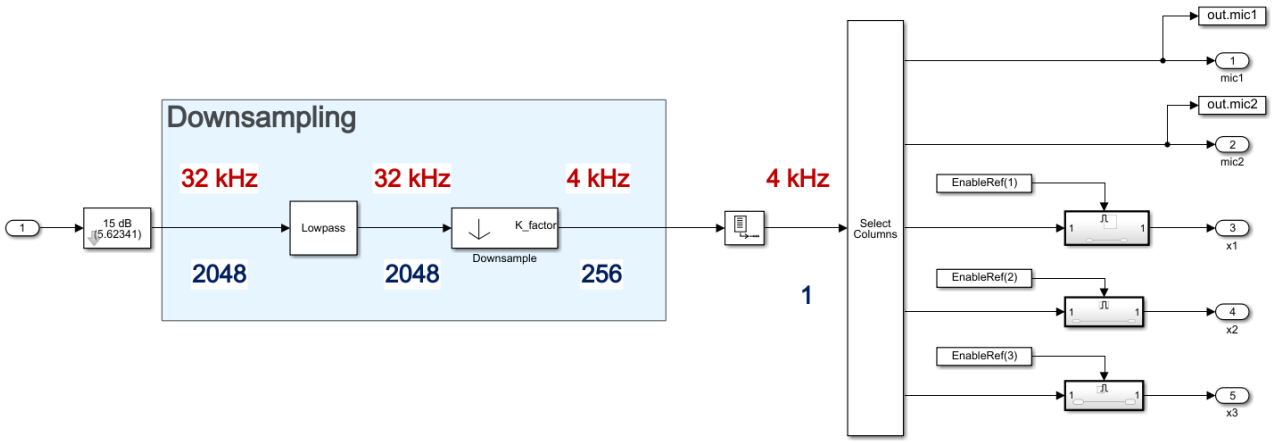

Figure 4.16: Acquisition Subsystem

From the acquisition phase just described, we obtain:

- The signals from the two error microphones named respectively e_mic1 (left ear position) and e_mic2 (right ear position);
- The reference accelerometric signals. In our case, three reference signals (x1, x2 and x3) are acquired from as many primary noise sources.

The error and reference signals are sent to the part of the model that is responsible for calculating the noise suppression signal. Being a "parallel" SISO system, an anti-noise signal is calculated for each error signal that will be emitted at the end by the speaker placed on the same side of the error microphone under examination. In addition, it is necessary to compensate for the influence of the anti-noise signal emitted by the speaker of the other SISO system for each error signal.

As an example, Figure 4.17 shows the calculation of the noise suppression signal y1, which from the left speaker acts on the left error microphone. All the considerations that will be made for the left SISO also apply to the right SISO.

The influence of the anti-noise emitted by the speaker of the other SISO subsystem is immediately subtracted from the error signal. The signal to be subtracted from the error signal is obtained by filtering the unwanted noise through the cross-path transfer function, which in the case of the left microphone corresponds to $\hat{S}_{12}(z)$. This is the z-transform of the estimated impulse response $\hat{s}_{12}(k)$ determined as described in the previous paragraph. The technique just described is called *cross-path compensation*.

Figure 4.18 shows the content of one of the subsystems that, by implementing the FxLMS algorithm, contribute to the calculation of y1. Each of these systems receives the error signal and one of the reference signals *x(k)* in input. As indicated by the principles of the FxLMS algorithm, set out in Chapter 2, the reference signal is filtered by estimating the secondary path $\hat{S}_{11}(z)$ before entering the Simulink block that implements the basic LMS algorithm. The latter, which is provided with an arbitrary value of the step-size *mu*, updates the coefficients of the adaptive filter. The output of this filter represents the anti-noise signal calculated based on the reference signal considered.

Ultimately, an anti-noise component is calculated for each reference signal which, added to those deriving from the other reference signals, constitutes the overall anti-noise y1.

All the considerations made for the left SISO system also apply to the right SISO system with the generation of the y2 anti-noise.

In order to allow a correct emission of the anti-noise signals y1 and y2 by the loudspeakers, the last operations performed in the Simulink model essentially concern a re-sampling of the signals from 4 kHz to 32 KHz.

In summary, the control model acquires the signals from the two error microphones and the reference signals. At the output, it emits two anti-noise signals that are sent separately to the two loudspeakers in order to create a parallel SISO system.

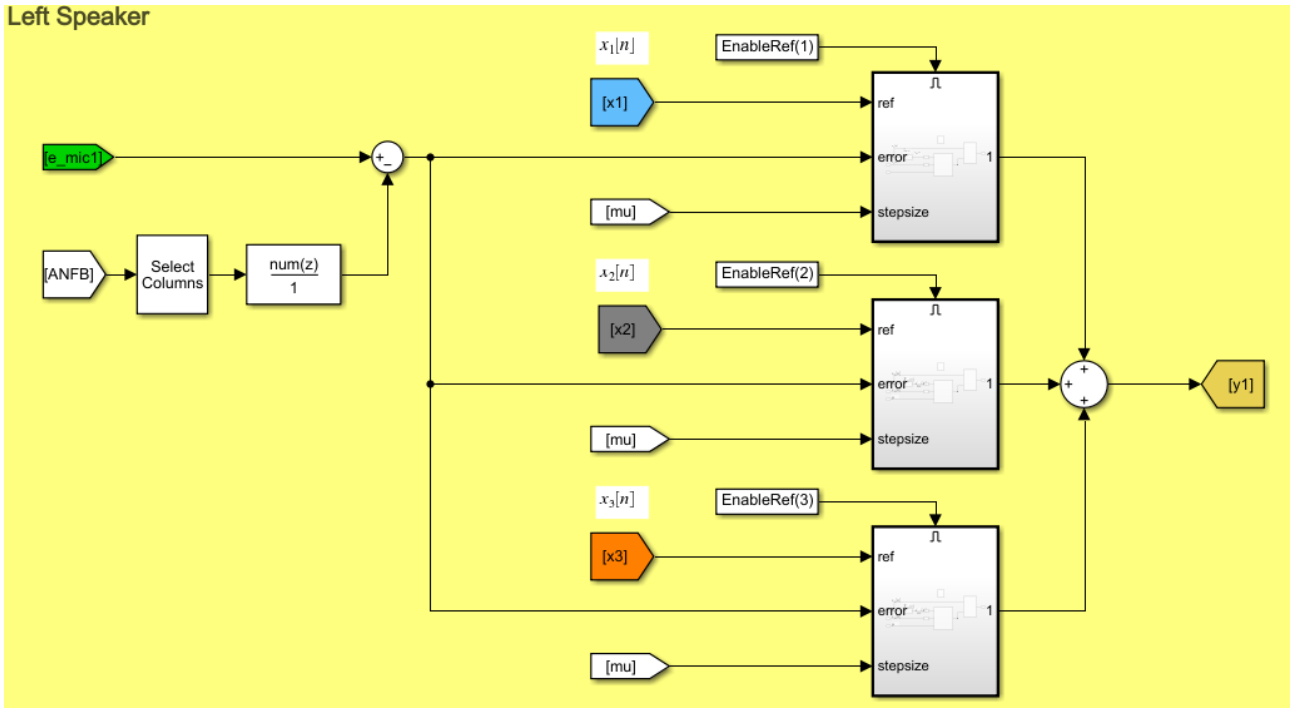

Figure 4.17: Left SISO ANC System, anti-noise calculation

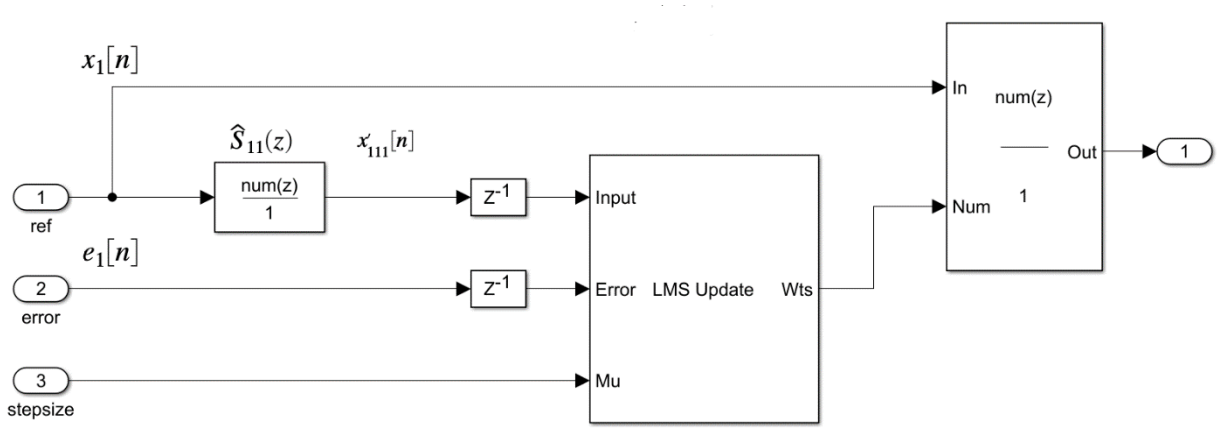

Figure 4.18: FxLMS Algorithm Implementation

Chapter 5: Active Noise Cancellation System Testing

The previous chapter described the process that led to the assembly of the prototype Active Noise Cancellation system. In addition, the Simulink models were described. They were created to acquire the estimates of secondary paths and cross-paths and to control the functioning of the system through the FxLMS algorithm. The prototype system obtained was installed on board a cabin (Figure 5.1) derived from the same model of tractor on which the measurements illustrated in Chapter 3 were carried out. This cabin was mounted on four supports that allowed the installation of electromagnetic shakers.
Before the description of the tests on the cabin, the results of *off-line* tests of a Simulink model of the ANC system will be illustrated, which represented the first version from which the final version described in the previous chapter was developed.

Figure 5.1: Cab derived from McCormick X7.690 tractor

5.1 Offline Testing

At the beginning of the software implementation of the control, a first version of the Simulink model was created in order to simulate the behaviour of the ANC system in "off-line" mode. In this phase, signal recordings acquired during the measurement sessions described in Chapter 3 on board the tractor were used. In particular, two signals acquired simultaneously were considered, consisting respectively of the recording of the noise in the cabin at the driver's ear and the recording of the accelerometric vibratory signal at one of the noise sources (Figure 5.2).

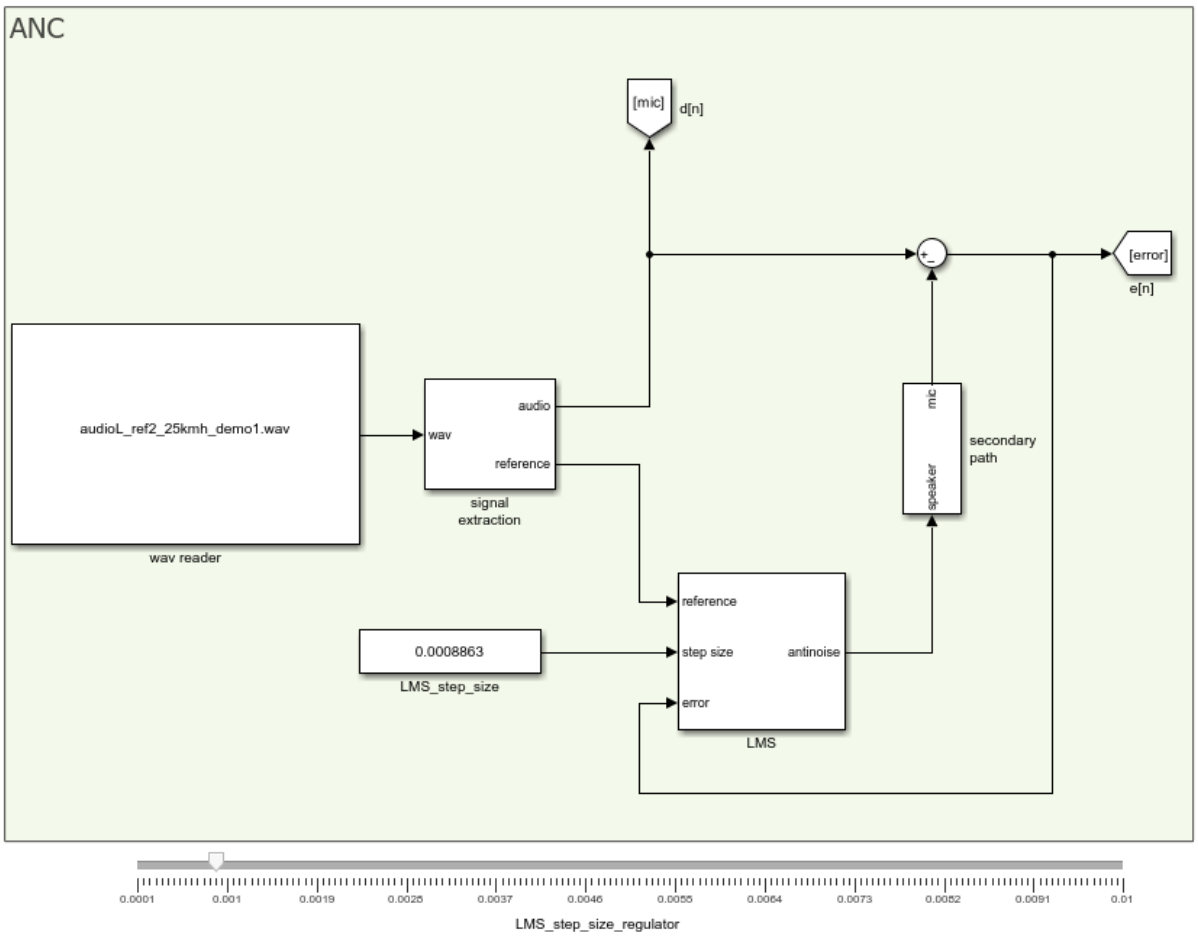

Figure 5.2: Off-line Simulink model ANC part

Describing the block diagram in Figure 5.2, we can identify the following steps that implement the ANC algorithm:

- The *wav reader* block reads a two-channel audio file that includes the recording of the microphone signal at the tractor driver's left ear and the recording of the accelerometric signal at one of the mechanical noise sources on the vehicle.
- The block that implements the LMS algorithm, whose internal subsystem is illustrated in Figure 5.3, receives the accelerometric reference signal, the step-size

value (which can be set using a slider regulator visible at the bottom of the model) and the error signal *e[n]*. The reference signal is filtered in the FxLMS-type algorithm by means of the secondary path, which, as already seen, represents an estimate of the transfer function of the acoustic system between the emission source of the anti-noise and the point at which one wants to obtain cancellation. In this first simulation phase, the secondary path was approximated with a simple delay applied to the signal of 70 samples.

- The *LMS_Update block*, available in the Simulink library, calculates the vector of the *Wts* coefficients to be supplied to the adaptive filter, which applied to the reference signal, outputs the desired anti-noise signal.

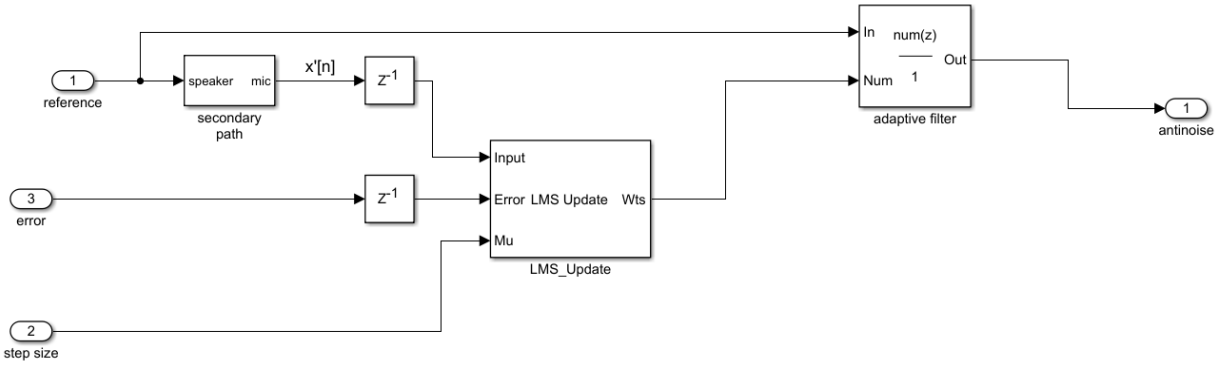

Figure 5.3: LMS block

- The anti-noise signal, to simulate the acoustic behaviour of the cabin, is filtered through the secondary path and subtracted from the audio signal representing the noise perceived in the position of the driver's ear. This subtraction simulates the acoustic cancellation, which is the goal of the whole system. This cancellation is naturally detectable in the error signal, which is then sent in feedback to the FxLMS block.

All the quantities and parameters involved in the model can be represented by graphs in order to have a visual confirmation of the functioning of the system. However, to simulate the actual sensation of cancellation, a practical method is to reproduce, through headphones or speakers, the original noise signal *d[n]* and the error signal *e[n]* in output from the model in order to perceive the differences (Figure 5.4).

5.1.1 Offline Testing: Results and Discussion

In this section we will analyse the performance of the FxLMS algorithm just illustrated using the vibro-acoustic signals of the second session of experimental measurements. In particular, the effects of the cancellation on the audio signal acquired in the left ear in the recording with the tractor moving at a constant speed of 25 km/h will be analysed. These recordings were made at the sampling frequency f_s = 25 kHz.

For simulation simplicity, the signals used will be a 1-minute segment within the recording (in particular the third minute). Performance will be studied in the presence of an "ideal" secondary path, which does not distort the transmitted signal but only introduces a delay of δ milliseconds. In particular, assuming a speaker to microphone distance of l_{SP} = 1 m and sound propagation speed v_{suono} = 343 m / s, we have:

$$\delta = \frac{\ell_{\mathrm{SP}}}{v_{\mathrm{suono}}} = \frac{1}{343} \simeq 3 \text{ ms}$$

The calculated δ corresponds for f_s = 25 kHz to 73 samples. This scenario represents an upper limit of the performances obtainable from the cancellation system with a realistic secondary path (measured, for example, on the system in the cabin that will be subsequently set up) which should approach the theoretical ones predicted by the coherence analysis. The FxLMS scheme of Figure 5.3 will be used as algorithm with λ= 1 and N= 1000 taps (for a duration of the impulse response of the filter of 40 ms for f_s = 25 kHz).

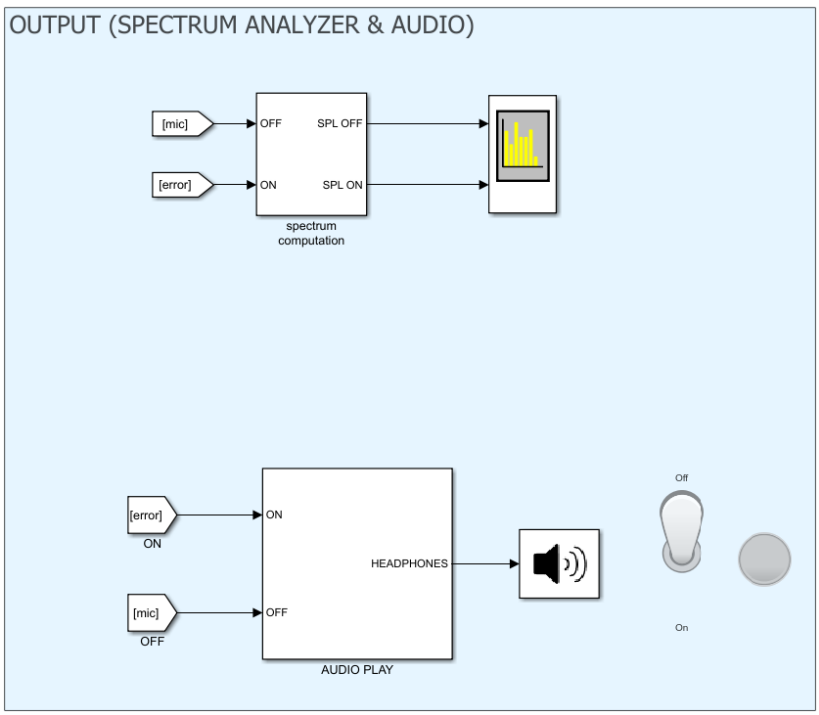

Figura 5.4: Offline Simulation

In Figure 5.5, the *A-weighted* audio spectrum is shown, comparing the absence and presence of the cancellation, using the reference signal acquired at the pump group for different step-size values μ. The SPL sound pressure level expressed in dB_A is therefore shown on the ordinate axis. It can be seen that for sufficiently small values of μ (for example $\mu = 10^{-4}$) the two curves are superimposed, as the filter is unable to adapt and the cancellation is not effective. For higher values (for example $\mu = 10^{-2}$ or $\mu = 10^{-1}$) we see how the cancellation becomes effective, especially at medium-high frequencies, where the coherence analysis had already shown high potential cancellations of the two peaks present, respectively, between 350 and 400 Hz (at approximately 375 Hz) and between 400 and 450 Hz (at approximately 425 Hz).

A similar analysis is shown in Figure 5.6 if the reference used is number 4 (reducer to the rear wheel). The same considerations of Figure 5.5 can be repeated also in this case, taking care to observe that the most coherent (and therefore cancellable) peak is that between 350 and 400 Hz.

To quantify the cancellation obtainable with the developed system, it may be of interest to define an *effective cancellation* function as:

$$\Delta = \mathrm{SPL}(d[n]) - \mathrm{SPL}(e[n]) \qquad (5.1)$$

where SPL($d[n]$) and SPL($e[n]$) represent the audio spectra (as for example from Figure 5.5) when the cancellation system is, respectively, OFF or ON. In other words, Δ measure of how many dB_A the noise perceived in the cabin is reduced. Figure 5.7 shows the effective cancellation for the two references considered and different values of μ. It can be seen that in both cases the best performances are obtained for $\mu = 10^{-1}$, while for $\mu = 10^{-2}$ the gains of the ANC system are reduced. However, for $\mu = 10^{-1}$ an increase in "negative" cancellation at some frequencies can be observed in both cases, corresponding, according to (5.1), to an increase in the sound level with the ANC system active. However, looking at the audio spectra it can be concluded that the increase in noise occurs at lower sound levels: this situation could be, from a psycho-acoustic point of view, tolerable.

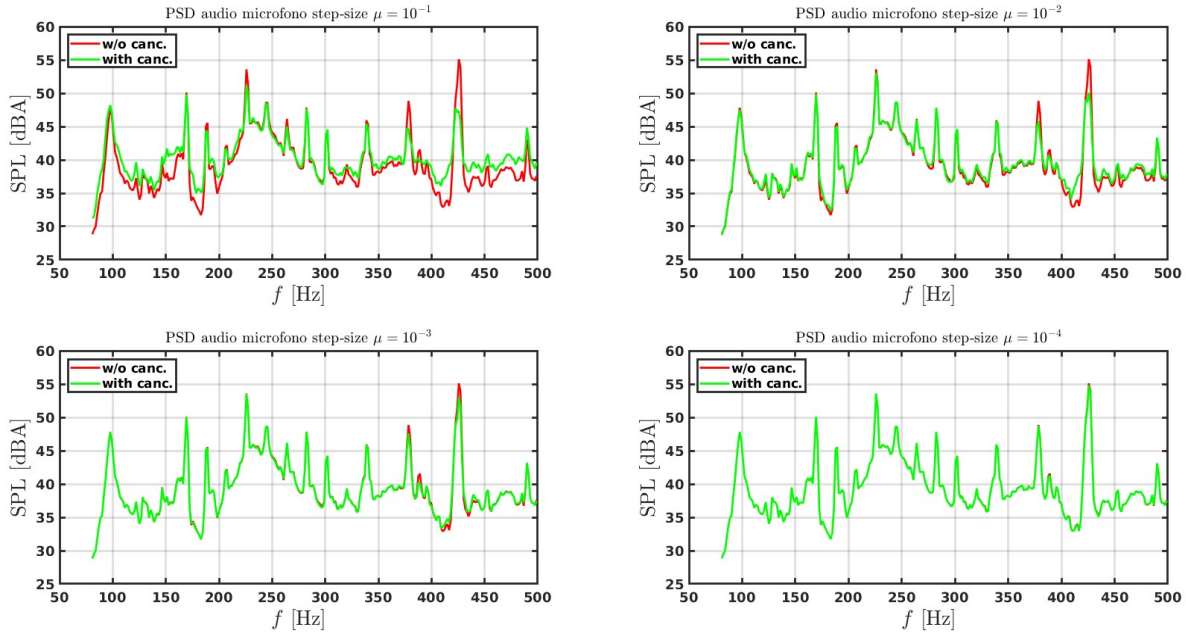

Figure 5.5: Audio spectrum, comparing absence and presence of cancellation, using reference 2 (pump group) for different values of step-size μ.

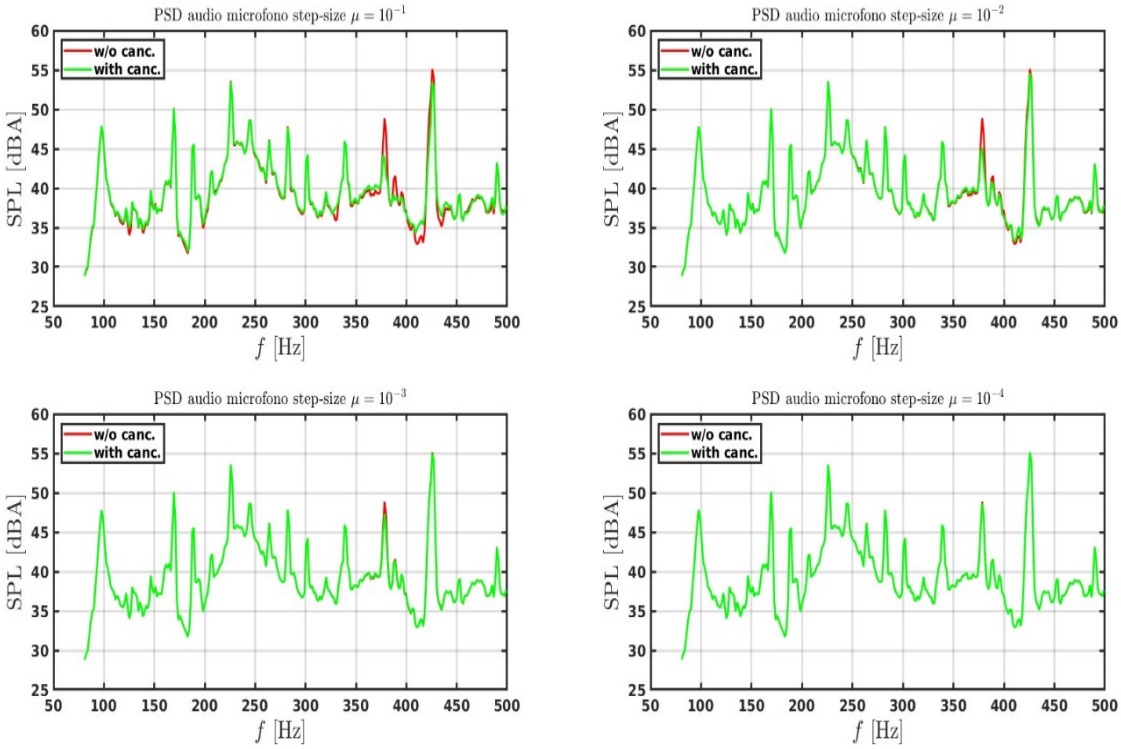

Figure 5.6: Audio spectrum, comparing absence and presence of cancellation, using reference 4 (reducer at the rear wheel) for different step-size values μ.

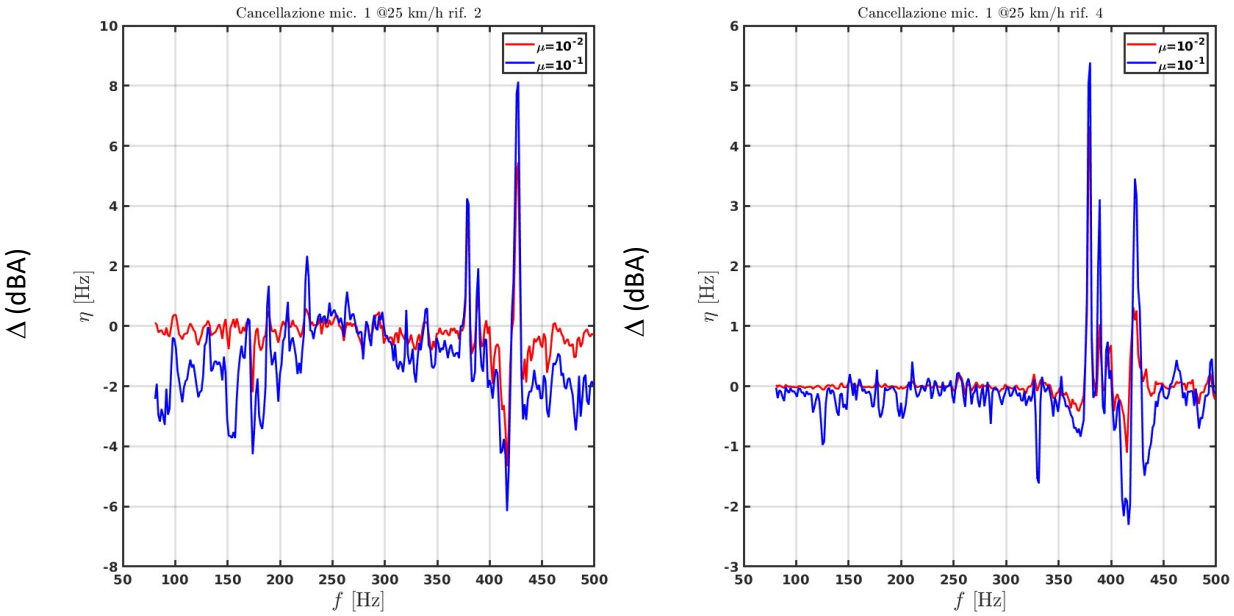

Figure 5.7: Effective cancellation for the references considered and different values of μ

5.1 Testing on Tractor Cab

At the end of the system development described in Chapter 4, the prototype was installed on board a cab from the model of the tractor on which the acquisitions, described in Chapter 3, have been carried out. This cabin was then installed on supports, which allow the insertion of electromagnetic shakers. Through these devices, to the structure can be provided signals of vibration of different nature ranging from pure single or double tones, passing by white noise signals up to the signals of reference accelerometrics previously recorded at noise sources on the tractor (hydraulic pumps group and transmission reducer to the rear wheel). The stress of the shakers causes a total vibration of the cabin, simulating the actual mechanical components of the tractor. This vibration will cause acoustic noise in the cabin that the ANC system will have to reduce.

As shown in figure 5.8, accelerometers were installed near the cabin stress positions. These accelerometers were used to provide reference signals for the ANC system. In these experimental conditions, where we have only noise sources due to the stress of shakers, the coherence between reference signals and the noise in the cab is high. This situation is less advantageous aboard the real tractor where the sources that contribute to the noise in the cabin are in more than those acquired with reference accelerometers.

To simulate the presence of an occupant inside the cabin, during a large part of the tests a mannequin was used placed in the driver's seat in the cabin. This has allowed

controlling the system from the outside, however, achieving results, in terms of acoustic response of the cabin system, assimilated to those of a busy cabin. In fact, it is known that the acoustic field in a closed environment is strongly dependent on what occupies it, or by the presence of material surfaces that interact with the acoustic waves absorbing or reflecting them.

At the position of the driver's ear, two omnidirectional microphones were installed in order to acquire the error signals in those interest positions. More precisely, the distance between manikin's ears and microphone is about 30 cm. For this work, two 1/2 inch omnidirectional ICP microphones for free-field measurements with a sensitivity of 31.6 mV/Pa by Brüel & Kjær, have been employed. The loudspeakers dedicated for the anti-noise emissions have been placed close to the manikin's head in order to improve the noise cancellation performance thanks to the reduced microphone/ loudspeaker distance (about 34cm). The considered setup described above is depicted in Figure 5.9.

The protocol adopted in the various tests that have been carried out will now be described. During all the tests, it was reputed to suspend all applications and all the Windows background processes on the NUC mini PC such as the one inherent in the antivirus. This choise was adopted in order to avoid unwanted buffering that could have influenced the execution of the Simulink control models. Furthermore, the model inherent in the FXLMS algorithm implementation, in all tests carried out, was executed in *Rapid Accelerator* mode. This execution mode fills out an executable, external to the Simulink calculation environment, which later controls the operation of the ANC system. The use of the described mode has allowed a significant reduction in calculation latencies compared to the standard *Normal Mode*.

Each test began with the measurement of the secondary path and cross-path transfer functions in the manner described in paragraph 4.2.1. As an example, in Figure 5.10, the magnitude response of the secondary path between the left loudspeaker and the left error microphone, i.e., |S11(f)|, is shown. It is possible to easily observe that this filter is band-limited within 600 Hz thanks to the introduction of a low-pass filter and equalization specification performed by the audio interface RME side. Moreover, note that very low-frequency contributions are also limited.

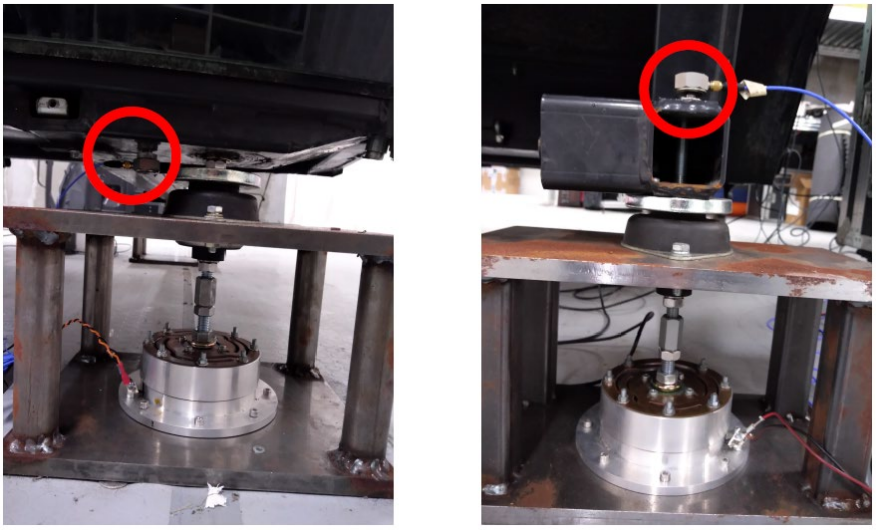

Figure 5.8: Cabin installation on shakers.

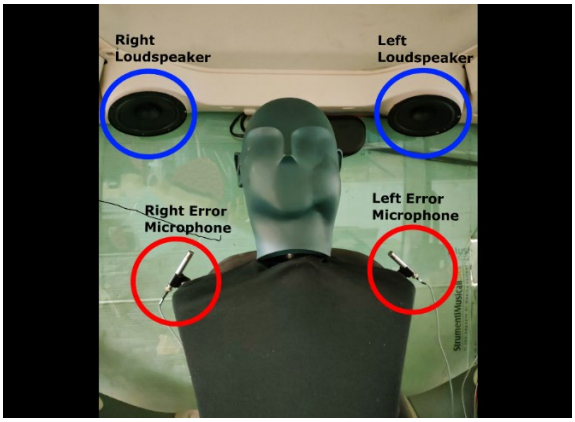

Figure 5.9: Experimental setup and measurements equipment: error microphones, loudspeakers for anti-noises emission and manikin at the driver's position.

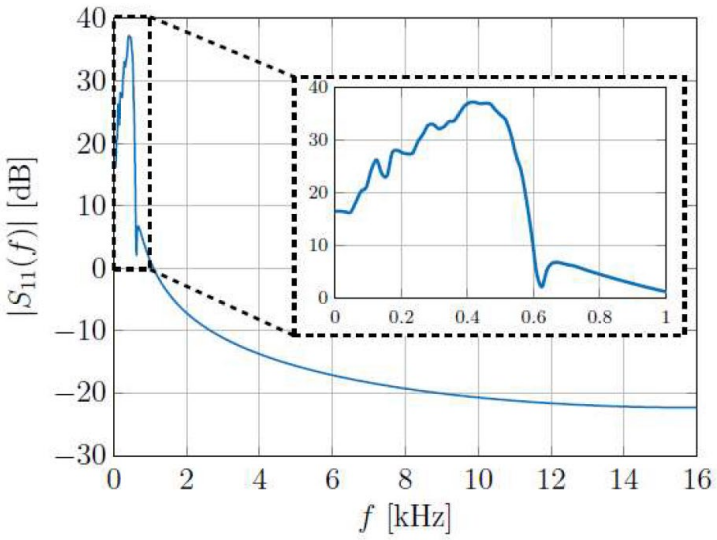

Figure 5.10: Magnitude response of the secondary path between left loudspeaker and left error microphone 1 |S11(f)|.

After the acquisition of the secondary paths, it was possible to test the actual ANC system. The electromagnetic shakers were supplied, through an external system consisting of a portable PC connected to a sound card and an amplifier, signals of different nature. These signals were transformed by the shakers into vibratory stresses applied to the cabin. As anticipated, the accelerometers designed to supply the ANC system with the reference signals were applied near the shakers' connections to the cabin.

Once the execution of the model described in paragraph 4.2.2 concerning the operation of the control system using the FxLMS algorithm has started, the signals relating to the two error microphones have been acquired. During each test, using a manual switch, it was possible to arbitrarily activate and deactivate the emission of anti-noise signals from the speakers. It should be noted that in the phases in which the speakers did not emit the cancellation signal, the algorithm continued to update the coefficients of the adaptive filter, thus updating the anti-noise signals.

The next paragraph will describe the signals that have been provided to the shakers from time to time, to generate the noise, and the resulting results obtained by activating and deactivating the emission of anti-noise signals.

5.2.1 Online Testing: Results and Discussion

As evidenced by the acquisitions made on the real tractor (Chapter 3), unlike the disturbing signals perceived by the microphones within a car, that are usually dominated by almost broad-band low-frequency regime, within a tractor cabin more tonal signals appear. For this reason, as representative of realistic vibrations, a sinusoidal signal at a fundamental frequency f_d = 300 Hz has been used to feed the shakers and excite the tractor cabin. The corresponding results for parallel SISO ANC system with cross-channel compensation are shown in Figure 5.11 and Figure 5.12 for the left and right error microphone, respectively. In particular, sub-figures (a) depict the microphone signal evolution as a function of time and sub-figures (b) show the SPL as a function of the frequency when the ANC system is OFF an ON. The ANC system starts in OFF mode and, after a small time interval, is turned ON. By observing the microphone signals evolution, in Figure 5.11(a) and Figure 5.12(a), it is possible to note that, initially, the ANC system is not effective: this is because FxLMS algorithm convergence is not achieved, yet. In fact, both microphones exhibit significant noise reduction after about 50 sec. By comparing the two microphone signals evolution, one can notice that the right microphone with respect to the left one perceives a higher level of sound and the disturbing audio signal is better mitigated. This can be confirmed by observing the corresponding SPL spectra for both microphones in Figure 5.11(b) and

Figure 5.12(b). The SPL of the right error microphone is higher than that of the left one and a noise cancellation up to 4.5 dB is exhibited at the considered tonal input at f_d = 300 Hz. Note that the ANC system cannot attenuate the second harmonic at 600 Hz, because of (i) the low-pass filtering of the secondary paths and (ii) the considerably small energetic level perceived by the microphones with respect to the fundamental one.

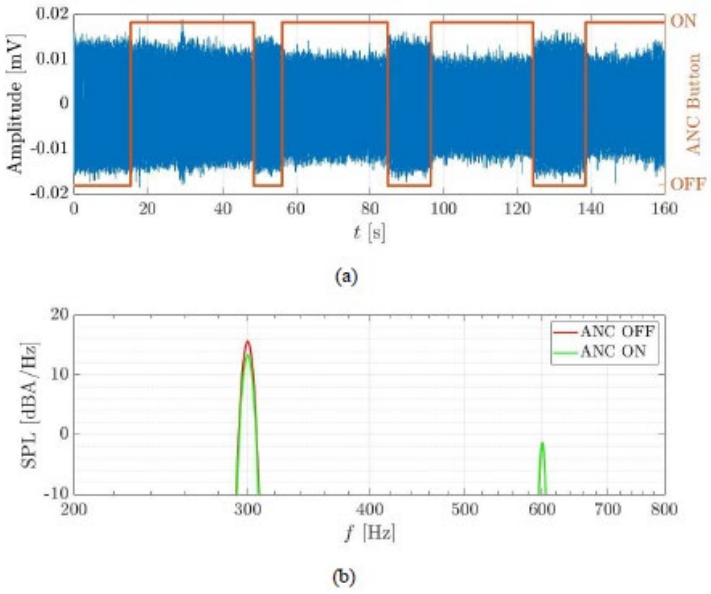

Figure 5.11: Results for tractor cabin excited by a pure tone at fd = 300 Hz. Left error microphone signal evolution against time (a) and SPL spectra (b) when ANC system is OFF and ON.

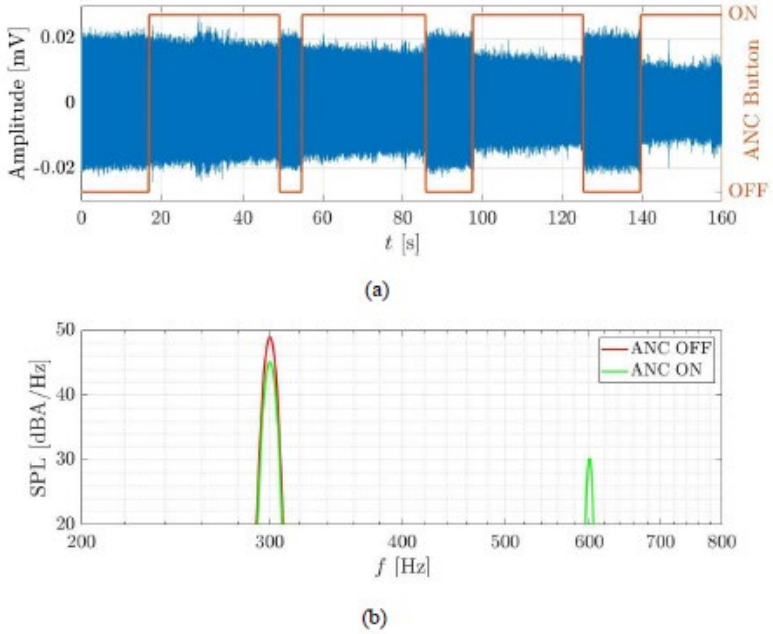

Figure 5.12: Results for tractor cabin excited by a pure tone at f_d = 300 Hz. Right error microphone signal evolution against time (a) and SPL spectra (b) when ANC system is OFF and ON.

In order to test the ANC system robustness under different scenarios and input signal type, two sinusoidal audio waves centered at f_{d1} = 260 Hz and f_{d2} = 440 Hz have been employed to the vibrate cabin. Experimental results, in terms of SPL spectra, for the left and right error microphone are shown in Figure 5.13(a) and Figure 5.13(b), respectively. Both error microphones nicely mitigate the disturbance signals. In general, the left error microphone exhibits better performance with the right one. Especially for f_{d2}, one can notice a noise cancellation level that up to 5 dB and 2 dB is obtained for the left and right error microphone, respectively. Unfortunately, the ANC system is not significantly effective for the pure tone centered at f_{d1}. In fact, both error microphones show a maximum noise reduction of about 1.5 dB at a frequency of 260 Hz. This may be due to the fact that, at this specific frequency, the secondary paths exhibits a low-gain and also by the lower energy level of the microphone signal compared to that experienced at 440 Hz.

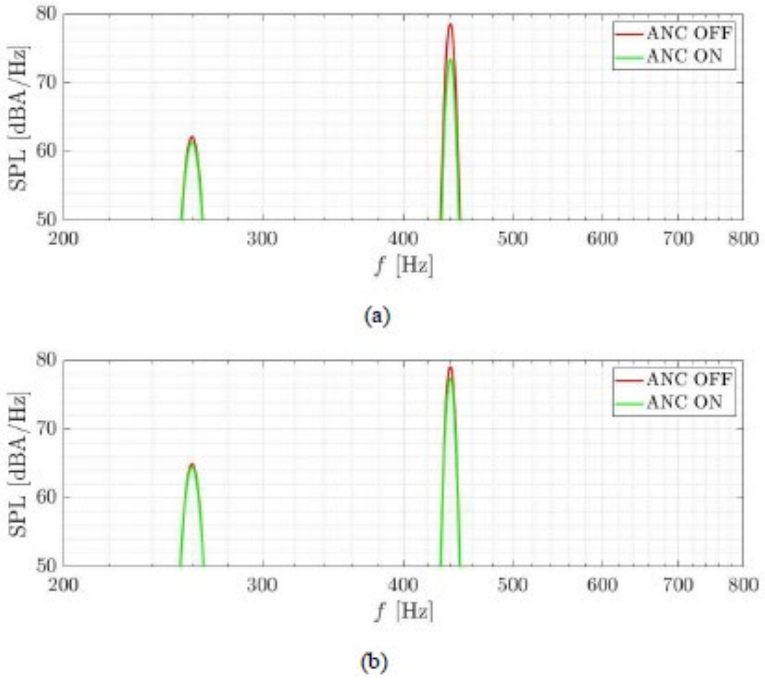

Figure 5.13: Results for tractor cabin excited by two pure tones at f_{d1} = 260 Hz and f_{d2} = 440 Hz. SPL spectra when ANC system is OFF and ON for left (a) and right (b) error microphone.

Finally, an experimental measurement of environmental sound propagating within the cabin of a tractor moving at a speed of 40 km/h has been used to shake the cabin and, thus, to test the ANC system under a realistic scenario. In this case, the experimental results are discussed in terms of mean square of the m-th error signal $e^2[n]$ when the ANC system is OFF and ON, i.e.,

$$\mathbb{E}\{\tilde{e}_m^2[n]\} = \frac{1}{N}\sum_{n=0}^{N-1} \tilde{e}_m^2[n] \qquad (5.1)$$

where: $\mathbb{E}$ denotes the expected operator; N is the considered window length (in terms of number of samples) for the mean square evaluation. In particular, this performance indicator has been evaluated as a function of the frequency band, i.e., the error microphone signal in (5.1) has been decomposed into 1/3 octave- bands. For the sake of compactness, only the left error microphone is considered. The corresponding results are shown in Figure 5.14, where f_c denotes the central frequency of the considered sub-band filter. As expected, due to time-varying nature and the presence of broadband frequency contributions of the disturbance signal, ANC system performance degrades. However, it is possible to note that, for the whole bandwidth, no amplification effects are obtained. On the other hand, for the mid-frequency range, small noise mitigation can be appreciated, e.g., within 199.6–501.2 Hz. Similar considerations can be drawn also for the right error microphone.

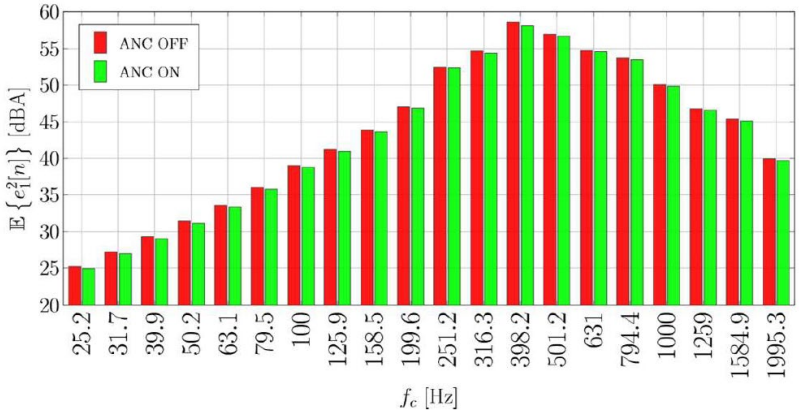

Figure 5.14: Results for tractor cabin excited by realistic environmental noise. One-third octave band when ANC system is OFF and ON for left error microphone.

The above results were obtained by using the pair of *mid-range* speakers visible in Figure 5.9. Some tests were performed using the pair of *woofers* that are described in Chapter 4 and represented in Figure 4.8. They are characterized by a good low frequency response. This is demonstrated by the test conducted by providing the shakers with two pure frequency tones f_{d1} = 125 Hz and f_{d2} = 500Hz, respectively. In practice, two frequencies close to the operating limits set for the operation of the ANC were chosen. From Figure 5.15 it is evident the cancellation that loudspeakers of this type are able to obtain for frequencies close to 100 Hz. This makes them suitable for reducing the noise due to the modal resonances of the booth structure. They are not efficient at cancelling mid-tones.

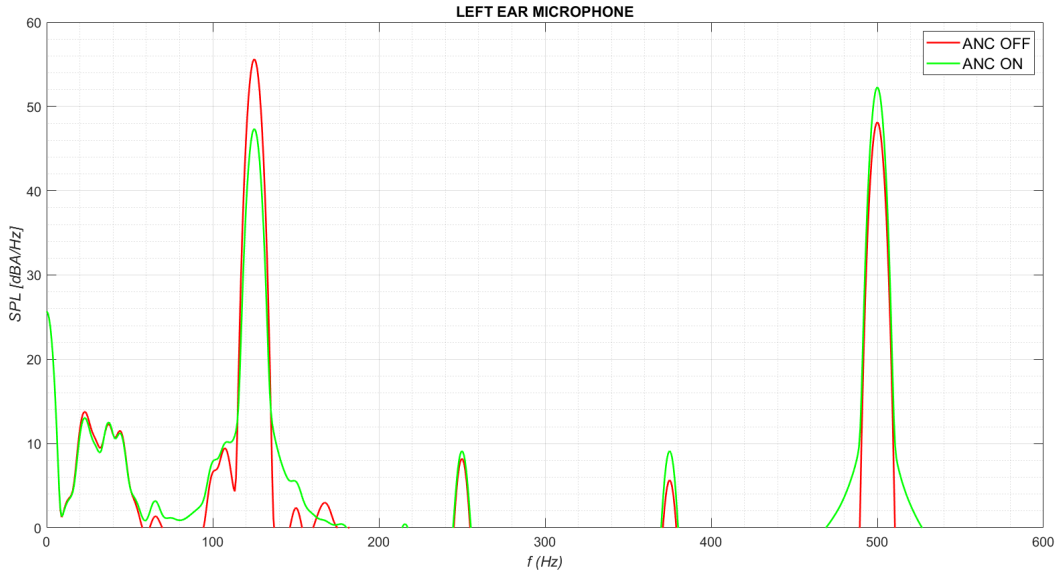

(a)

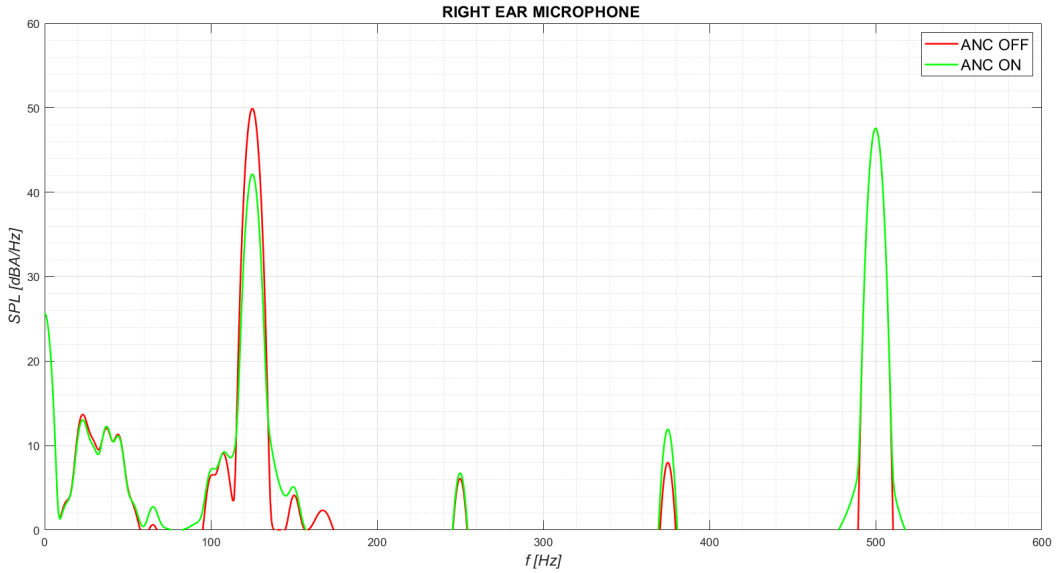

(b)

Figure 5.15: Results for tractor cabin excited by two pure tones at f_{d1} = 125 Hz and f_{d2} = 500 Hz. SPL spectra when ANC system is OFF and ON for left (a) and right (b) error microphone.

Chapter 6: Conclusions and Future Work

In this work, a low-cost and practical ANC system implementation for realistic agricultural machinery has been presented. General-purpose devices were used, such as the RME audio interface or the mini PC NUC, and control system programming based on Simulink block models was performed. These features make the developed system an excellent starting point for all those who want to approach, in an academic or industrial context, the field of Active Noise Cancellation. To replicate the studies described in this work, basic skills in digital signal processing are required while all the devices used are easily available on the online market.

Experimental results, on the tractor cabin mounted on shakers, show that ANC prototype is able to nicely mitigate disturbance signals with periodic behaviour at different frequencies. System performance degrades when realistic time-varying disturbance signals are considered. However, no noise amplification occurs within the whole frequency band and slight small noise cancellations are obtained under realistic and stressful conditions.

The system, in the very last part of the project, was tested aboard a real tractor. These tests have not been dealt with in the present work as they represent a preliminary phase of a plausible development of the research. The cancellation results on board the tractor, although present, need to be consolidated through above all a long work of setting the internal parameters of the system, whose hardware and software structure has in any case already proved to be suitable for application on a real vehicle.

The main problems encountered during the research process in implementing the system concerned:

• Choice of the type and location of the cancellation speakers: the cancellation speaker of each of the two parallel SISO systems had to be close to the error microphone designated for cancellation. The type of loudspeaker then had to have a good response at the medium-low frequencies, i.e. those where cancellation was desired. All these considerations translate into the need to install decent sized speakers in the cabin at a short distance from the driver's head. This purpose was achieved through the design and 3D printing of speaker stands specifically designed for installation in the cabin.

• Choice of the position of the reference accelerometers: this is especially important when the system is installed on a real vehicle. The whole characterization process described in Chapter 3 must be carried out. It is necessary to identify the sources for

which there is a high coherence between the acoustic field in the cabin and the vibration measured in correspondence with these mechanical components.

• Reduction of latencies throughout the control system: this was the most important aspect in the software implementation of the ANC system. This problem was addressed by choosing the whole series of filtering and re-sampling described in Chapter 4. In particular, the reduction of the sampling frequency of the signals from 32 kHz to 4 kHz, before being processed by the FxLMS algorithm, was fundamental. This has significantly reduced the computational load.

• Reduction of the mutual interference of the two parallel SISO systems: this problem was addressed by introducing the technique of *cross-path compensation* in which the anti-noise signal produced by the other system was subtracted from the error signal of each SISO system, filtered by the cross-path transfer function. This operation was carried out before the FxLMS algorithm acquired the error signal.

Based on an evaluation of the entire research process described in this work and the results obtained, it is considered right to make some considerations regarding the possible future developments that may derive from it.

The first goal, for a possible future development, concerns the installation of the prototype system on a real tractor. In this case, the vibro-acoustic system in which the ANC system would work is more complex in terms of variables that affect the acoustic field in the cabin and the operation of the ANC system itself. In fact, during the real working conditions of a tractor, there can be multiple causes that can affect the stability and efficiency of the control system. For example, the actual transfer function of the secondary path can change during system operation due for example of the opening of a door or the presence of a second occupant on board cabin. The estimate therefore of the secondary path inserted in the FXLMS algorithm, following a measurement carried out before activating the ANC system, may differ greatly from the actual secondary path. This affects cancellation efficiency. Another cause of instability can consist of impulsive noise due to impacts or other non-rare causes during a tractor's work. It is therefore necessary to work on the calibration of the internal parameters of the ANC system by finding compromise values between reactivity to change the sound field and stability of the control system.

An interesting research route would be to switch to two cancellation speakers for each error microphone. For example, a solution would be to use two different type speakers in terms of frequency response to cancelling on a microphone. A woofer could take care of the cancellation of the noise components at low frequencies such as the one

generated by rolling tires and from the lower orders of the engine. A *mid-range* speaker could instead deal with medium frequency components due for example to the hydraulic system. In this case, the system would pass by two to four speakers going to increase the cancellation efficiency on a very wide spectrum. The problem linked to this development is the increase in the acoustic paths that must be managed in the control of the ANC system.

In this work, the cancellation of structure-borne noise components was treated by using accelerometric reference signals. To increase system efficiency, it may also be considered the use of additional reference signals from microphones placed inside the cab. This solution would be advantageous from a point of view of the high consistency between error signal and reference signal. However, it is sensitive to problems of acoustic feedback that could cause instability. In fact, the reference microphone can also perceive the anti-noise signal. *Feedback compensation* must therefore be operated.

To conclude this thesis work it can be said that the solutions found during the implementation of the ANC system represent an excellent starting point for all those who intend to approach this field. In fact, the fundamental steps of development that have been treated can be retrieved by all those who, with a signal processing and vibro-acoustic basic knowledge , want to try using the active cancellation method to solve exposure reduction problems at high acoustic levels or improve sound quality on board of the cabin of any vehicle.

References

[1] Consiglio dei Ministri della Repubblica Italiana, "Decreto Legistrativo 9 Aprile 2008, n.81, Testo Unico sulla Salute e Sicurezza sul Lavoro," *Gazzetta Ufficiale,* vol. 101, 30 April 2008.

[2] "Trattori - ARGO TRACTORS," Argo Tractors S.P.A, [Online]. Available: https://www.argotractors.com/. [Accessed 11 November 2021].

[3] A. M. Abd-El-Tawwab, S. Abouel-Seoud, F. El-Sayed and T. Abd-El-Hakim, "Characteristics of agriculture interior noise," *Journal of Low Frequency Noise, Vibration and Active Control,* vol. 19(2), pp. 73-81, 2000.

[4] H. Fastl and E. Zwicker, Psychoacoustics – Facts and Models, 3rd ed., Berlin: Springer, 2007.

[5] DIN 45692:2009, *Measurement technique for the simulation of the auditory sensation of sharpness.*

[6] P. Lueg, "Process of silencing sound oscillations". U.S. Patent 2,043,416, 9 June 1936.

[7] S. M. Kuo and D. R. Morgan, "Active noise control: a tutorial review," *IEEE,* vol. 87, no. 6, pp. 943-973, June 1999.

[8] S. Elliott, I. Stothers, P. Nelson, A. McDonald et al, "The active control of engine noise inside cars," in *INTER-NOISE and NOISE-CON 1988*, Avignon (France), 1988.

[9] K. Gulyas, G. Pinte, F. Augusztinovicz, W. Desmet et al, "Active noise control in agricultural machines," in *ISMA 2002*, Leuven (Belgium), 2002.

[10] "NOISE CANCELLING HEADPHONES & EARBUDS," Bose Corporation, [Online]. Available: https://www.bose.com/en_us/products/headphones/noise_cancelling_headphones.html. [Accessed 1 12 2021].

[11] "Hyundai's World's First Road-Noise Active Noise Control, RANC," Hyundai Motor Group, [Online]. Available: https://tech.hyundaimotorgroup.com/article/hyundais-worlds-first-road-noise-active-noise-control-ranc/. [Accessed 1 12 2021].

[12] S. M. Kuo and D. R. Morgan, Active Noise Control Systems Algorithms and DSP Implementations, USA: John Wiley & Sons, Inc., 1996.

[13] A.Opinto, M. Martalò, C. Tripodi, A. Costalunga et al, "Performance Analysis of Feedback MIMO ANC in Experimental Automotive Environment," in *14th International Conference on Signal Processing and Communication Systems (ICSPCS)*, Adelaide (Australia), 2020.

[14] A. Farina, "Simultaneous measurement of impulse response and distortion with a swept-sine technique," *Journal of the Audio Engineering Society,* February 2000.

[15] P. Welch, "The use of fast Fourier transform for the estimation of power spectra: A method based on time averaging over short, modified periodograms," *IEEE Trans. Audio and Electroacoustics,* vol. 15, no. 2, pp. 70-73, June 1967.

[16] L. White and B. Boashash, "Cross spectral analysis of nonstationary processes," *IEEE Trans. Inform. Theory,* vol. 36, no. 4, pp. 830-835, July 1990.

[17] S. Kay, Modern Spectral Estimation, Englewood Cliffs, NJ, USA: Prentice-Hall, 1998.

[18] "LattePanda: a Windows 10 Computer with integrated Arduino," LattePanda, [Online]. Available: https://www.lattepanda.com/. [Accessed 1 December 2021].

[19] "Intel NUC," Intel, [Online]. Available: https://www.intel.com/content/www/us/en/products/ boards-kits/nuc.html/.. [Accessed 1 December 2021].

[20] "Fireface UCX," RME, [Online]. Available: https://www.rme-audio.de/fireface-ucx.html. [Accessed 1 December 2021].

[21] "Behringer MIC100," Behringer , [Online]. Available: https://www.behringer.com/product.html?modelCode=P0207. [Accessed 1 December 2021].